Design and Fabrication of on-chip Mid-infrared Emitter and LVOF

Yaonian Cui

Design and Fabrication of on-chip Mid-infrared Emitter and LVOF

by

Yaonian Cui

to obtain the degree of Master of Science
at the Delft University of Technology,
to be defended publicly on Monday October 29, 2018 at 2:30 PM.

Student number:	4594452	
Project duration:	October 29, 2017 – October 29, 2018	
Thesis committee:	Dr. ir. R. F. Wolffenbuttel,	TU Delft, supervisor
	Dr. M. Ghaderi,	TU Delft, daily supervisor
	Dr. ir. A. Bossche,	TU Delft
	Dr. ir. S. Vollebregt,	TU Delft

This thesis is confidential and cannot be made public until October 29, 2019.

An electronic version of this thesis is available at http://repository.tudelft.nl/.

TU Delft

Abstract

In this thesis,two essential parts of microspectrometer are designed, fabricated and measured. They are a hot wire of polysilicon with constant temperature profile that used as the IR light source, and the LVOF which is aimed at IR spectral range.

In order to have the desired IR source, the hot wire should have temperature distribution as uniform as possible based on black-body emission. Thus, the thermal mechanics inside the hot wire is fully studied including heat generation, conduction, convection and radiation.

The thermal energy is electrically generated by voltage and current source. While the heat loss causing non-uniformity on temperature is mainly induced by heat conduction between the hot wire body and substrate, and to surrounding air. For the first one, the geometry including the length, width and thickness, the resistivity profile of hot wire and the meander bridge at the end of hot wire body are designed. The meander bridge works as the connection and interface to substrate which to some extent determines the heat conduction through it. Moreover, it can bear tensile force induced by thermal expansion. Besides, the meander middle bridge is added to hot wire as well in some design plans for stronger mechanical stability.

On the other hand, since the temperature on hot wire is significant related to air pressure due to heat conduction to surrounding air, all hot wires are designed to operate in vacuum environment. Finally, a bunch of hot wires with different geometry, resistivity and TCR are designed and fabricated.

To design the LVOF aimed at IR band, the working schematics and properties of LVOF are firstly studied in depth. All factors such as reflectance, incident angle, cone angle and so on that might affect its performance which includes the most important transmittance are researched. The LVOF is also designed in different length and tilt angle. The case that the LVOF with the hot wire as IR source is paid special attention to.

Eventually, the electrical property and optical performance of hot wire is measured in vacuum chamber by FLIR IR camera. So far, the hot wire that has best performance is the one comprised of array of short hot wires. The result is fully discussed and divergence between actual performance and design plan is analyzed from many aspects.

Acknowledgement

I would really like to show my sincere respect and gratitude to My supervisor and Dr. Reinoud Wolffenbuttel who gave me the chance to do such wonderful thesis project, and the chance that I might publish it on transducer which is a famous European conference. He also kept encouraging me to try the ideal position in company which I don't dare to, and willing to be my reference. Really I'm grateful to him.

And my advisor Dr. Mohammadamir Ghaderi, who gave me a lot of help throughout the thesis project, same thanks to him. I was always having many questions and problems, but he was constantly patient no matter how stupid my problem is. The thesis project can not be finished without him. Huge thanks to him as well.

My best friend, Jinzi Qi, gave me selfless support every time I need help on daily life affairs. Jiang Bo and Guanchu Wang, as older experienced student, also gave me much advice on academic advice. Special thanks to them and all other friends that ever helped me.

Of course, the most important, My parents. Thank them for their emotional and financial support to every decision that I made. I can not even achieve anything without them. Really really thanks to them.

Finally, I want to thank myself for never giving up. Hope I can keep running until the day I touch my rainbow.

Yaonian Cui
Delft, October 2018

Contents

1 Introduction **1**
1.1 Spectroscopy . . . 1
1.2 Microspectrometer as a sensing system . . . 2
1.3 Linear variable optical filters (LVOF) . . . 3
1.4 Hot wire as infrared emitter . . . 4
1.5 Thesis outline . . . 5

2 The design of polysilicon hot wire as infrared light source **7**
2.1 Thermal generation . . . 7
2.2 Heat transfer mechanisms . . . 8
2.2.1 Thermal conduction . . . 8
2.2.2 Thermal convection . . . 8
2.2.3 Radiation . . . 9
2.3 Analytical solution . . . 10
2.4 Mechanical design of a Hot-wire . . . 10
2.5 Polysilicon hot wire design approach . . . 11
2.5.1 The initial design of hot wire . . . 11
2.5.2 Geometry design . . . 15
2.6 Resistivity of hot wire . . . 21
2.7 Comparison of the change of geometry and resistivity . . . 24
2.8 The rectangle hot wire with smaller beams at ends . . . 26
2.8.1 Design approach . . . 26
2.8.2 Results of Final design . . . 28
2.9 Hot wire design in longer length . . . 31
2.9.1 1mm hot wire design . . . 31
2.9.2 Meander beams at ends . . . 35
2.9.3 Lateral beams . . . 39
2.9.4 Lateral meander bridges . . . 41
2.9.5 4 and 5mm hot wire with middle bridges . . . 44
2.9.6 All designs of hot wire . . . 45

3 Optical design of a linear variable optical filter (LVOF) **49**
3.1 Theoretical background . . . 50
3.1.1 Bragg Reflector . . . 50
3.1.2 Schematics of FP filter . . . 52
3.1.3 Schematics of wedged FP filter . . . 53
3.2 Characterization of LVOF . . . 56
3.2.1 FSR, FWHM and finesses . . . 56
3.2.2 Reflectivity of two mirrors . . . 57
3.2.3 The number of reflections (p) . . . 58
3.2.4 The thickness and tapering angle of resonant cavity . . . 59
3.2.5 Incident angle . . . 60
3.2.6 Cone angle . . . 61
3.2.7 Separation between LVOF and detector . . . 63
3.3 LVOF with hot wire light source . . . 63

4 Layout design and fabrication of Polysilicon hot wire emitter **67**
4.1 Layout design 67
4.2 Fabrication process 70
4.2.1 Thermal oxidation 70
4.2.2 Polysilicon deposition 70
4.2.3 Doping of hot wires and bridges 71
4.2.4 Etching of polysilicon 71
4.2.5 Interconnect. 71
4.2.6 Spacer 72
4.2.7 Removal of SiO_2 layers 72
4.3 Fabrication results 72
4.4 Wire-bonding 76

5 Measurement and discussion **77**
5.1 Measurement on resistance 77
5.2 Measurement on IR emitting performance 80
5.2.1 Measurement set-up 80
5.2.2 The effect of pressure 81
5.2.3 The effect of voltage source 85
5.2.4 Hot wire array 88
5.2.5 Error source analysis 88

6 Conclusion and future work **93**

Bibliography **95**

1 Introduction

In this thesis, the design, fabrication and measurement of hot wire and Linear Variable optical filter (LVOF), which are two essential parts of microspectrometer for operation in infrared (IR) band is presented.

The microspectrometer is based on the combination of spectroscopy and micromachining technology. It basically consists of one hot wire made in polysilicon as infrared light source and a LVOF. The spectral range is aimed at 1.6 to 2.2μm. The main tool for simulation is COMSOL Multiphysics for hot wire emitter, which is a Finite element simulation tool. The optical design of LVOF is carried out using COMSOL and numerical computation using Matlab. Based on large amounts of simulation results, the polysilicon hot wire and LVOF are fully-designed then fabricated.

In this chapter, firstly the the fundamental concepts of spectroscopy technology are introduced. Secondly, a short introduction to microspectrometer including basic theory, classification and comparison among them is given, a short introduction to LVOF based spectrometer is followed. Subsequently, a general introduction to infrared light source and especially the type of polysilicon hot wire is given. Finally, the structure of thesis is given.

1.1. Spectroscopy

Spectroscopy is a study of the interactions between electromagnetic radiation and matters. By analyzing the radiation intensity in the function of wavelength or frequency, various measurements can be made such as identification for composition of mixed gas [1] and sample fluid [2] in chemical chromatography. The device used is referred as spectrometer.

The main concept of spectroscopy is resonance and corresponding resonant frequency or wavelength. When light that emitted by radiant source goes through material, energy exchange happens between atoms of material and photons. It becomes strongest when the energy of photon matches the difference of two energy states of atoms. Thus, the produced spectrum will be maximum at the corresponding resonant wavelength.

The interaction between material and radiation is generally represented in three forms, absorption, emission and scattering. When light passes through matter, photons with the energy that matches the gap between two states of atoms can be absorbed by atoms and molecules. The atoms go to higher energy state. That causes the decrease of transmission portion of light which is the basis of absorption spectroscopy. By comparing some calculations, and the spectral intensity before and after the absorption, the component and its amount in measurand can be determined. It is a powerful analysis method in many applications.

The activated atoms and molecules can subsequently get back to the original energy state by releasing the energy that absorbed before in the form of photons, the emission spectrum is then generated. This behavior can be described by Planck's equation: $\Delta E = h\nu$, where ΔE is the energy difference between the two states and ν is the frequency (wavelength) of the photons that are emitted and absorbed. h is Plan's constant which equals to $6.626 \times$

$10^{-34}Js$. The black body spectrum, for instance, is a type of emission spectrum that can be determined by the temperature of material, and the infrared emitted can be measured by specific instruments. Emission spectroscopy is a measuring method that takes advantage of this phenomenon. Emission peaks in spectrum represent the presence of certain material and its energy state, which can be used to identify component in measurand as well. In fact, it is often used in astronomy and chemistry.

Another interaction is scattering. When light hits the measurand, it can be redirected due to non-uniformity in matter. there are generally two cases that have small differences in between. When light that redirected in different angles is same as incoming light, it is called Rayleigh or Mie. While it is Raman scattering when light has a wavelength shift after passing through the measurand. In this case light changes its energy state. Scattering is proved to be a reliable and non-destructive method that used in matter analysis [3].

Absorption spectroscopy in infrared spectral range is one of the most commonly and widely used spectroscopic technologies [4] which particularly focuses on the interaction between infrared and measurand. It is often employed to analyze material component in gas and biofluids. As mentioned before, When infrared goes through the mixed gas, some of wavelength have almost no loss while some wavelengths are absorbed due to the unique absorption spectra of each individual gas. By measuring the percentage transmittance and other useful factors such as peak positions, widths and shapes at particular wavelength on infrared spectrum, then comparing the acquired results with the database, components in the gas can be identified. Compared to other methods such as measuring in ultraviolet and visible region, infrared spectroscopy is easier, faster and more sensitive. The infrared region in this thesis is initially aimed at around 1.6-2.2 µm, which is useful for absorption spectroscopy in organic materials such as ethanol.

1.2. Microspectrometer as a sensing system

Spectrometer is the major device that implements infrared spectroscopy. It is an instrument used for producing spectral lines. Using an spectrometer the light intensity at different wavelengths over an intended spectra is measured, which are used to identify material. The conventional spectrometer is typically bulky and expensive benchtop equipment. It is made for general purposes and thus usually has stronger performance than what is needed in applications. However, these spectrometers are bulky, more expensive, requiring larger volume of measurand and longer testing time [5]. Therefore, sometimes the high resolution has to be sacrificed for smaller size and low-cost. An effective way is to seek the theoretically possible spectral resolution within the limit of a relative small volume of measurand, which depends on the length of optical path in spectrometer. That is how microspectrometer is proposed.

With the development of optical microelectromechanical system (MEMS) technology, fabrication of various of microspectrometers were achieved [6]. In contrast with traditional benchtop instruments, it not only made a huge progress on downscaling, but also found a better solution between high-cost and high-resolution. It has huge potential in many applications because of its superior properties. Three major parts in microspectrometer are light source, disperse element and detector arrays. The working principle is that, light is absorbed by the measurand between the light source and disperse structure, then optical detectors can measure the absorption by material and analyze the component of incident light. Micromachining technology is often applied for manufacturing the infrared light source and the small disperse element.

Microspectrometer can be mainly classified into several types according to the type of optical detector and dispersion element. Basically, it can be categorized into grating-based microspectrometer and optical filter based microspectrometer based on the operation mechanism of dispersion element. Moreover, based on whether an array of detector or only one calibrated detector is used, it can be further classified into four types: moving grating and calibrated detector, fixed grating and detector array, tunable optical filter and calibrated detector, and the last one is one optical filter with detector array. But the system used in this thesis is linear-variable optical filter (LVOF) which consists of a tunable optical filter and an array of detectors. It can measure unique spectral response at different position.

Grating is a common structure used as wavelength-selective element in microspectrometer. The uniform distribution of narrow slits with equal spacing leads to the diffraction of incident light which is then separated into different wavelength in different angle at certain diffraction order [7]. By combining it with an array of detectors or a calibrated detector, the resulting wavelength can be presented in a more straightforward way. Figure 1.1 shows a grating based MEMS spectrometer composed of two bonded silicon chips with the grating and suspended thermopile detector arrays. Nevertheless, grating-based microspectrometer requires a comparative long optical path length which in a MEMS structure translates into a big limitation on optical throughput and power efficiency. It makes the grating-based microspectrometer not suitable for wafer-level miniaturized system despite of its compactness.

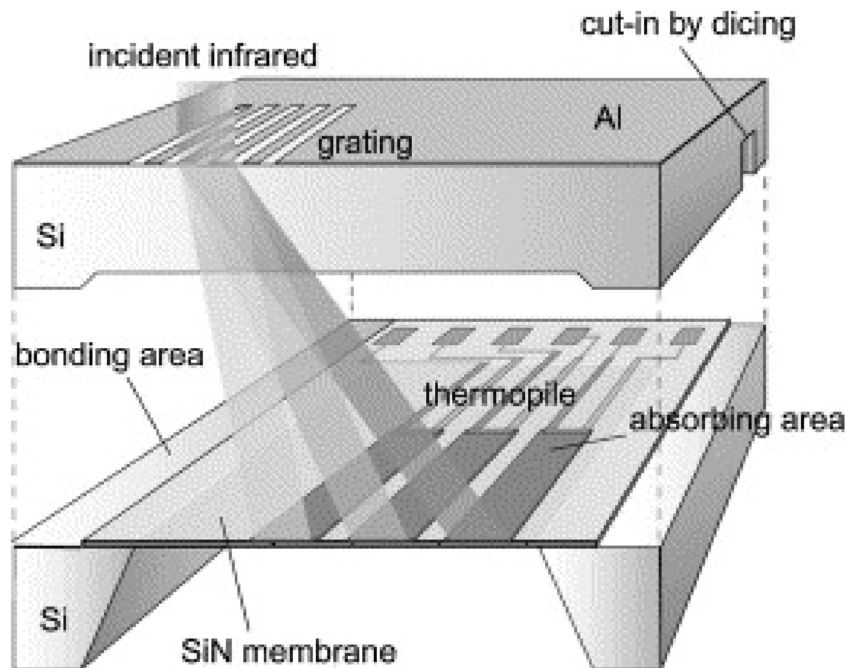

Figure 1.1: The schematic structure of the IR grating spectrometer [8].

Optical filter based microspectrometer is a better choice for miniaturization [9]. It uses interference filter such as Fabry-Perot filter to separate incident illumination into different wavelength. Typical resonator is composed of two parallel mirrors separated by a medium with a certain thickness that can be air or other optical material. As incident light travels inside the medium, the thickness decides the resulting wavelength of the light passing through the filter. In order to achieve a wide-band operation, an array of fixed resonators with different thickness such as LVOF or mechanically moving one of the flat mirror such as in a tuanble FP filters is used. or both of them, parallelism is vital for high resolution. High parallelism can be certainly achieved in fixed filter array by careful fabrication process, but the spectral resolution is limited by the number of spectral channel which means the number of filters. Although tunable FP filter can increase resolution by continuous mechanical movement on one of flat mirrors, parallelism again becomes an issue.

1.3. Linear variable optical filters (LVOF)

A Linearly variable optical filter (LVOF) as, shown in Figure 1.2, is composed of two highly reflective mirrors with a taper resonator inside. One mirror is flat while the other one slightly tilts. The thickness of resonator varies linearly over the length, which is equivalent to an array of fixed FP filter [10] see Figure 1.3. However, an LVOF can have a better resolution compared to discrete devices as it has many continuous spectral channels. Besides, compared to tunable FP filter it has stronger robustness as they are fixed. However, to ensure enough parallelism between the mirrors for proper operation, the LVOFs must be long. The

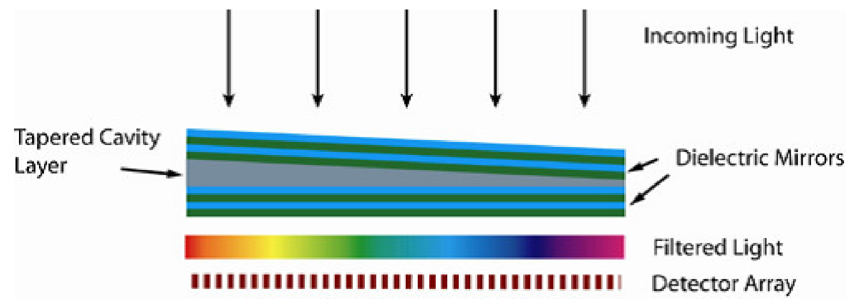

Figure 1.2: A schematic view of a tapered Fabry-Perot type of Linear-variable Optical Filter [10].

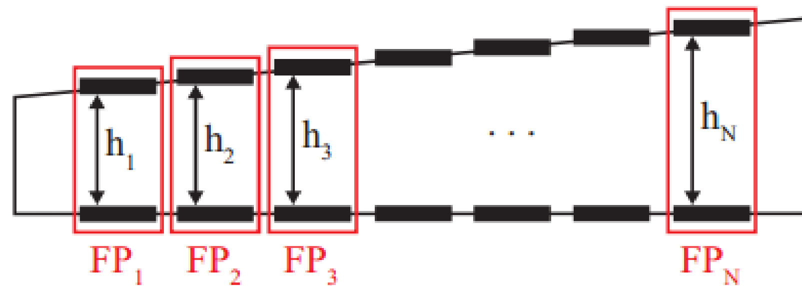

Figure 1.3: Analogy with multiple discrete FP filters.

most crucial factor of LVOF is the thickness of resonator that determines the spectral range. The resolution of a FP filter in part depends on the order of the filter (n) which translates into resonator thickness equal to $(2n-1)\lambda/2$. Other factors that determine spectral resolution are mirror flatness and reflectivity. By combining with a detector array to measure the radiation intensity at different position, a high resolution wide-band spectrum can be obtained.

1.4. Hot wire as infrared emitter

Infrared (IR) radiation is first found from the refracted light from sun. Theoretically, it is emitted by any heated glowing objects, which is also called black-body emission. The spectral intensity of thermal radiation from the surface of black-body radiator can be described by Planck's law, which is the function of emitting wavelength and absolute temperature of heated object. Emissivity is one of influential factors, but for easy simulation it is often assumed to be 1. It represents an ideal black-body that absorbs everything reaching it and reflects nothing. Based on the Wein's law for a blackbody, the spectral range, peak wavelength and its intensity, and total radiation power are determined by the temperature of heated object. An increasing emission can only be achieved by higher temperature which also causes the shift of peak emission towards shorter wavelength [11]. The other thing is, application in spectroscopy requires extremely uniform IR source to guarantee the accuracy of results. It means the emitted wavelength and its intensity has to be same all over the emitting surface of heated object. Thus, temperature has to be as equal as possible anywhere according to Planck's law.

In addition to black-body, there are some other types of IR sources such as IR-LEDs and IR-lasers. For instance, CO_2 laser is a common commercial IR source offering high power and coherent IR emission [12]. However, they are limited for applications that requires small size, high mobility and low power. The spectral range of these emitters is not easy to adjust either. Most importantly, they are not applicable for miniaturized system that at wafer level such as used in IR microspectrometer. Therefore, a miniaturized, low-power, easily adjustable and fabrication available IR source is required, such as a polysilicon hot wire which based on black-body thermal emission.

Hot wire is basically a conductive filament made from a special material (polysilicon in this thesis). It is widely used in the velocity measurement of gas and fluid in many applications,

which is called hot-wire anemometer [13]. Its use can date back to 1800s [14] and has been continuously improved for better precision [15]. Except that, it is also used to measure the heat conductivity and heat diffustivity of many material in different phase. It is called the transient hot-wire method which can go back to 1975 [16], in which hot wire serves as both heating unit and electrical resistor [17].

Hot wire is also used as IR emitter in many different way, such as metallic photonic crystal modified micro hot plate [18] and suspended serpentine silicon filament [19]. Later, The micro heater of polysilicon is proposed as a more advanced IR emitter in 2011 [20]. Furthermore, a rough surface is made on the light source for higher emissitivity thereby optical performance [21].

Similar in this thesis, hot wire is used as heating unit that emits IR light for microspectrometer. As electrical property such as resistivity of polysilicon can be modulated by doping of ions of other species, it can be equivalent to a heating resistor. By adding an electrical source no matter voltage source or current source to the two sides, it can be electrically heated according to Joule's first law. The resulted higher temperature causes thermal energy exchange to surroundings in the form of thermal convection, thermal conduction and thermal radiation, which means it is just like a black-body that emits IR to surroundings. Besides, a hot wire has a quite simple and regular structure that is easy to design and model in simulation tool. Moreover, fabrication of hot wire is not a tough task combining the advanced micromachining technology. Therefore, hot wire is a desired IR light source that can be applied in the microspectrometer.

Polysilicon is the basic material for hot wire. As mentioned before, the temperature is the dominant factor of thermal radiation in a black-body. According to Jouling heating, one of effective methods that adjusts generated heat power is changing resistivity. By implanting different types and concentration of dopant, the electrical properties involving resistivity of polysilicon is easy to modulate thereby making it a simple way to control thermal radiation. Besides, the thermal conductivity in doped polysilicon depends on dopant concentration as well [22]. Bascially, polysilicon itself is easy to transfer heat energy inside.

Actually, except polysilicon, silicon carbide as an alternative also has fascinating properties. It is much tougher thereby it is not easy to melt under a higher temperature. Compared to the maximum 500 °C of conventional polysilicon, the capacity to heat of SiC reaches to approximately 2700 °C that ensures a larger adjustable temperature range [23]. On the other hand, the strong toughness brings problems to patterning and etching in fabrication processing while it is opposing situation for polysilicon. Furthermore, the doping concentration to SiC is hard to figure out and control without large amounts of experiments. However, it is demonstrated in the later thesis that the effect of resistivity is not as obvious as assumption. SiC might be a choice for hot wire.

1.5. Thesis outline

The thesis is mainly divided into 6 chapters. Firstly, the introduction to the thesis project is already given. It explains the detailed concept of microspectrometer, LVOF and hot wire used as IR emitter. Secondly, the design of specific hot wire is described in chapter 2. Hot wires with various geometry and resistivity are simulated in COMSOL to get highest temperature and most uniform distribution along it. Thirdly, the design for LVOF is given. All possible influential factors are simulated in MATLAB. The special case of LVOF which is with hot wire as IR source is focused on. Next, the fabrication process of hot wire is introduced. It includes the layout design, fabrication flow and wire-bonding of the chip. Then the measurement on electrical properties and optical performance of hot wire is presented. Error sources that diverts the actual result away from design plan is analyzed and discussed. Finally, it is the conclusion and future work. Both unfinished work and next step for the project are discussed in this chapter.

2

The design of polysilicon hot wire as infrared light source

In this section, the design of polysilicon hot wire which is used as the IR source in microspectrometer is presented. It refers to the complicated interlacement in thermal, electrical and mechanical domain [24]. One reason that polysilicon hot wire is suitable for this application is, it is a simple structure and easy to design, control and fabricate. Functionally, it is similar to a heated resistor that emitting thermal radiation characterized by IR. Besides, the temperature distribution along the hot wire has to be as same as possible in order to obtain a required IR source for spectroscopy application. To achieve the goal, three aspects including the electrical source supplied, the geometry of hot wire and its adjustable electrical properties are mainly focused on. They are major factors that modulate the thermal energy exchange occurring inside or on the surface of hot wire, according to basic thermal theory.

2.1. Thermal generation

For hot wire, heat is electrically generated from provided power supply that submits to Joule's law:

$$P = I^2 R = \frac{V^2}{R} \tag{2.1}$$

Where P is the heat power produced, R is electrical resistance of hot wire, I and V are whether voltage source or current source supplied. Both of them are applied in this thesis.

For resistance,

$$R = \rho \frac{l}{w \cdot h} \tag{2.2}$$

Where ρ is resistivity, l is the length of hot wire and w and h are width and thickness separately. It can be seen that either electrical source or electrical property of material is a good way to manipulate heat generation thereby temperature of hot wire. As for resistance, all of parameters in geometry can also be used. The resistance is proportional to length of hot wire while inversely proportional to the area of cross-section which equals to $w \cdot h$ in rectangle shape. Thus, both width and thickness can be used which is actually the main method. The resistivity ρ of the wire can be also varied for obtaining required resistance.

Another important aspect of resistance is thermal coefficient of resistance (TCR). It describes that resistance is associated with changing temperature:

$$R = R_{ref}(1 + \alpha(T - T_{ref})) \tag{2.3}$$

Where R is the resistance at temperature T, R_{ref} is the resistance at reference temperature T_{ref} which is usually room temperature and α is TCR. TCR might be positive, negative or zero. When it is positive, it means the the resistance will be larger as temperature tends to increase. It's similar in negative case, the resistivity, and resistance, decreases with temperature. TCR

basically depends on doping concentration in material. The change in TCR with doping has to be considered while changing resistivity by doping level to to manipulate the maximum temperature in hotwire.

2.2. Heat transfer mechanisms

Generally, heat transfer on hot wire is characterized by thermal generation, conduction, convection and radiation which is based on different mechanisms.

2.2.1. Thermal conduction

It is always understood that heat is transferred from hot objects to cold ones. The driving force of heat flux is the thermal gradient which can be characterized by thermal conduction, convection and radiation. Basically, heat conduction occurs inside solids due to nonuniformity of temperature. It comes from collisions of molecules and movement of electrons, and obeys to Fourier's law:heat flux resulted from heat conduction which is a vector quantity is proportional to magnitude of temperature gradient and opposes to its sign. However, the scaler form is used in this thesis for simplicity since it flows in one dimension and only the steady-state is considered.

$$q = k\frac{\Delta T}{L} \tag{2.4}$$

where q is heat flux the unit W/m^2, k is thermal conductivity in W/m□K. ΔT is the temperature between two objects that heat conduction occurs and L is the thickness in the direction of heat flux. Thermal conductivity is the most important parameter that proportional to molecule speed and specific heat. Under the condition of steady-state, it is assumed to be a constant number.

For a deep understanding, the complete three-dimension dynamic heat conduction is as follows,

$$\Delta \cdot k\Delta T + \dot{q} = \rho c\frac{\partial T}{\partial t} \tag{2.5}$$

Where ρ is the density of material and c is specific heat. To obtain the total conducted thermal energy of heat flux through a cross-section:

$$Q = qA \tag{2.6}$$

Where A is the area of cross-section.

Note that, for polysilicon hot wire designed in this thesis, heat conduction between hot wire body and substrate, and to the surrounding is two main conduction process that has large effect on temperature distribution. Especially, heat conduction to air is the murder for high temperature in the middle of hot wire. It can be observed a huge decrease there with this heat conduction. Therefore, to avoid the effect from heat conduction to air, all hot wires designed in this chapter are assumed to work in vacuum environment.

2.2.2. Thermal convection

Heat convection is a process that carries heat away by a heated fluid. The adjacent region between the moving fluid and hot object forms the boundary layer where viscous effect is significant. Heat is conducted to this layer and fluid thereby being heated and rising while cooler fluid drops down which forms a cycle of heat convection. This behavior can be described by Newton's law:

$$q = h\Delta T \tag{2.7}$$

Where Δ is the temperature difference between the hot object and moving fluid. h , with the unit of W/m^2□K, called heat transfer coefficient that indicate the driving force for the flow of heat between them. In this case it denotes the local transfer coefficient at each point on the surface. when it is a forced convection which means the fluid is forced past the object and temperature difference between them is not too large, h is independent of temperature. While in natural convection it varies as $\Delta T^{1/3}$ or $\Delta T^{1/4}$ along the fluid direction.

In fact, both thermal conduction and convection occurs when the fluid passing by. Thus, Nusselt number is used to represent the ratio of them across boundary:

$$Nu = \frac{q_{conv}}{q_{cond}} = \frac{h\Delta T}{k\Delta T/L} = \frac{hL}{k} \tag{2.8}$$

When Nu=1, it means a pure thermal conduction.

Actually, heat convection which is characterized by heat flux in COMSOL has much less effect on temperature distribution which is even negligible (It will be proved later).

2.2.3. Radiation

IR can be obtained by a heated black-body emitting electromagnetic radiation. The intensity and peak wavelength of this radiant energy depends on temperature and nature of surface of hot wire. The monochromatic emissive power can be described by Planck's law:

$$E(\lambda,T) = \epsilon(\lambda,T)\frac{2\pi hc^2}{\lambda^5}\frac{1}{e^{\frac{hc}{\lambda kT}} - 1} \tag{2.9}$$

The unit of thermal emittance is W□sr^{-1}□m^{-3}, where h is Plank's constant, c is speed of light, λ is the wavelength emitted, k is Boltzmann constant and T is the absolute temperature of heated object, ϵ is emissivity of black-body.

It can be seen that it involves steradian which is the unit of solid angle. It is defined as a spherical segment with the area equal to the square of its radius r. Actually, the emissive power on the area that is at a radius r, angle θ from y axis and ϕ from x axis relative to radiation source depends on solid angle. But for simplicity, the solid angle is not considered in this thesis. Thus, the unit of emissive power is $\mathrm{W/m^2}$.

In practice, there is no perfect black-body which means there is always the case that the heated object emits less radiation. Emissivity ϵ is used on such an occasion to characterize the non-ideal part:

$$e_{non-ideal} = \epsilon e \tag{2.10}$$

Where $0<\epsilon<1$. Though emissivity is a function of temperature and wavelength, it is assumed to to be a constant number 0.96 for simplicity in this thesis.

To get the total radiant energy, it should be integrated over the whole spectrum:

$$e(T) = \int_0^\infty E(\lambda,T)d\lambda \tag{2.11}$$

As for the dependency of radiant energy on temperature despite of wavelength, it can be described by Stefan-Boltzmann law:

$$e(T) = \sigma T^4 \tag{2.12}$$

where σ is Stefan-Boltzmann constant having the value $5.67\times10^{-8}\mathrm{W/m^2}$□K^4, T is the absolute temperature.

The relation between the wavelength where the intensity of radiation is maximum and temperature can be given by Wien's displacement law:

$$\lambda_{max} = \frac{b}{T} \tag{2.13}$$

b is Wien's displacement constant which is 2897.77 μm□K, T is absolute temperature.

In addition to radiation intensity which describes the radiation leaves from surface, radiosity B with unit $\mathrm{W/m^2}$ is defined as the total flux of radiative that away from surface. If H is defined as irradiance which is the flux of energy irradiates at surface per unit area, the radiaosity can be written as the sum of irradiated energy that reflects away from object and the radiation that it emits:

$$B = \rho H + \epsilon e \tag{2.14}$$

Therefore the net heat flux that object emits is

$$q_{net} = B - H = B - \frac{B - \epsilon e}{\rho} \tag{2.15}$$

It has unit W/m^2. When H is 0, the surface does not reflect irradiance and radiosity is the radiant heat flux that the object emits [25].

In fact, for a heated IR source, radiant energy only takes a small portion of all thermal energy activity compared to heat conduction and convection. That is why the temperature has to be high enough to acquire an acceptable radiation intensity.

2.3. Analytical solution

To design a hot wire with desired temperature distribution, a simple mathematic model of hot wire is derived initially. As demonstrated in Figure 2.1, the ideal hot wire is characterized by a thin and long cylinder where the energy balance is maintained. Here is only one increment of hot wire shown in Figure 2.1.

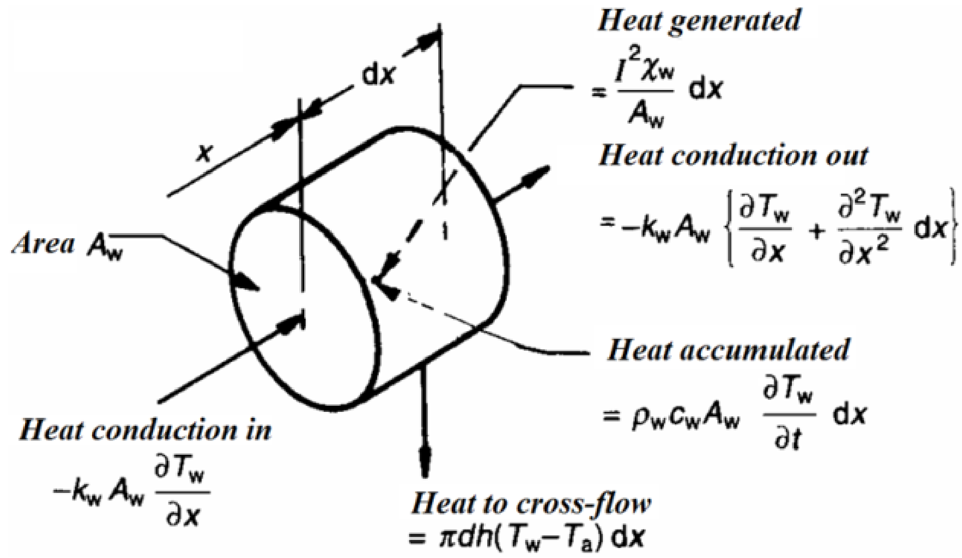

Figure 2.1: Heat balance in an incremental element of hot wire [26].

Most heat processes occurring in heated hot wire are presented in the figure except for the heat conduction to the surrounding air. I is the current passing through hot wire (assuming current source here) and χ_w is resistance of increment at local wire temperature T_w. A_w is the cross-sectional area and k_w is the thermal conductivity of the wire material. ρ_w is the density and c_w is the specific heat per unit mass. d is the diameter of wire and h is the heat-transfer coefficient contributing to heat convection between surface of hot wire and surroundings.

Under the condition of steady-state $\frac{\partial T_w}{\partial t} = 0$, it can be simplified to the equation 2.16 that can be performed to describe this energy balance in hot wire with the assumption that temperature is uniform over the cross-section [26].

$$k_w A_w \frac{d^2 T_w}{dx^2} + (\frac{I^2 \chi_w \alpha_0}{A_w} - \pi d h)(T_w - T_a) + (\frac{I^2 \chi_a}{A_w}) = 0 \tag{2.16}$$

Where, χ_a and χ_w are the values of the resistivity at ambient fluid temperature T_a and at reference temperature. α_0 is temperature coefficient of resistivity at the reference temperature.

2.4. Mechanical design of a Hot-wire

Thermal expansion is a phenomenon that matter will expand when heated and contract when cooled. It is due to the change of average molecular kinetic energy of material when

heated or cooled. It is limited by the size of matter and can only occur over certain range of temperature. Coefficient of thermal expansion (CTE) is the property of material that indicates the extents to which matter expands to because of thermal energy. It measures the fractional change in size for per unit change in temperature at a constant pressure. It has three types:volumetric, area and linear expansion. For the linear thermal expansion:

$$\frac{\Delta l}{l_0} = \alpha_l \Delta T \tag{2.17}$$

Where l_0 and Δl are the original length of matter and the change in length after heated and cooled. α_l is coefficient of linear thermal expansion with the unit 1/K. ΔT is the temperature difference.

For volumetric thermal expansion:

$$\frac{\Delta V}{V_0} = \alpha_V \Delta T \tag{2.18}$$

Where V_0 and ΔV are the original volume of matter and the change in volume after heated and cooled. α_v is coefficient of volumetric thermal expansion with the unit 1/K. Both equations ignore the effect of pressure.

Linear thermal expansion focuses on the change in one dimension such as length, which opposes to volumetric thermal expansion that measures the resultant change in volume of matter. In many material, CTE is anisotropic which means it depends on the crystallographic direction along which it is measured.

2.5. Polysilicon hot wire design approach

In this section, several hot wire of different geometry is designed to be used as IR source. The design method and its working mechanism are specifically presented with corresponding simulation results. Finally, all finished desirable designs are listed. Note that, as mentioned before, all hot wire are assumed to operatre in vacuum environment to avoid the large effect of heat conduction to surrounding air.

2.5.1. The initial design of hot wire

A cylindrical hot wire is indeed easy to theoretically analyze in model. However, according to 2.2, a rectangle hot wire has both width and thickness that can be taken advantage of, compared with the only diameter in cylindrical. Hence, the hot wire is initially designed to be a long thin micro-strip. Two types of hot wire are thereby designed, one with two small beams such as two rectangles at ends in Figure 2.2 while the other one has not any beams just a rectangle hot wire body.

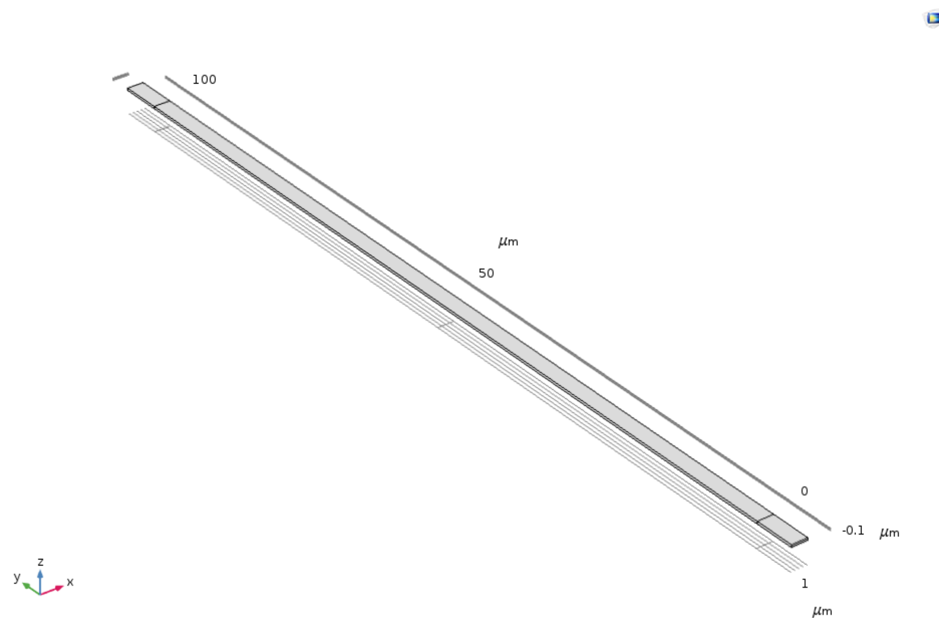

Figure 2.2: The initial design of hot wire.

Firstly, the comparison between with and without beams is made. For the one with beam, the end face of two beams is set to mechanically fixed which means it is connected to substrate. The temperature is constant 25 °C on this side, because the substrate has relatively huge area maintaining room temperature and polysilicon is a material that good at heat diffusion. While the other one without beam has no boundary conditions at end face of hot wire body, thus it neither has constant temperature nor be mechanically fixed, i.e. the hot wire is thermally isolated from the substrate.

By the result of comparison in Figure 2.3, the one with beam has not only a large decrease in temperature, it also tends to be slightly curving. The reason decrease is due to strong heat conduction from hot wire body to substrate, which is through beams. And the non-balance between small heat generation on the bridge and heat conduction to substrate causes the slight curve in temperature profile. Generally, it shows that the heat conduction to substrate has strong effect on temperature. A current drive which is 0.1mA is applied on these two sides of beams in both cases.

It can be manifested later that thermal generation and conduction are two dominant heat processes in the hot wire. Therefore, thermal generation at two ends has to be larger than in middle in order to compensate for the heat consumption of conduction due to two beams connecting to substrate. It is also the main important problem that trying to be solved for hot wire in this thesis. Several methods including many different geometry of hot wire and change of resistivity with different electrical source are applied based on equations listed above. Figure 2.4 is a overview of comparison of these methods in temperature profile. By changing factors as list, temperature on hot wire has changeable magnitude and distribution. Each line represents the change in one parameter by a factor of 10 while the rest is kept same. It can be seen that change of geometry is a more effective way for adjustment of temperature than that of resistivity.

Another important selection is the electrical source. Theoretically, for voltage drive there is a gradient from one end to another, while in terms of current source it can achieve same electric field anywhere on the hot wire when the resistance is same. However, the simulation result in Figure 2.5 shows that there is not much difference on electrical field between them. For the section of verification of design method, current source is used.

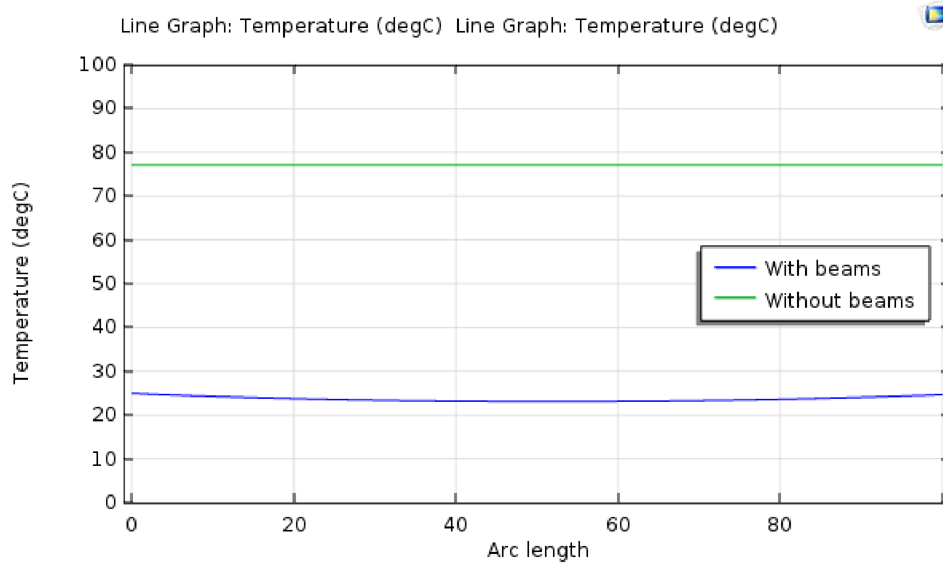

Figure 2.3: Comparison between with and without two beams. Arc length means the coordinate in y direction.

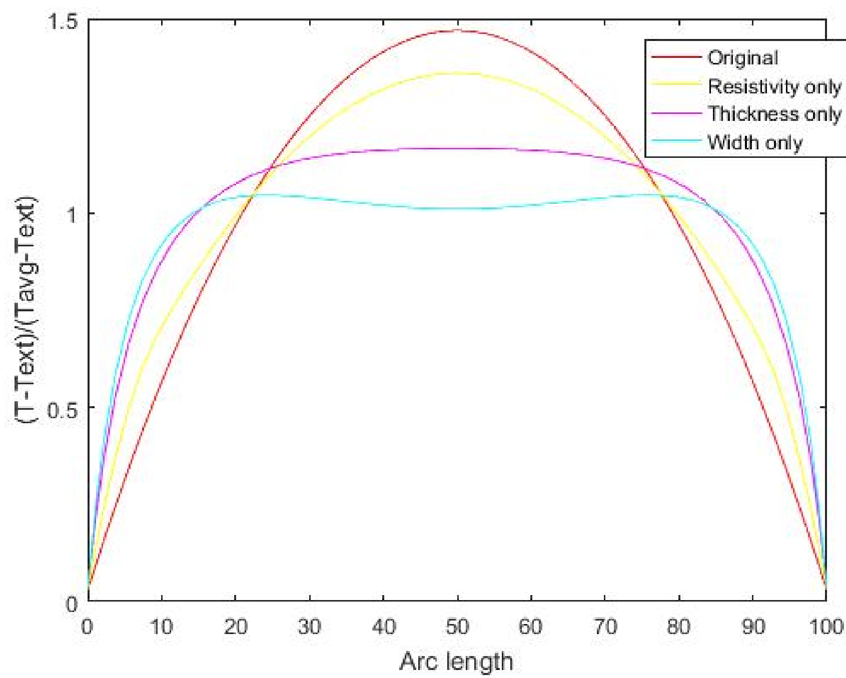

Figure 2.4: Comparison between all methods. x axis represents the normalization of temperature.

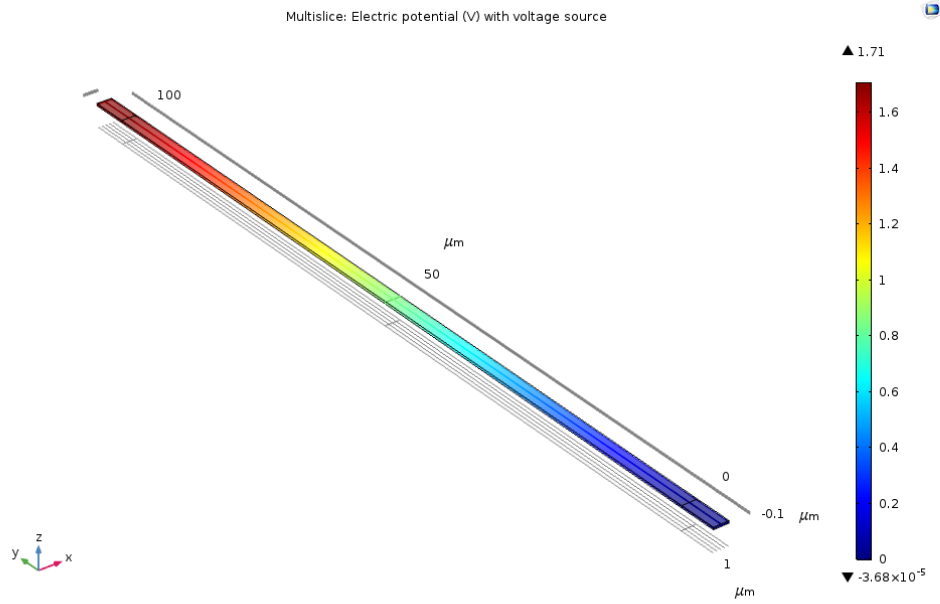

Figure 2.5: a. Electrical field with voltage source.

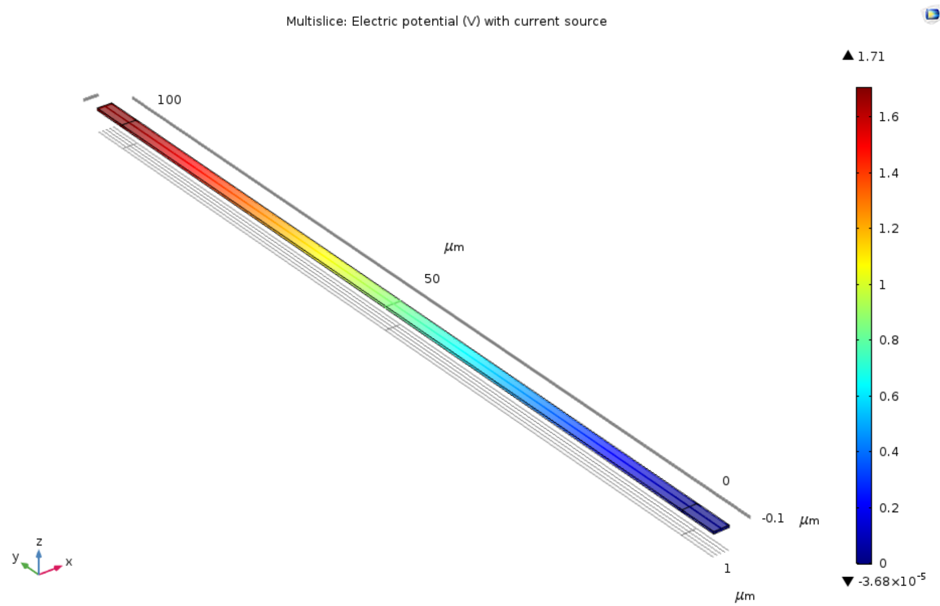

b. Electrical field with current source.

2.5.2. Geometry design

In this section, only the effect of change of geometry on hot wire is studied thereby the resistivity remaining constant 0.0031 Ω□cm which can be achieved by adjustment of doping level. The corresponding TCR is 0 according to the figure of TCR versus doping level in highly Boron-doped polysilicon [27]. The working environment is still vacuum.

Length of hot wire

The length of hot wire is the first parameter being studied. Two values, 100µm and 1000µm are simulated with 2.2mA and 22mA current source supplied separately. The result is in Figure 2.6.

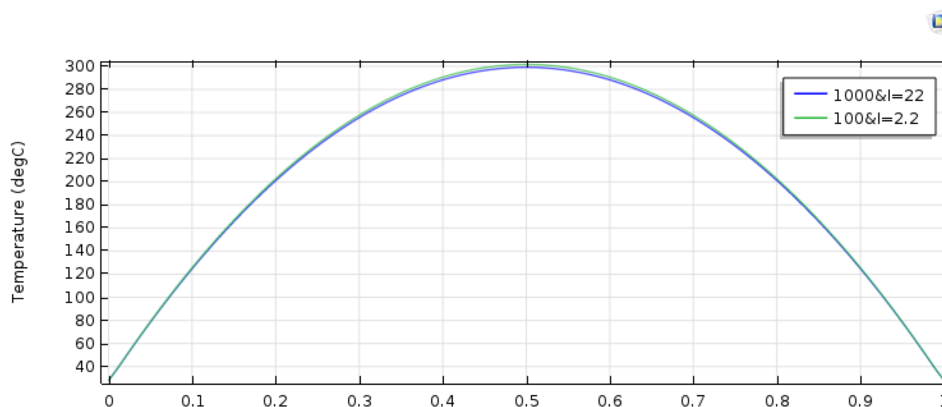

Figure 2.6: The effect of length. The x axis shows the normalized position on the wire.

It can be seen from the figure that an extended hot wire does not help to the uniformity of temperature distribution, it is even worse that more current is needed for same temperature. Although the resistance and heat produced should increase with a larger length according to 2.2, the area for thermal convection with surrounding air increases as well. More current is required to compensate for larger heat loss. In the section of verification of design method of hot wire, 100µm is used.

Thickness

The thermal conduction between hot wire and substrate via short beams is the main cause to non-uniformity of temperature profile on hot wire. From 2.2, a smaller area of interface between them will result in higher resistance thereby stronger heat generation and much weaker thermal conduction in accordance with 2.4 and 2.6. The strong suppression of heat loss will bring a better uniformity and the increasing portion in heat generation can also largely compensate for the lost. Therefore, if hot wire is thicker in the middle, the interface to substrate is relatively smaller on comparison. The geometry in Figure 2.7 can satisfy the requirement, and the simulation results are in Figure 2.8.

It can be seen that the change in thickness is linear. In Figure 2.8, it is clear that with thinner ends or a thicker center, the temperature distribution is more uniform by a increasing temperature at the part close to ends. It demonstrates that thermal conduction is indeed weaken and the change of thickness is an effective way. However, limited by the micromachining technology the gradient of thickness is hard to control.Thus, it is not easy to achieve the taper like hot wire in etching. Current drive here varies to get a same highest temperature.

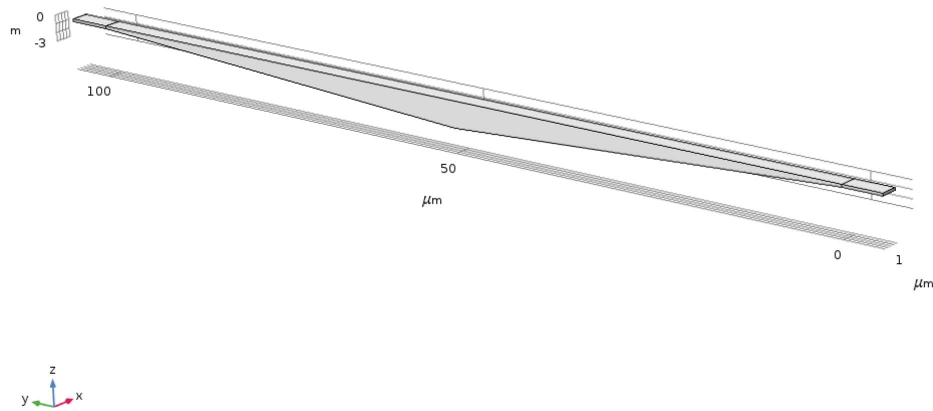

Figure 2.7: The hot wire with thicker center than ends.

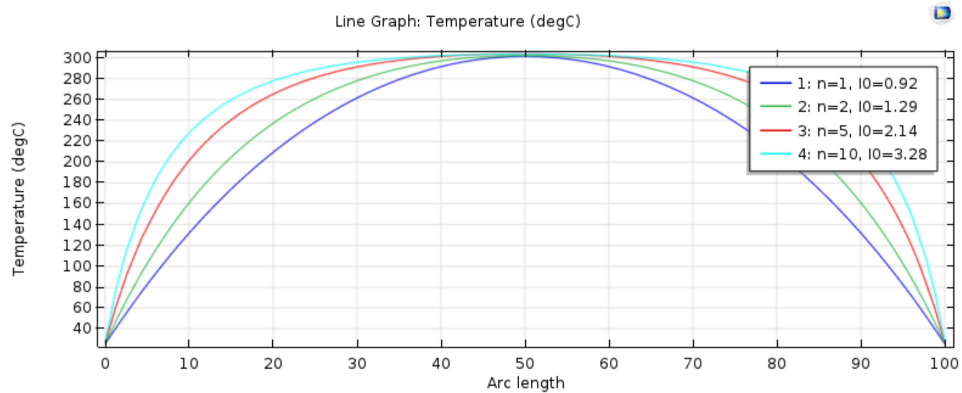

Figure 2.8: The effect of thickness. n is the ratio of thickness at center and ends. It means the thickness at center is 0.9, 1.8, 4.5, 9μm respectively while that at ends is 0.9μm. I0 is in mA.

Width

Similar to what is done with thickness, narrower ends or a wider center on hot wire can reach the same smaller interface to substrate and higher resistance.

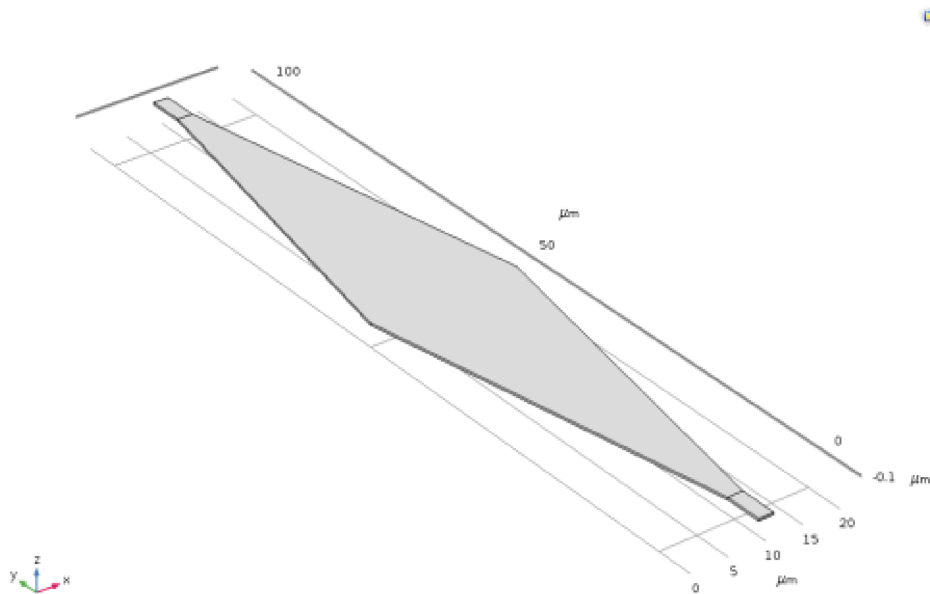

Figure 2.9: The wire with wider center than ends.

Similarly, the change in width is linear as well. In Figure 2.10, temperature becomes more uniform with a wider center thereby narrower ends on hot wire based on same mechanism. Compared with the linear thickness, playing with geometry within a plane is much easier in fabrication processing as it is simply a matter of mask. Nevertheless, a rhombus upper side of hot wire can not generate same emissive power anywhere on the surface. It can not meet the requirement of uniform IR light source. Current drive varies to get a same highest temperature.

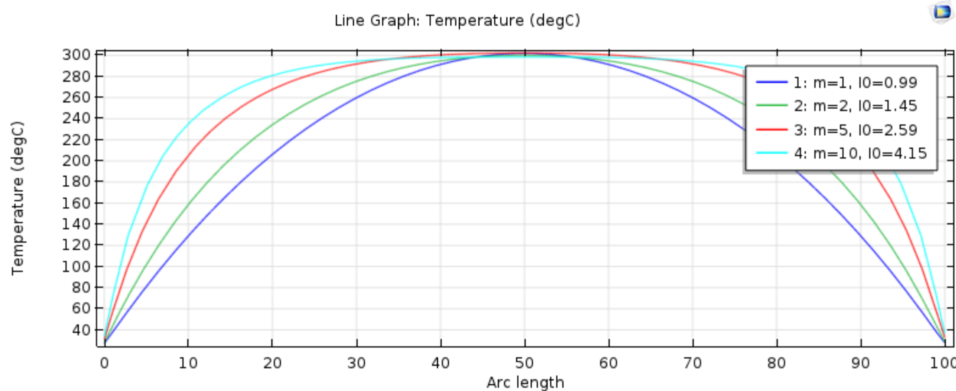

Figure 2.10: The effect of width. m is the ratio of width at center and ends. It means the width at center is 5, 10, 15, 20μm respectively while that at ends is 5μm. I0 is in mA.

Combination of thickness and width

Since the change of either thickness and width works well, the combination of two methods can also be useful way.

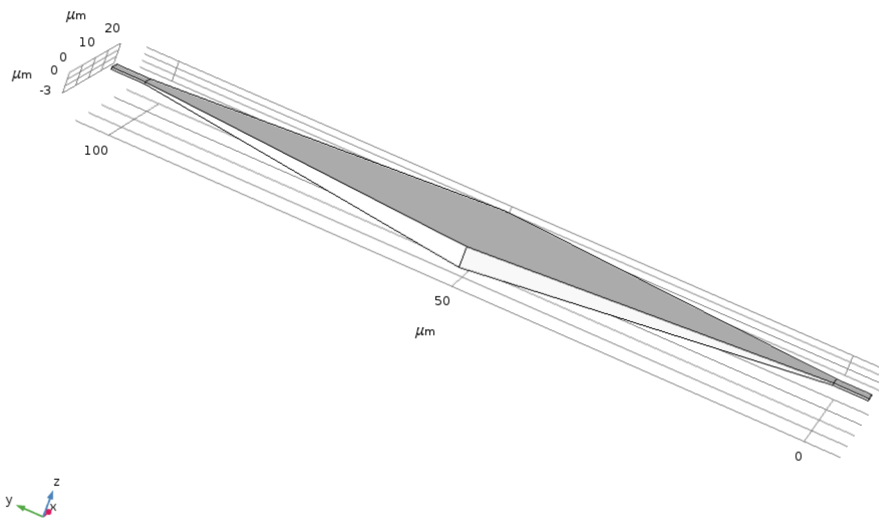

Figure 2.11: The combination of the change of thickness and width. The upper side is rhombus and flat while the lower side is linearly slanted from the center to the end due to the change of thickness.

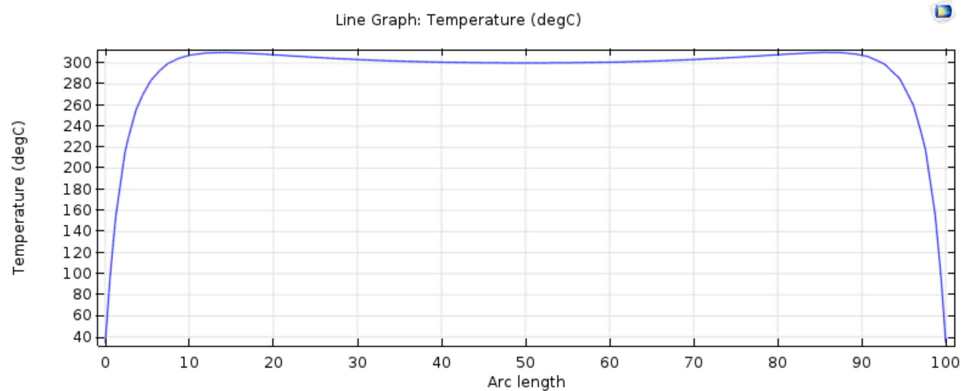

Figure 2.12: The temperature profile with the combination of change of thickness and width. At the ends, the thickness and width are 0.9 and 5µm respectively, while they are 9 and 50µm respectively at the center. The current drive 3.85mA.

In contrast with 2 previous results, the uniformity on temperature has an expected significant improvement. A relative constant value of 300°C with an error of 10 °C is maintained from 10µm to 90µm on the wire, which is a direct provident of the strong influence of change of geometry on temperature distribution. But it still can be seen two small bumps at ends which is within 10°C , either slightly changing thickness or width can improve it.

The reason for these two bumps in Figure 2.13 is that local heat generation at two ends overcomes thermal conduction to substrate. The solution is to strengthen thermal conduction here then trade off redundant heat generation. Increasing the area of interface to substrate, for instant increasing thickness and width at ends can work as well which is shown in Figure 2.13. By a slight increase of thickness and width at ends, the uniformity of temperature distribution gets much better. Finally, a initial design of hot wire with a relatively uniform temperature distribution is determined. The thickness at end of hot wire h1=0.9µm and width w1=3µm, while they are 9 and 50µm respectively at the center. The temperature on hot wire generally remains 300°C with an error of 2°C in the range of 20µm to 80µm on the hot wire.

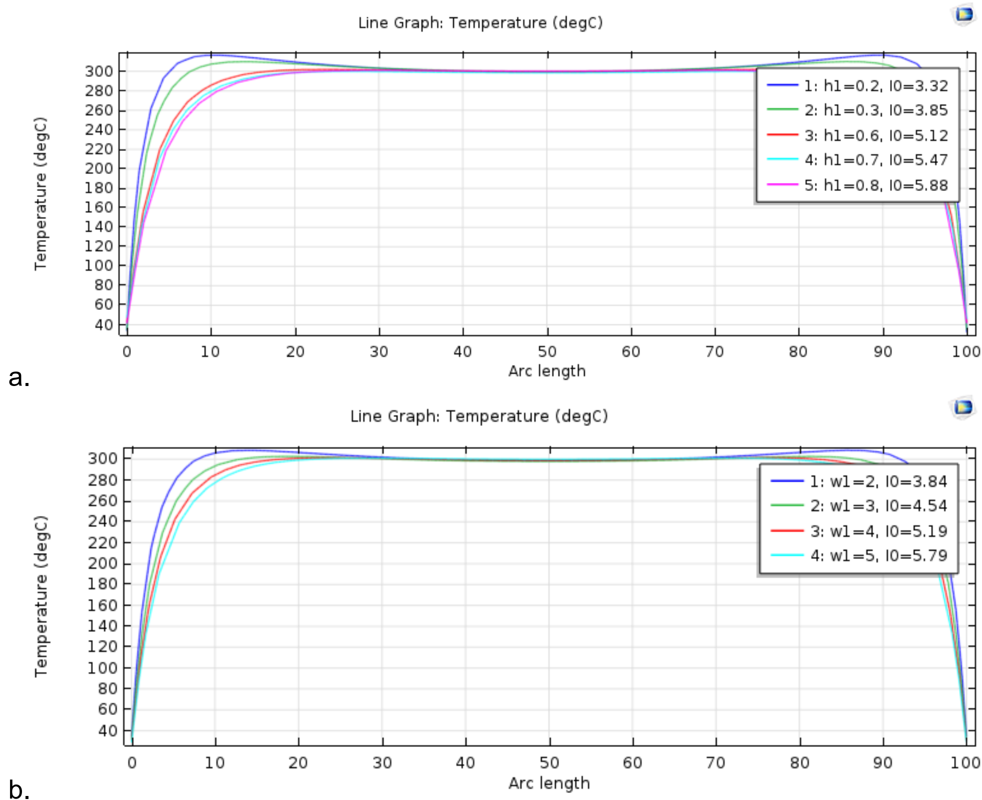

Figure 2.13: Changing thickness and width at the ends to remove small bumps close to ends. a. changing thickness. h1 is the thickness of the ends of hot wire while that at center remains 9 µm. b. w1 is the width of the ends of wire while that at center remains 50µm. The unit for both is um and I0 is in mA.

Natural convection

So far, the hot wire is assumed to operate in the air which is achieved by no heat conduction to air. In reality, perfect vacuum does not exist which mean there is always some air flow surrounding hot wire. Though it is not strong enough to exert heat conduction on the hot wire, heat convection can still take effect. However, heat convection is so weak that can induce much less influence.

In COMSOL simulation, heat convection can be characterized by the boundary conduction of heat flux with external natural convection and internal natural convection. The first one, which is applied in all previous simulation, means that heat flux between the object and air flows goes freely from hot to cold without any forcing drive. However, to achieve the vacuum environment, the hot wire has to work in an enclosing vacuum chamber. In this case, internal natural convection boundary condition should be applied. The comparison between external and internal heat convection is shown in Figure 2.14.

For internal natural convection condition, the hot wire in simulation is assumed to be put in a chimney composed of two parallel plates with 100µm long and a distance of 10µm between each other. As a result, thermal convection between surface of hot wire and surroundings is further weakened and the current that needed to reach same maximum temperature is smaller. However, the uniformity of temperature is influenced as well. That is probably also due to a decreased current drive so that the thermal conduction between hot wire body and substrate (not heat conduction to air) surpasses the heat generation at two ends of hot wire. The solution for this problem is as same as before, to adjust the area of interface to substrate by changing width and thickness at ends. In fact, it is a really efficient and powerful way to acquire a desired temperature profile. Finally, the thickness at end of hot wire h1 is decided to be 0.9µm and width w1=2µm, while they are 9µm and 50µm respectively at the center.

Since the heat transfer coefficient h in thermal convection is related to air pressure. The relation between temperature on hot wire and air pressure around on the basis of heat con-

vection is studied further.

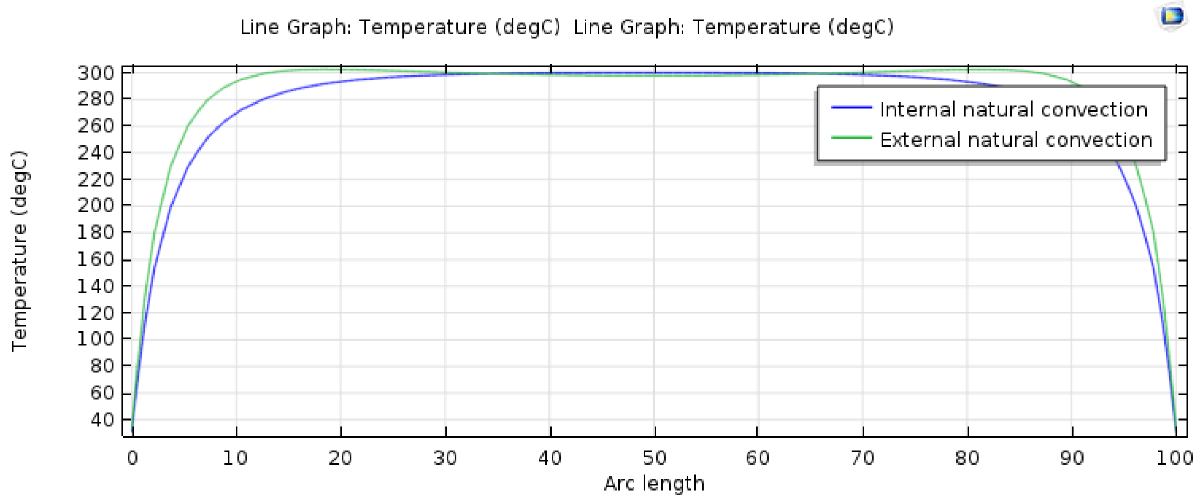

Figure 2.14: Comparison of internal and external natural convection. The current for internal natural convection is 3.6mA, and 4.54mA for external natural convection. Other geometric parameters are same.

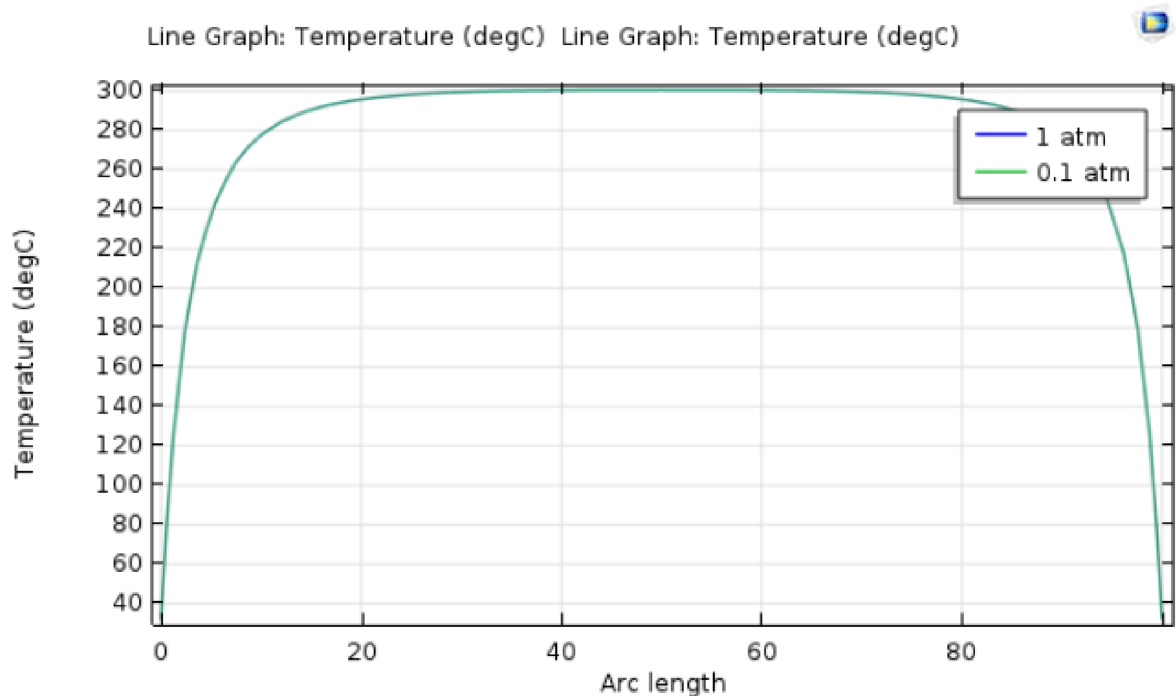

Figure 2.15: The comparison of air pressure

In Figure 2.15, two results with different air pressure are almost overlapped, which means there is barely difference in the temperature profile. Though air pressure might have some influence on the thermal convection which is characterized by thermal transfer coefficient h, the heat convection itself is so weak that can be negligible. In addition, thermal conduction between hot wire body and substrate is the strongest effect that determines the temperature distribution in this case. Therefore, air pressure has almost no influence on temperature on the basis of heat convection.

However, the influence of air pressure on thermal conduction from hot wire to surrounding air which is not considered yet is pretty huge. It is explained in chapter 5.

Radiation

Based on equation 2.12, the emissive power of each wavelength can be calculated easily. Figure 2.16 shows the spectral intensity at the central point on top surface of hot wire. It is obvious that with a larger current, the intensity of spectrum increases significantly. The peak wavelength shifts to shorter value in the meanwhile. It is consistent with equation 2.12 and higher temperature resulting from larger electrical source can produce stronger thermal radiation. In the range of current source given, the spectrum is within IR.

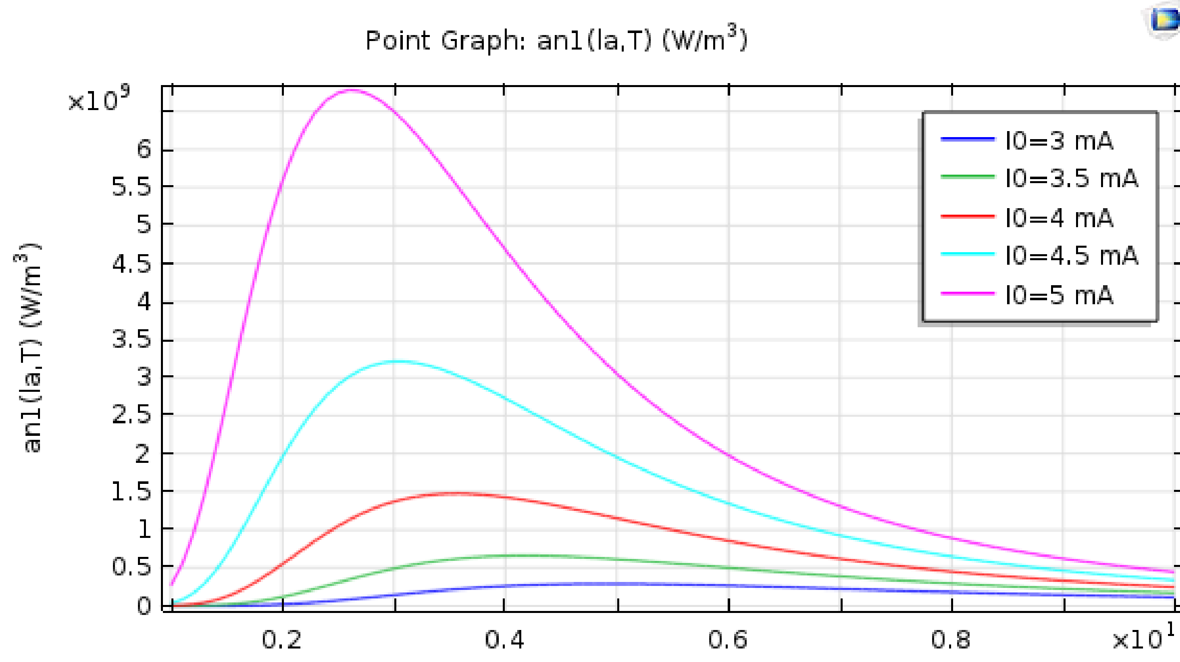

Figure 2.16: The spectral density at center point on top surface of hot wire. The unit of x axis is µm.

2.6. Resistivity of hot wire

Linearized resistivity

In the first case, a linear variation in resistivity is considered. In this case, the resistivity decreases linearly along the length of the hot wire and up to the center where it has the lowest resistivity as shown in Figure 2.17.

Resistivity at ends is 10 or 100 times than at center which can generate more heat with current supply as compensation. In addition, the effect of TCR has to be taken into account since the resistivity is no longer 0.0031 Ω□cm. Although the change of resistance due to TCR is 100 times smaller than to increase of resistivity according to calculation.

The result for the two different cases is shown in Figure 2.18. While the temperature profile for a 100x variation in resistivity is comparatively more uniform, the difference is quite small. The change of temperature is smaller than 5°C which means a linearized resistivity is too mild to make many impacts on heat generation and to manipulate temperature distribution.

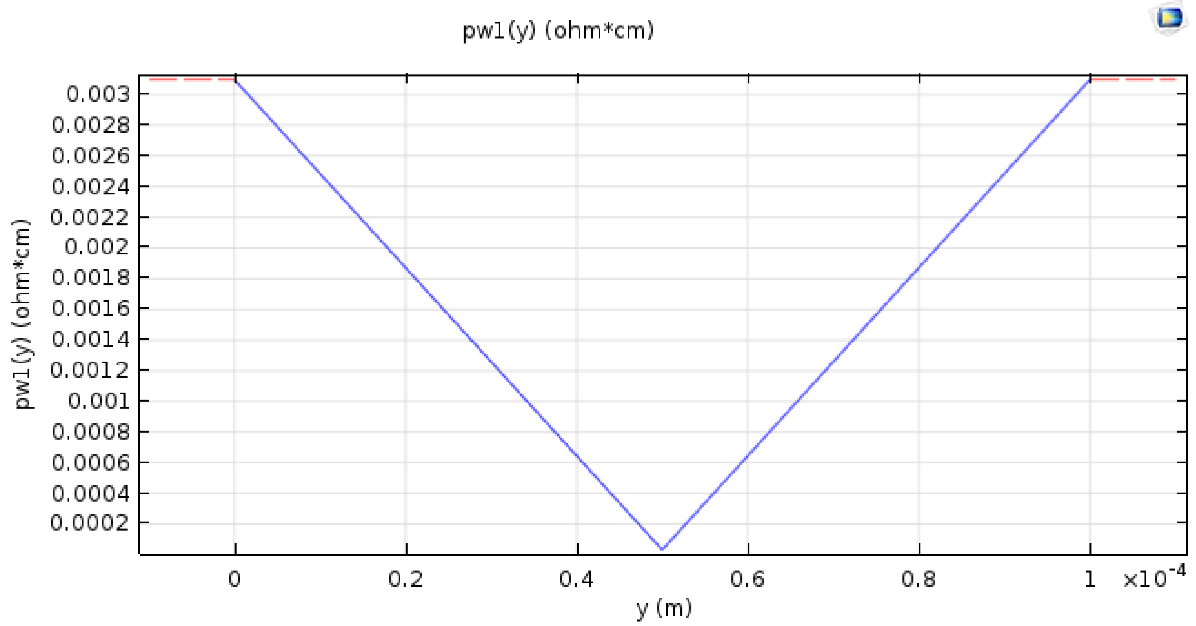

Figure 2.17: The resistivity of hot wire changes linearly.

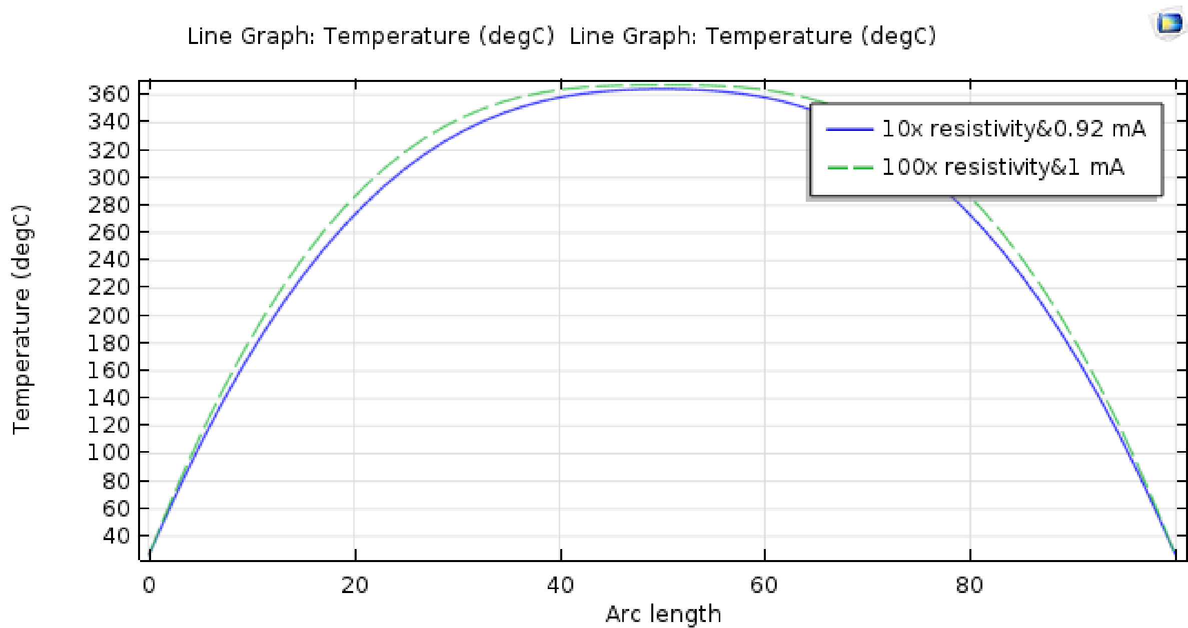

Figure 2.18: The result of linearized resistivity profile. It is 10 times and 100 times larger at ends than at center.

Piecewise resistivity

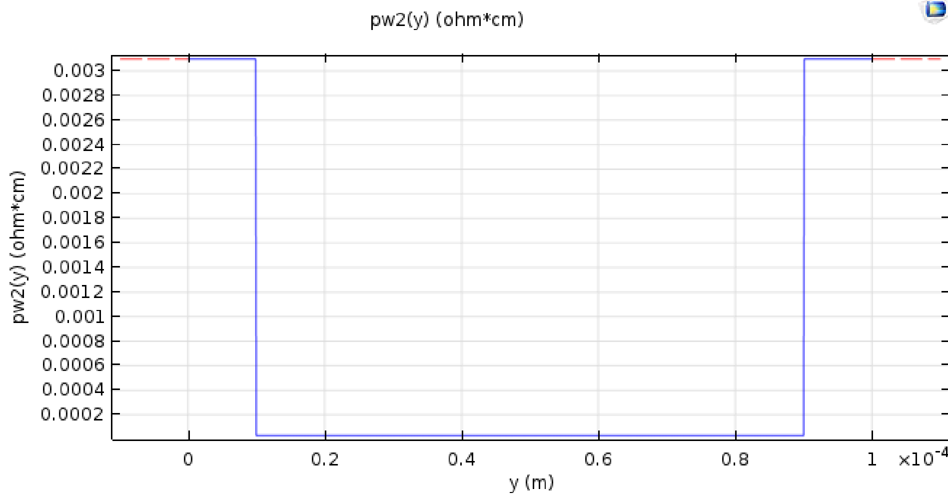

Figure 2.19: The resistivity of hot wire changes in piecewise.

In Figure 2.19, the resistivity profile on hot wire is separated into 3 segments. The two parts connecting beams at ends have same resistivity while it is 100 times larger than that in the middle part with similar reason in linearized resistivity.

It is shown in Figure 2.20 that the piecewise resistivity does help a lot to uniformity on temperature. There is a obvious turning point on temperature before it starts to significantly decrease. It indicates that heat is blocked in middle because of discontinuous resistivity on hot wire, which can contributed to uniformity on temperature. The next step is to further improve this effect, therefore the ratio of length of 3 segments is studied.

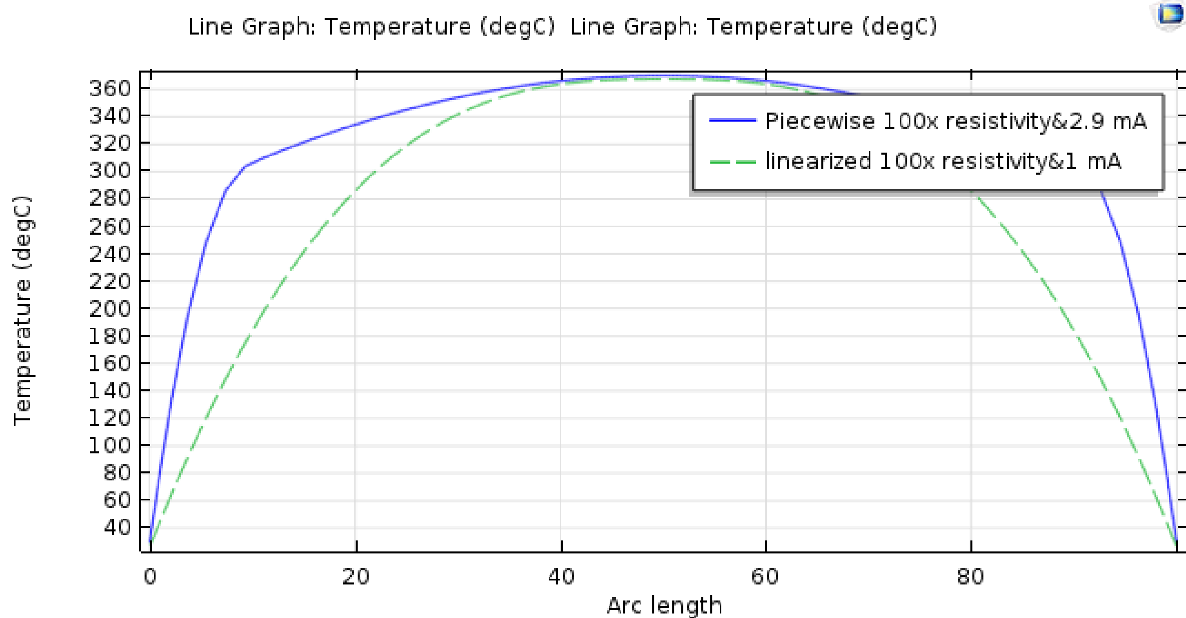

Figure 2.20: The comparison of linearized and piecewise resistivity.

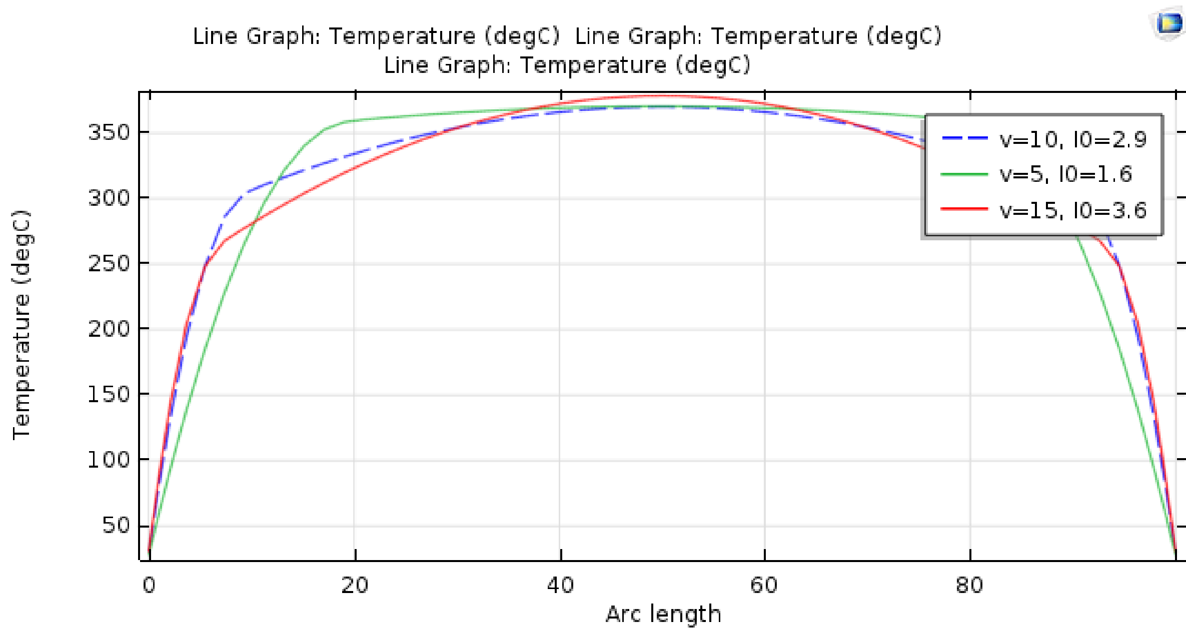

Figure 2.21: The comparison of different ratio of length of segments v. v=15 means both of two small segments at ends account for 1/15 of the hot wire while the middle part takes account for 13/15 of the wire. I0 is in mA.

To study the effect of the length of the high resistive part, the beam s divided into 'v' parts with the first and last parts having a 100x higher resistivity than the rest. The temperature profile for the v=5, 10 and 15 are shown in Figure 2.21. It shows that the smaller the segment of high resistivity is, the later the temperature starts to decrease. It is reasonable that two small segments with higher resistivity is used to resist thermal conduction, the dramatic decrease of temperature only occurs once heat flux gets into them. On the other hand, the smaller these two segments are, the more non-uniform the temperature is in the middle because of the weaken resist to thermal conduction.

2.7. Comparison of the change of geometry and resistivity

It can be included from previous results that change of resistivity does not have equally strong effect on temperature profile of hot wire as geometry does. The change of geometry manipulates heat transfer in hot wire directly by the control of thermal conduction which is a dominant factor. In contrast, resistivity is in charge of heat generation which is much weaker than thermal conduction in this order of dimension of hot wire. The result of comparison of two methods are shown in Figure 2.22. The change of resistivity is used to replace the effect of change of geometry including width and thickness of hot wire.

It is clear that the combination of change of thickness and width maintains a uniform temperature over 70µm on hot wire while it is around 30µm when one of it replaced by change of resistivity. Thus, the control of thermal conduction to substrate by adjustment of area of interface is a more efficient method. Therefore, the change of geometry is the major way for the uniform temperature profile on hot wire.

Nevertheless, it does not mean that change of resistivity is needless and useless. As mentioned before, either change of thickness or width only has its own disadvantages that not meet the requirement of a qualified IR light source. Therefore, the change of resistivity is used as back-up method.

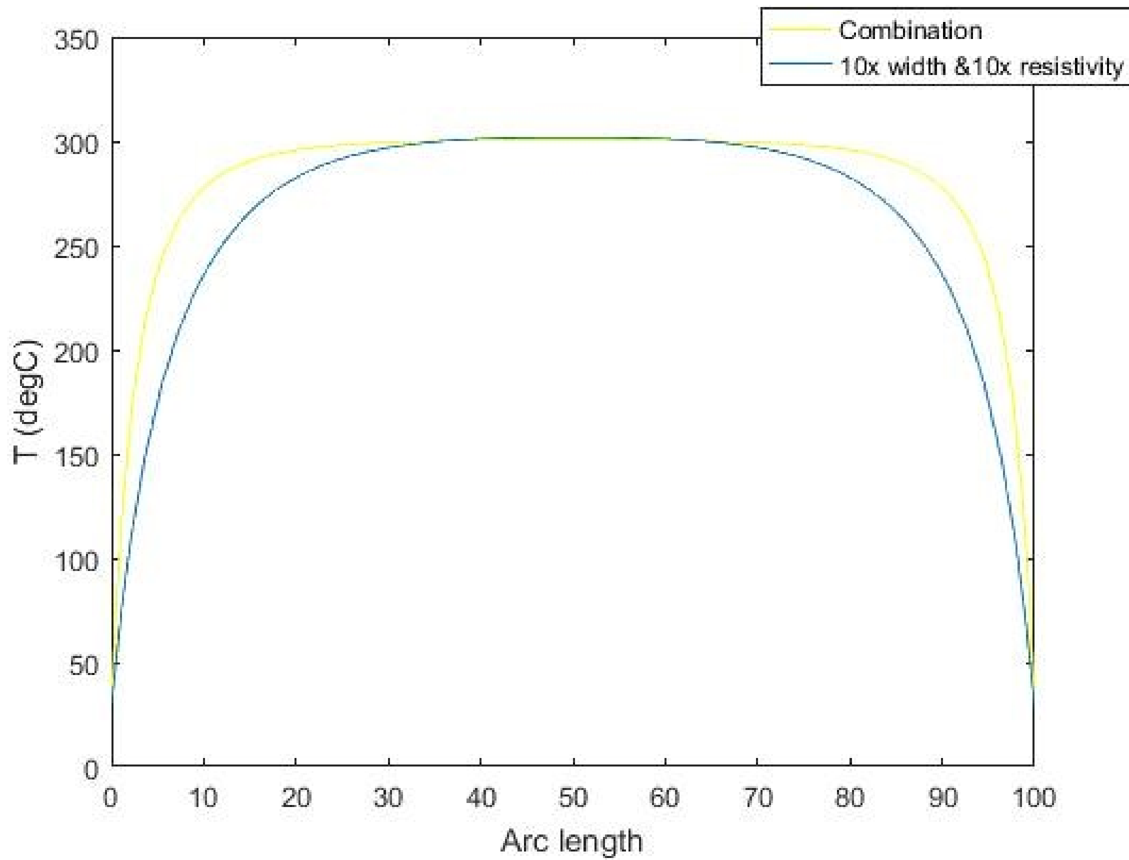

a.

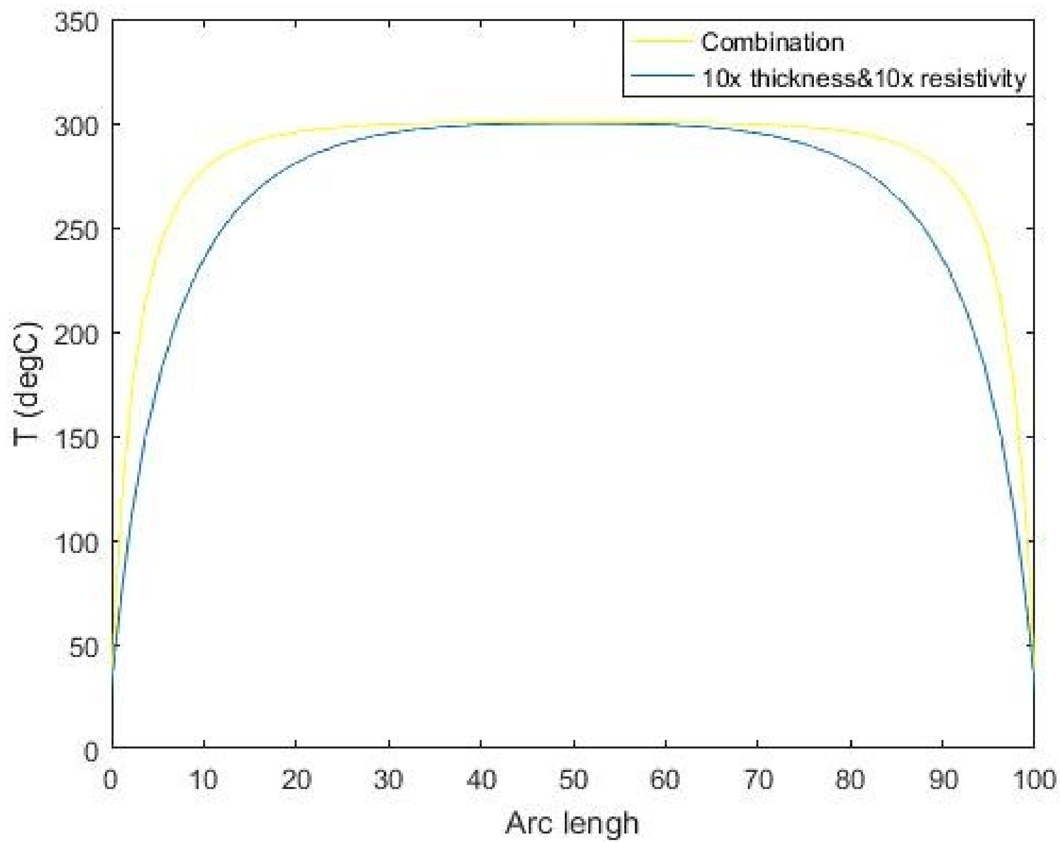

b.

Figure 2.22: The comparison of the change of geometry and resistivity. a. Changing Width and resistivity. The width at center is 10 times larger than that at the ends, while the resistivity at ends is 10 times larger than that at center. b. Changing thickness and resistivity. The thickness at center is 10 times larger than that at the ends, while the resistivity at ends is 10 times larger than that of center. Combination means the design that used change of both width and thickness of hot wire as shown in previous results.

2.8. The rectangle hot wire with smaller beams at ends

It is suggested that heat conduction to two beams is the major problem that needed to deal with. And the most effective way is to decrease the area of interface between hot wire and substrate. A new design of wire is in Figure 2.23. By two narrower beams at ends, the thermal conduction is strongly limited that a better temperature profile is acquired.

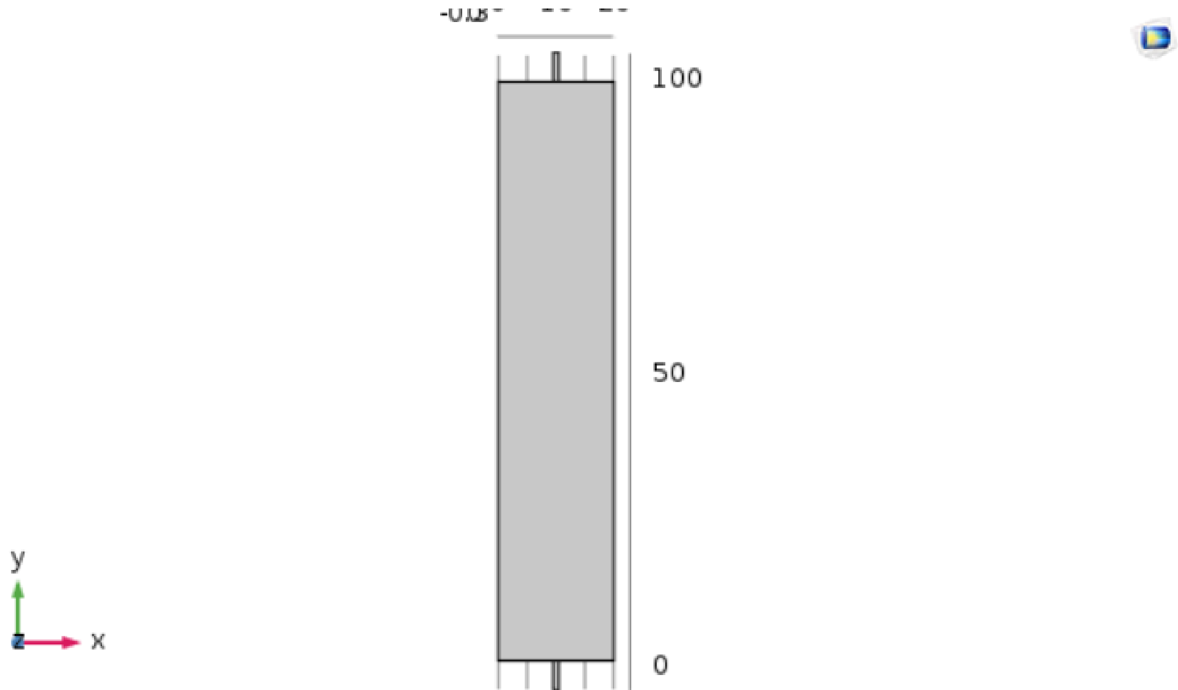

Figure 2.23: A desired shape of hot wire.

2.8.1. Design approach

Geometry

In this section, the effect of length and width of two beams at two ends in is simulated. For simplicity of fabrication, the thickness of two beams is 0.3μm, same as that of hot wire. For the wire, length is 100μm and width is 20μm.

Two beams at two ends are transition areas for heat flux from hot wire to substrate. If more heat generated in them, it can largely compensate the heat loss due to thermal conduction to substrate. Most importantly, the area of interface can be directly changed by the width of beams. Thus, the geometry and resistivity of two ends works on temperature distribution of hot wire as well.

From Figure 2.24 and 2.25, both increase of length which can produce more heat, and decrease of width which suppresses thermal conduction can lead to a more uniform temperature profile. It is in correspondence to the conclusion mentioned before. Therefore, thel_b of 5μm and w_b of 1 μm are selected.

It can be seen from the figure that 1μm increase in length of beams will cause about 15 °C increase on temperature at position of 10μm. If the uniformity is defined as the temperature difference between that at 10μm and center over the maximum temperature 1-(T_{max}-T_{10})/T_{max}, it is 86%, 93.7%, 99% respectively when l_b=1, 2, 5μm which is 100, 50, 20 times shorter than hot wire. And it is 99.3%, 94.3%, 83.3% respectively when w_b is 1, 2, 5μm which is 20, 10 and 4 times narrower than hot wire. Temperature uniformity increases by 13% with 5 times longer beams, while it increases by 16% with 5 times narrower beams. Still, design of geometry is a useful method for temperature manipulation.

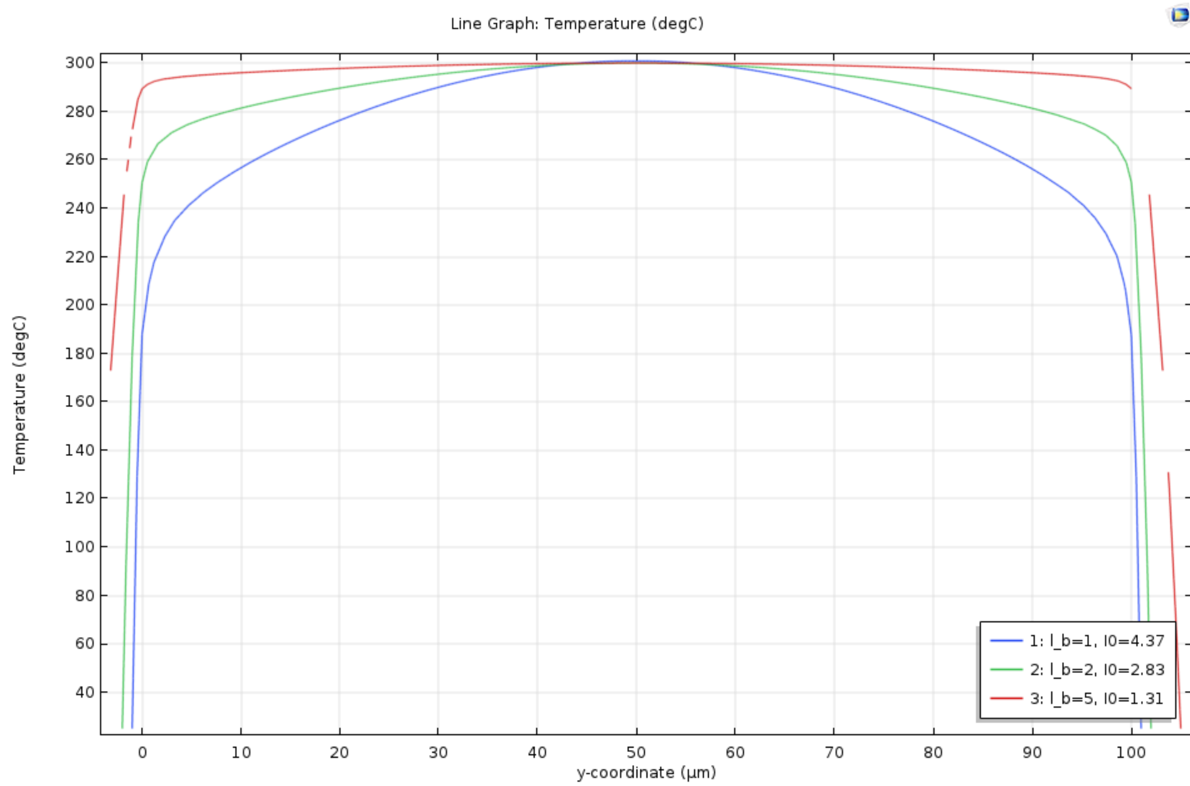

Figure 2.24: The effect of length l_b of beams.

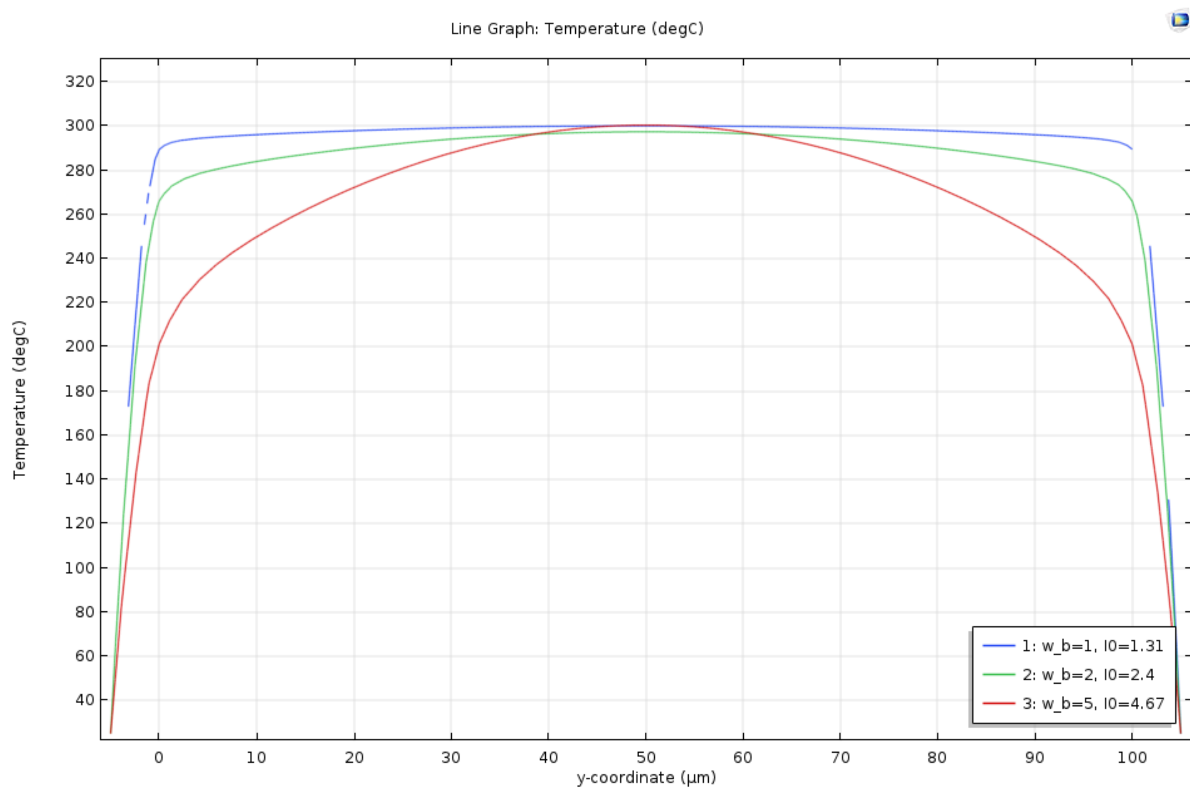

Figure 2.25: The effect of width w_b of beams.

Resistivity

In this section, the impact of resistivity of beams is studied. TCR is taken into account.

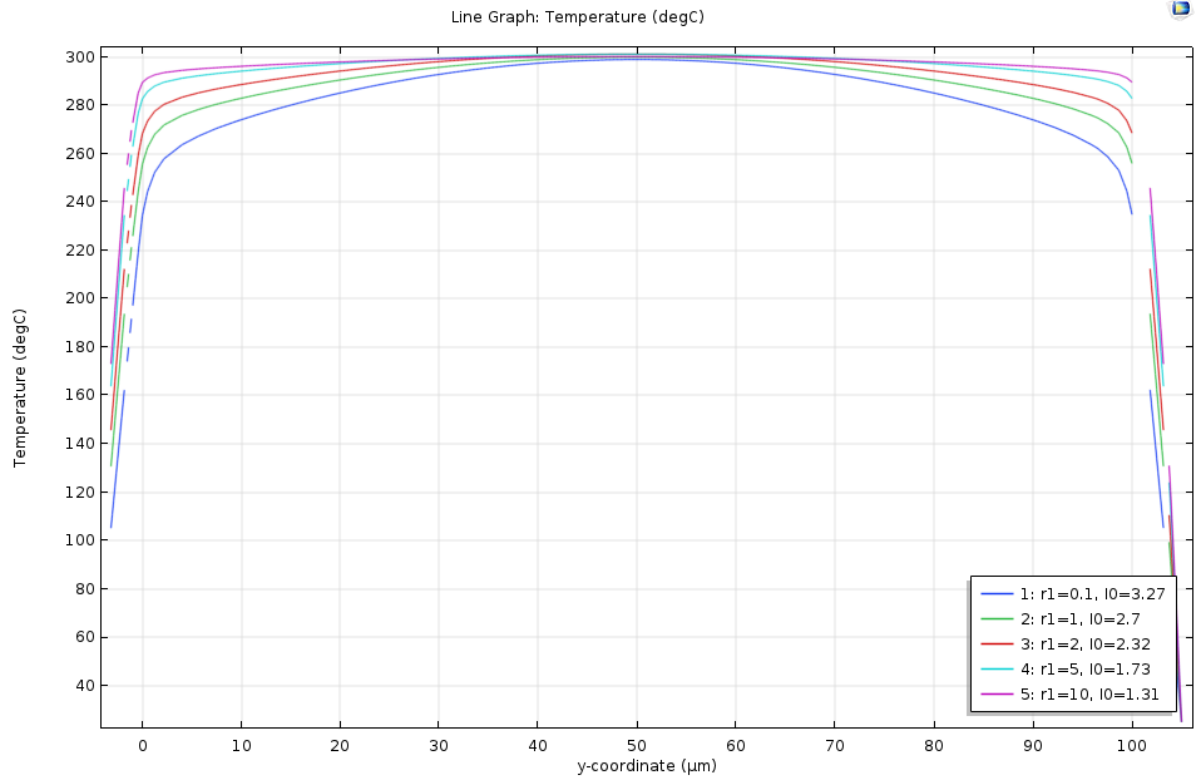

Figure 2.26: The effect of resistivity of beams. r1 is the ratio of resistivity of beams and hot wire. ρ of hot wire is 0.001 σ□cm, while that of beams is r1 times larger. I0 is in mA.

As resistivity of beams is different from hot wire, it just like the resistivity in piecewise studied above. Here the resistivity is considered to be r1 times of that of the hot wire body. It can be seen from figure 2.26 that a larger resistivity produces more thermal energy. The uniformity of temperature for r1=0.1, 1, 2, 5, 10 is 91.7%, 94%, 96%, 99% and 99.3% respectively. Since the doping level that the main way to change resistivity can not be as accurate as it is initially designed, an error range should be considered. With higher resistivity, the change in temperature uniformity due to uncertainty of resistivity becomes smaller. It is 2% when r1=1 and 2, and 0.3% when r1=5 and 10. Thus, the larger resistivity of beams the better for temperature. Moreover, it has to be in a reasonable range considering TCR which is unknown beyond the range. Therefore, r1=10 is selected.

All in all, the final design of 100µm is as listed,

Object	length[µm]	Width[µm]	Thickness[µm]	Resistivity[ω□cm]
Hot wire	100	20	0.3	0.001
Beams	5	1	0.3	0.01

Table 2.1: The final design of 100µm hot wire

2.8.2. Results of Final design

Temperature profile

Based on all simulation results before, the final structure of hot wire is determined. The geometry of hot wire is 100, 20 and 0.3µm for length, width and thickness respectively. While they are 5, 1 and 0.3 µm for two beams. So far, the highest temperature on the wire is 300 °C, it is not enough to emit IR in the interested range . Therefore, the current drive used is increased to 1.4mA to increase temperature. The final temperature distribution is in Figure

2.27, the highest temperature is nearly 350°C and the uniformity of temperature is about 98% which is a quite high value.

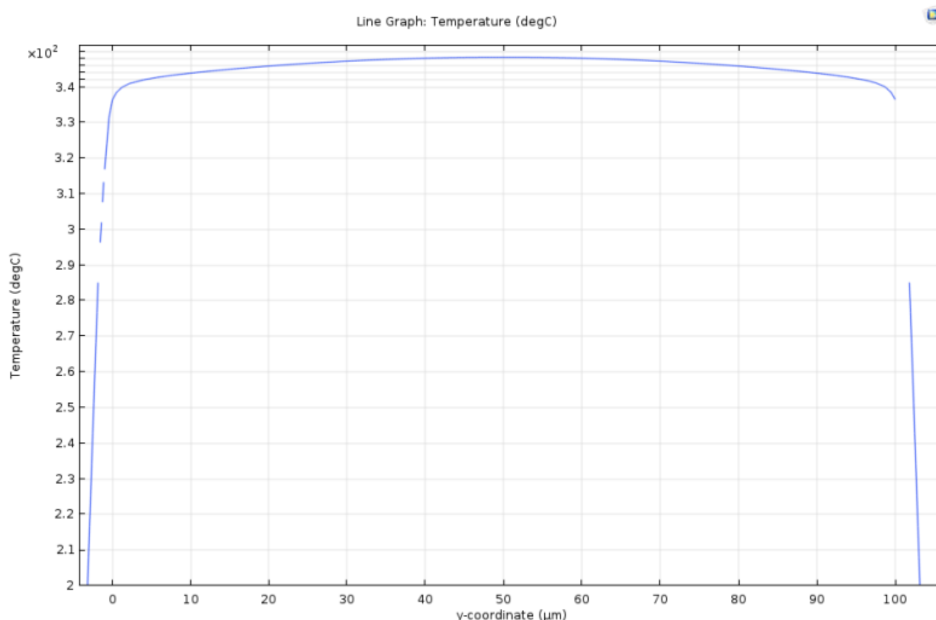

Figure 2.27: Temerature profile of final design

Radiation

Radiosity and net radiant heat flux is shown in Figure 2.28 and 2.29. Radiant heat flux is slightly smaller than radiosity which looks reaonable according to 2.14 and 2.15. Since the hot wire works in vacuum envirnment, there is no way for reflection of irradiation. But it is also assumed that small amount of air is still left, it might be the cause.

Along the middle line from center to two ends, there is generally 7.5% change of radiosity. Besides, there is almost no difference in the lateral direction since the hot wire is too narrow to have changes. The current drive is 1.4mA.

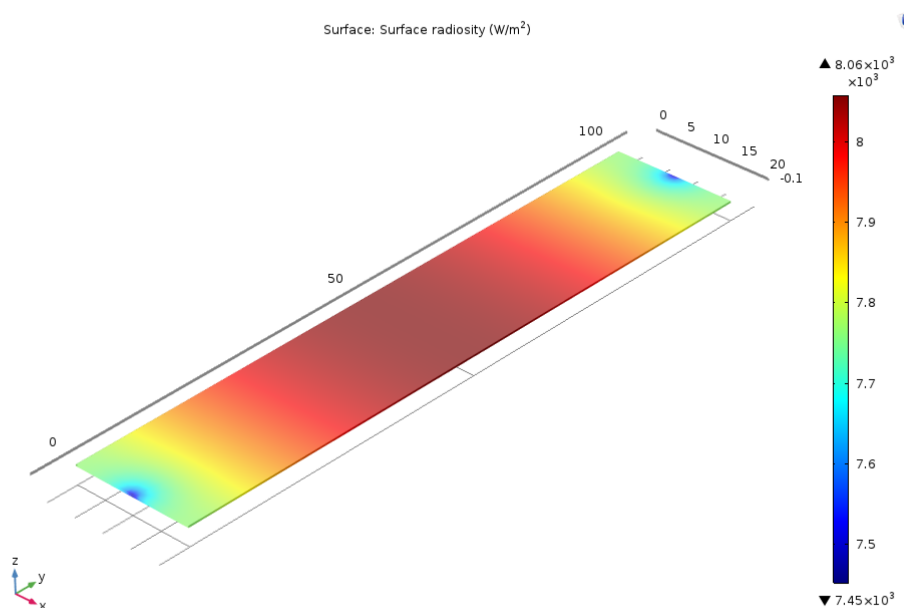

Figure 2.28: Surface radiosity

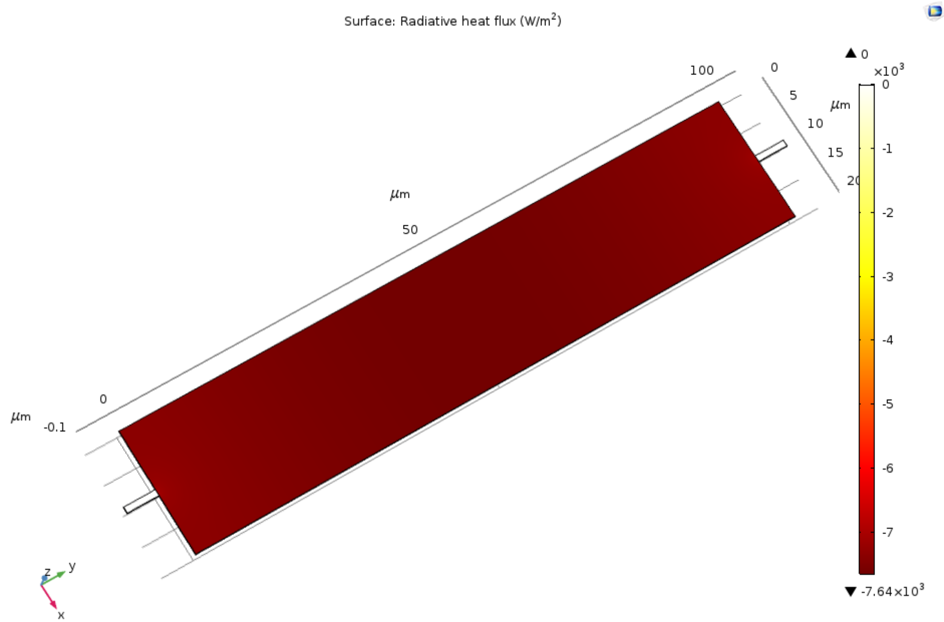

Figure 2.29: Radiative heat flux

Peak wavelength with highest emissive power is shown in Figure 2.30. From 10µm to 90µm on hot wire, the peak value is among 4.6-4.7µm with nearly 0.5µm deviation. However, the hot wire used as IR source is designed to be in 1.6-2.2µm. The temperature has to be further increased by probably a higher electrical source to shift the peak wavelength to shorter value.

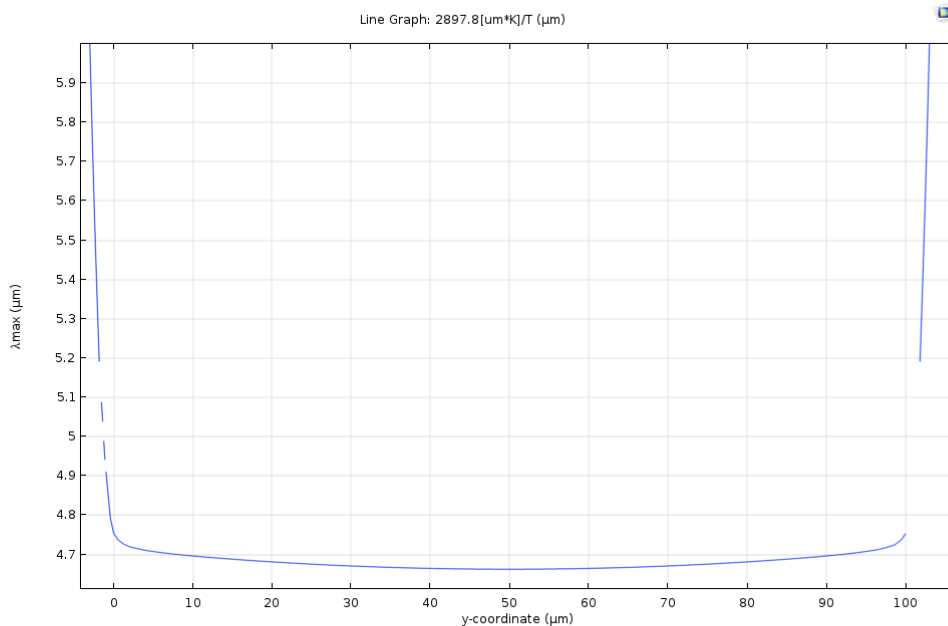

Figure 2.30: Peak wavelength

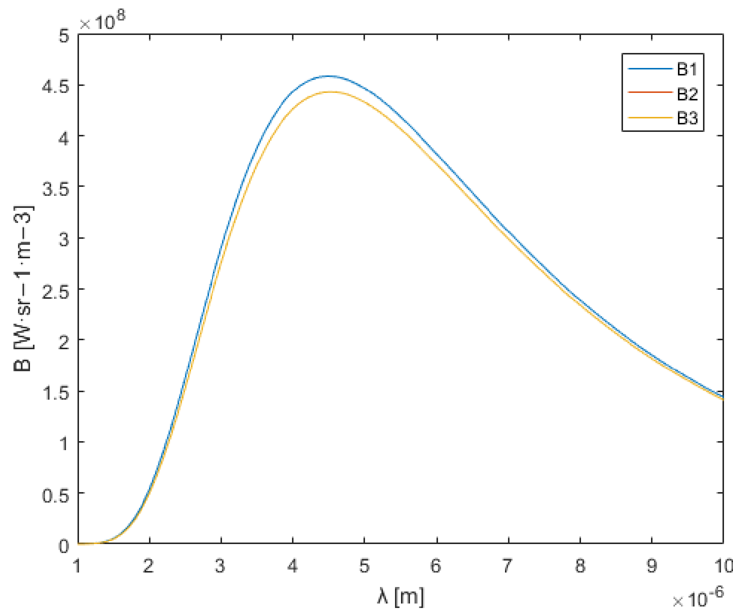

Figure 2.31: The spectral density at 3 different points on top surface of hot wire. B1 is at the position of 10µm, B2 is at 50µm which is the center point and B3 is at 90µm.

In order to observe the emissive power for each wavelength, 3 different points are selected. It can be seen that there is no much difference on profile of spectral density as well as magnitude, it almost overlaps for B2 and B3.Therefore, it is a quite uniform light source.

2.9. Hot wire design in longer length

some longer hot wires are designed including 0.5, 1, 2, 4 and 5mm to fit the resolution of IR camera. Same methods are used for them and the electrical drive applied in this section is voltage source.

2.9.1. 1mm hot wire design

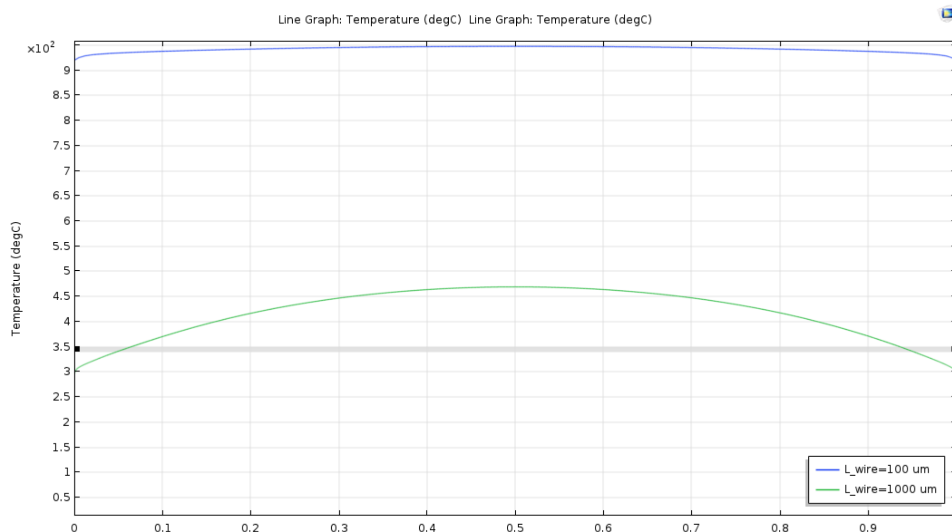

Figure 2.32: The comparison of 0.1 and 1mm hot wire with original setting. Y coordinate is normalized by dividing it by 1mm and 0.1mm respectively. Only hot wire part is shown.

From Figure 2.32, if the hot wire of 1mm long but with previous geometry and resistivity of 0.1mm, both temperature magnitude and distribution change a lot. Since voltage source is applied, it is a inverse case for current source according to 2.1. As it is 10 times longer now, resistance is 10 times larger as well. Thus, heat generation is much weaker than before. It can be seen that almost 500 °C decrease on temperature. Besides, thermal energy balance in hot wire is broken, temperature is no longer uniform. That is why 1mm hot wire has to be re-designed.

Another aspect needed to pay attention is that, as hot wire is 10 times long, the area of surface for thermal convection from hot wire to surroundings gets 10 times larger as well. It may strengthen the effect of thermal convection on temperature distribution. For 1mm hot wire, it is not so strong that the major factor is still thermal conduction. However, for longer hot wire such as 2, 4 and 5mm hot wire, it should be treated more carefully.

The design for two beams

As the geometry of two small beams have a huge influence on temperature of hot wire, the width of beams determines directly the area of interface to substrate for instance, the design method used in this section is mainly on two beams which means width and thickness of hot wire is still 200 and 0.3µm respectively. Besides, the effect of change of resistivity is manifested much weaker than that of geometry. Thus, resistivity is 0.01Ω□cm for beams and 0.001Ω□for hot wire, same as before for simplicity.

In order to generate more thermal energy in beams and restore the energy balance, beams has be shorten to reduce resistance with the voltage source applied. Figure 2.33 demonstrated that temperature does increase much when beams become shorter.

For width of beams, it is a little complicated. Two thermal processes which oppose to each other are both improved when width increases. Resistance will decrease which means stronger heat generation and higher temperature, while the path for heat loss to substrate due to thermal conduction is larger as well which means lower temperature. The trend of change of temperature depends on which one is stronger. In Figure 2.34, it shows that temperature increases when width increases. It indicates heat generation overcomes thermal conduction in beams and a small change in width can induce large change on temperature, which also demonstrates the design for only beams is an efficient way. Therefore, two straight beams are 20µm for length and 1.2µm for thickness.

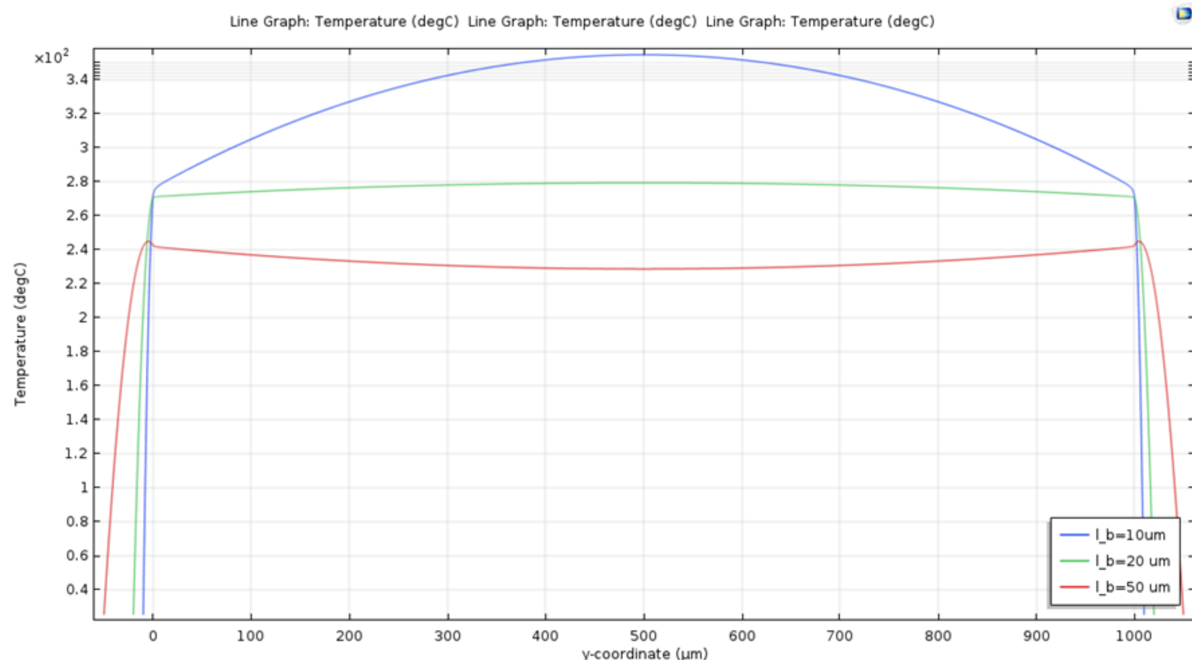

Figure 2.33: The effect of length of beams. Voltage is 6V.

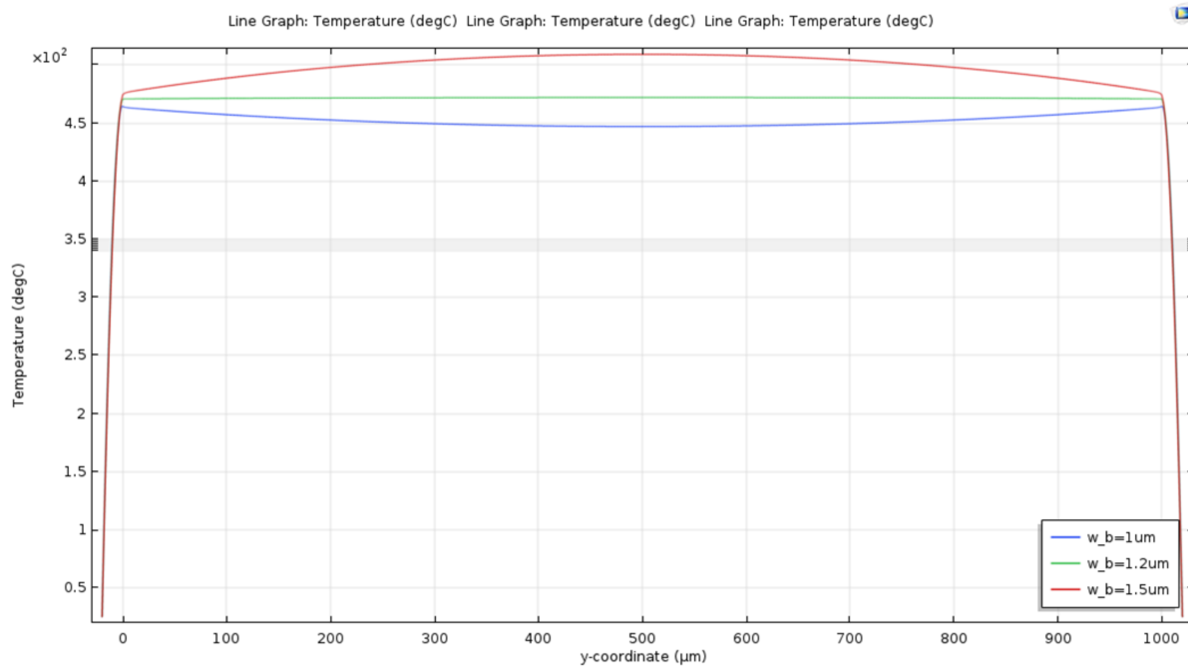

Figure 2.34: The effect of width of beams. Voltage is 9V.

The first design of 1mm hot wire has a big problem that the fabrication resolution is 1µm, it is hard to make a beam changing by 0.1µm in width. Therefore, the width of beams has to an integral number, 2 and 3µm for instance. Thus, two more design of 1mm hot wire is made.

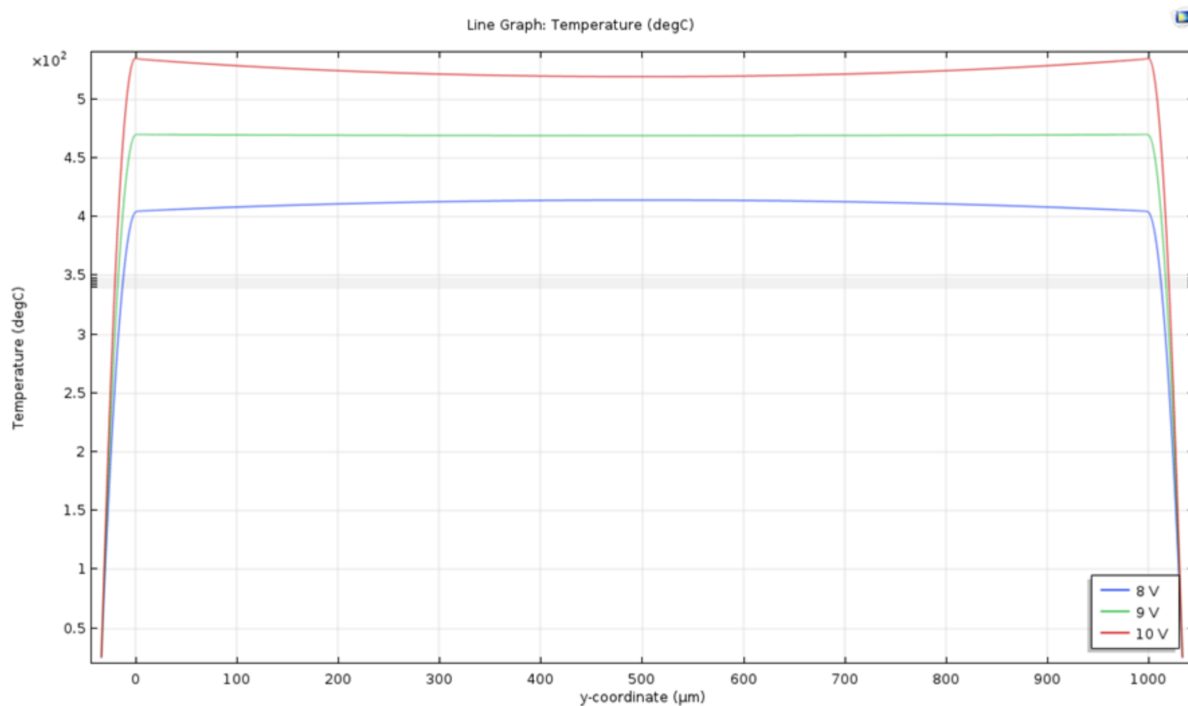

Figure 2.35: The second design for 1mm hot wire

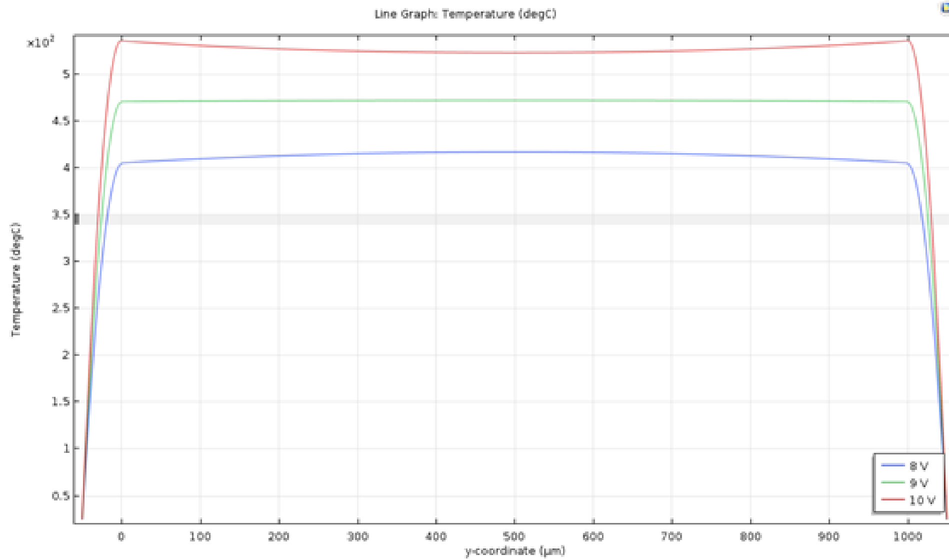

Figure 2.36: The third design for 1mm hot wire

For the second one, beams are 34μm in length and 2μm in width. The maximum temperature on hot wire is 470 °C which is within the tolerable range of polysilicon, and 1°C difference from center to two ends. For the third one, they are 50μm in length and 3μm in width. Temperature is 470 °C and deviation is 2 °C.

It can be seen that, the change of electrical source not only works on the magnitude of temperature but also temperature distribution. Thus, it has to find the most suitable value of electrical source combining with other variables to give a uniform temperature profile within maximum limit.

Figure 2.37 and 2.38 shows the radiation of the second design for hot wire. The peak wavelength is around 4μmand not change much along the surface. The maximum spectral intensity is approximately 9×10^{8}W/m^{3}, it can be increased by a larger voltage supply, here it is 9V.

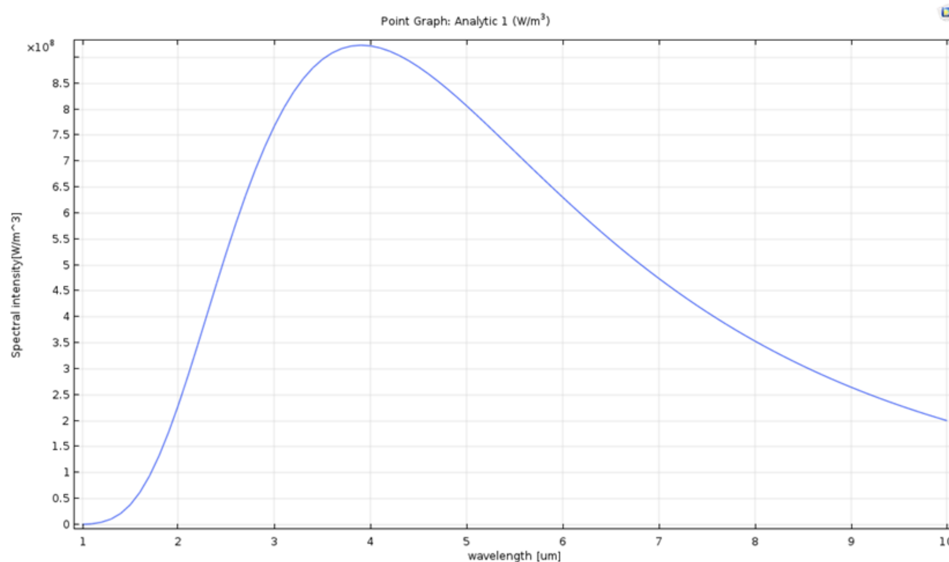

Figure 2.37: Spectral radiation intensity at central point

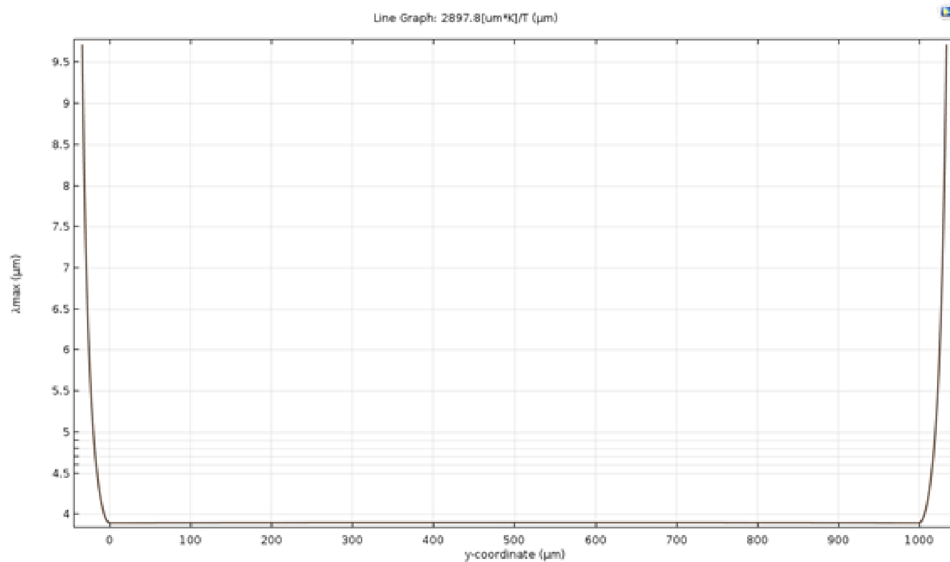

Figure 2.38: Peak wavelength along the middle line on the top surface of hot wire

2.9.2. Meander beams at ends

According to 2.17 and 2.18, the hot wire will undergo thermal expansion when heated by electrical source. It expands in all directions and especially gives a tensile force to two beams at ends. When beams are just straight blocks with no space accommodating such expansion, the hot wire has chance to bend over and even break off in the end. Therefore, in order to mechanically keep stable on hot wire, beams at ends are designed to be meander that the interspace in curved segment on meanders can deal with the elongation of hot wire due to thermal expansion. Two meanders at both ends can help to mechanically maintain balance in orthogonal direction.

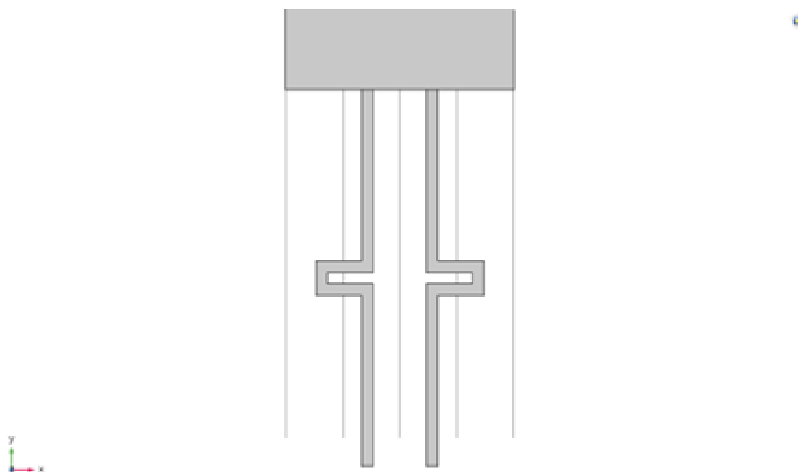

Figure 2.39: Meander beam

1mm hot wire

The length of meanders is the major factor studied. As mentioned before, the length of meander can affect temperature distribution on hot wire a lot by heat generation. In addition, the interspace in meander has to be larger than the elongation of hot wire due to thermal expansion. If the length of interspace is $l_b m1$ and that of rest is $l_b m2$. Both of them are measured in various value to find the best combination. The change of temperature profile on hot wire with total length of meander is same as which is with straight beams at ends.

When meanders become longer, temperature reduces as in Figure 2.33. $w_b m$ is the width of beams. To weaken the thermal conduction to substrate through beam, it keeps 1μm for each beam in all following simulations.

Eventually, an appropriate design for 1mm hot wire with meanders at ends is made, which is shown in Figure 2.40 and 2.41.

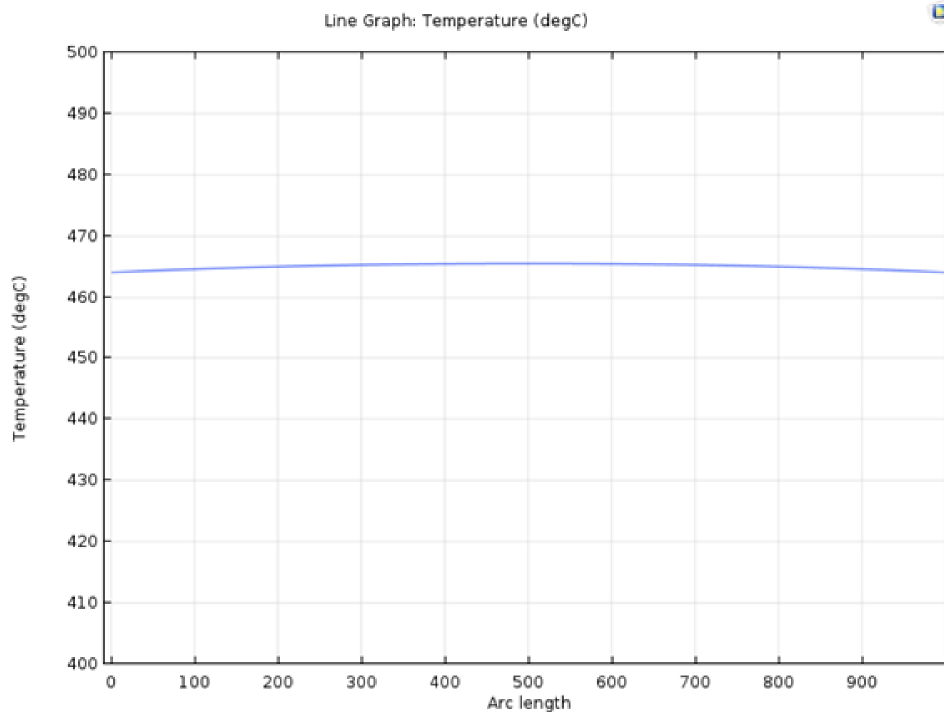

Figure 2.40: Temperature profile of 1mm hot wire with meander beams

In this design, the geometry and resistivity of hot wire is same as before, which is 1mm in length, 20μm in width and 0.3μm in thickness for both hot wire and meanders. Resistivity is 0.001 ω□cm for hot wire and 0.01 ω□cm for meanders. The geometry of meander is $l_b m1$=4μm and $l_b m2$ is 32μm.

From the result, the maximum temperature on hot wire is 465°C with a deviation of 1.5°C. For simplicity, only thermal expansion in the direction that along the hot wire is observed which means linear thermal expansion. The maximum displacement in y direction is 0.6[μm]. It is not too much, but it is demonstrated that the interspace in meander does work to the elongation of hot wire due to thermal expansion and helps to mechanically stable.

0.5mm hot wire

By using the same design method for 1mm hot wire, a 0.5mm hot wire with meanders is made. It uses same meanders as 1mm hot wire. The maximum temperature is 475°C with 1°C deviation which is 10°C higher than 1mm hot wire. As length is smaller, resistance of hot wire reduces while power of heat generation increases. The maximum displacement in y direction is 0.32μm which is smaller in 1mm hot wire. It makes sense according to 2.17.

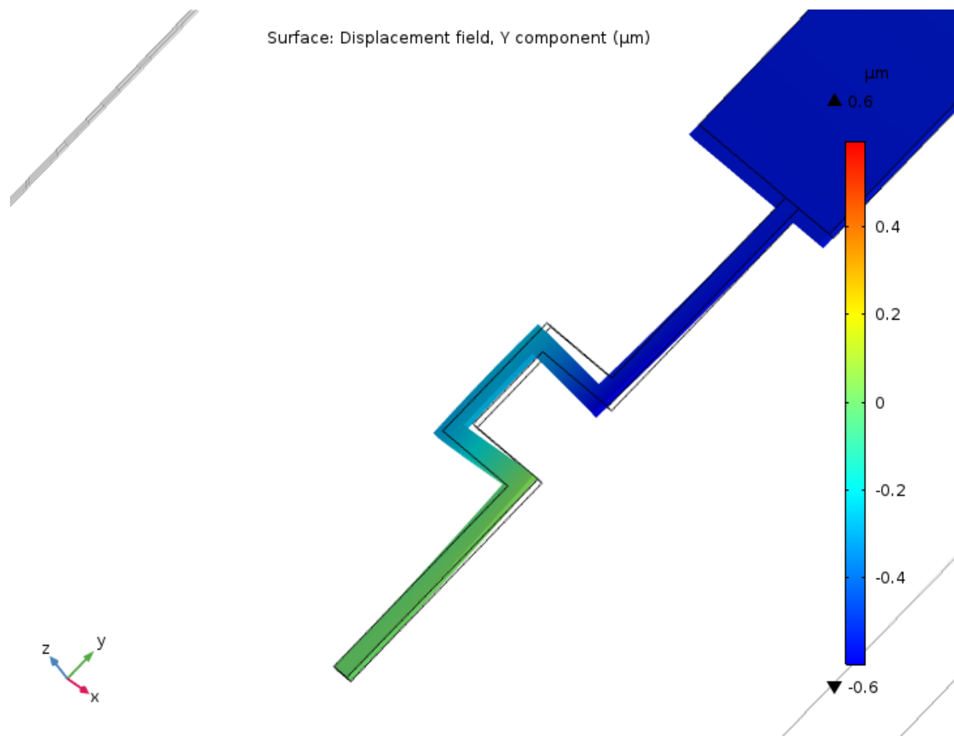

Figure 2.41: The contraction of meanders on 1mm hot wire

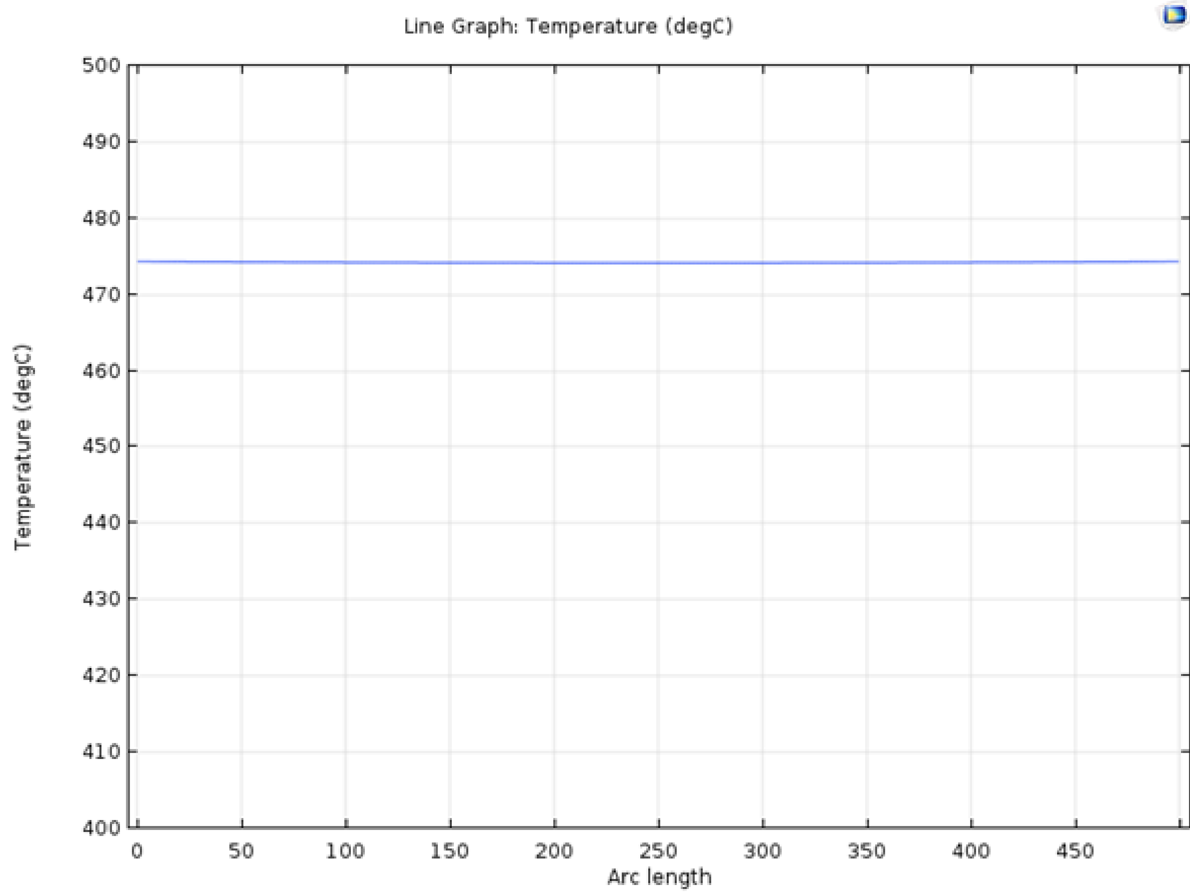

Figure 2.42: Temperature profile of 0.5mm hot wire with meander beams

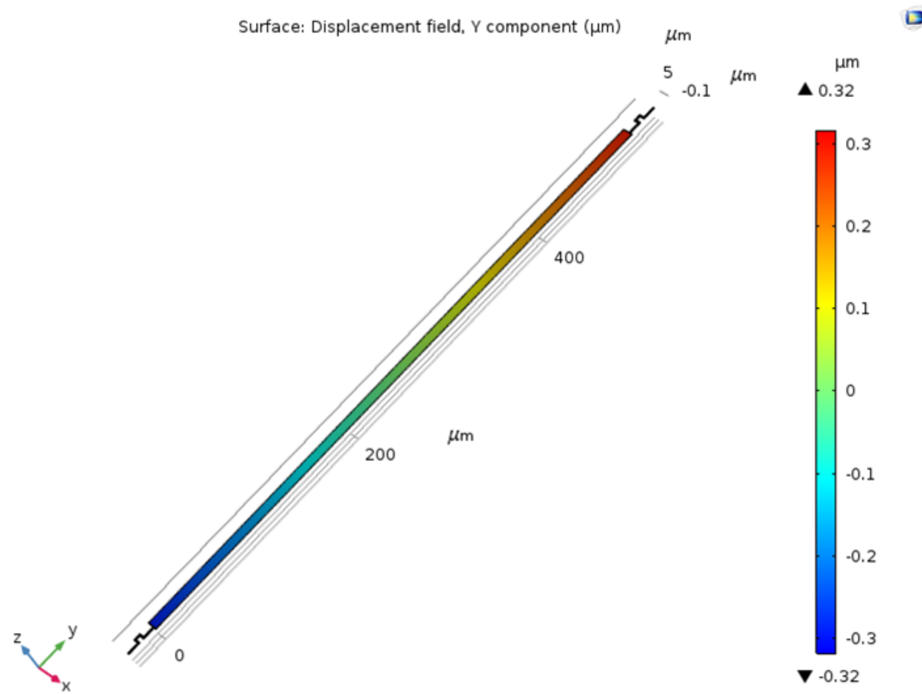

Figure 2.43: The contraction of meanders on 0.5mm hot wire

2mm hot wire

A 2mm hot wire with meanders is designed as well. The meander has to be longer as the length of hot wire is twice which means it more vulnerable to thermal expansion and easier to break off. The meander is 3µm and totally 34µm in rest. Figure 2.44 shows that the maximum temperature is further smaller to 450 °C.

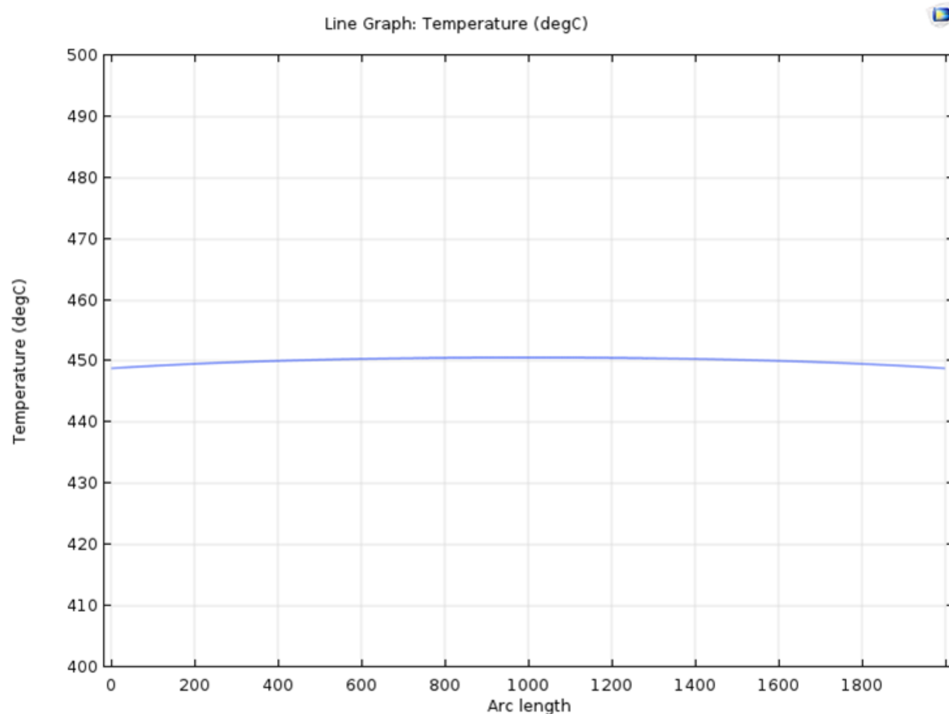

Figure 2.44: Temperature profile of 2mm hot wire with meander beams

2.9.3. Lateral beams

The mechanical disturbance comes not only from the thermal expansion, but also environment outside. The outside force that occasionally applied on the device may destroy it, falling down on the ground during shipment for instance. From the view of fabrication, basically hot wire is etched from a polysilicon layer which is deposited on another layer of oxide as substrate. When making the suspending hot wire and removing the needless part of polysilicon that underneath it, the water residue adhere to hot wire that comes from etching resolution can pull it down and touch the substrate. It can cause the destroy of hot wire. Therefore, in order to mechanically keep more stable for hot wire, two small straight beams are put on the lateral side of it.

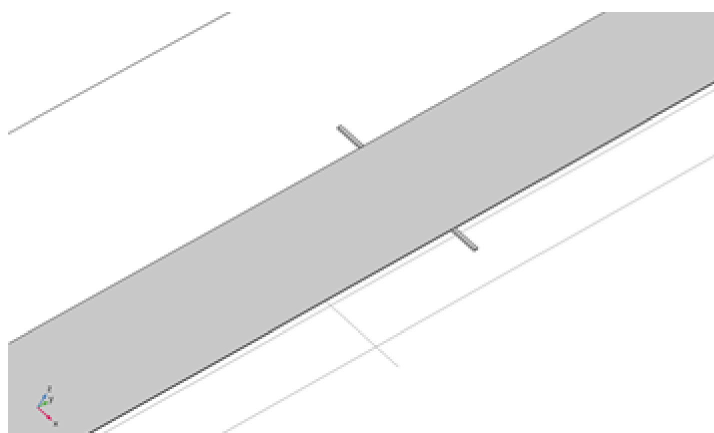

Figure 2.45: Lateral beam

The boundary condition for these two beams is that, similar to the beams at ends, the spare side is set to mechanically fixed as it connects the polysilicon layer. Thus, the strong thermal conduction from hot wire to polysilicon layer cause a large dip on temperature in the middle of hot wire, which is shown in Figure 2.46.

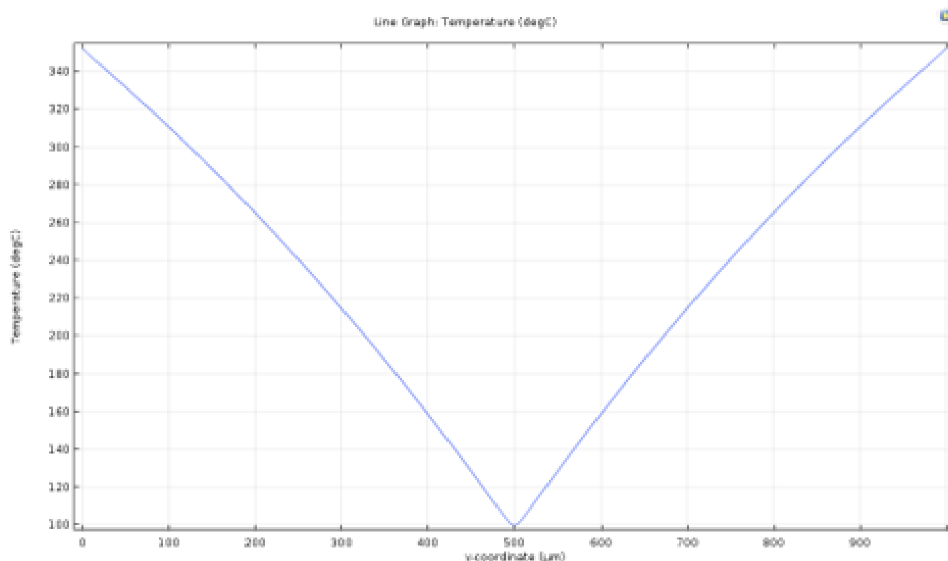

Figure 2.46: Temperature profile for hot wire with lateral beams

Same as before, three aspects are tried to remove the huge decrease of temperature: length, width and resistivity of lateral beams.

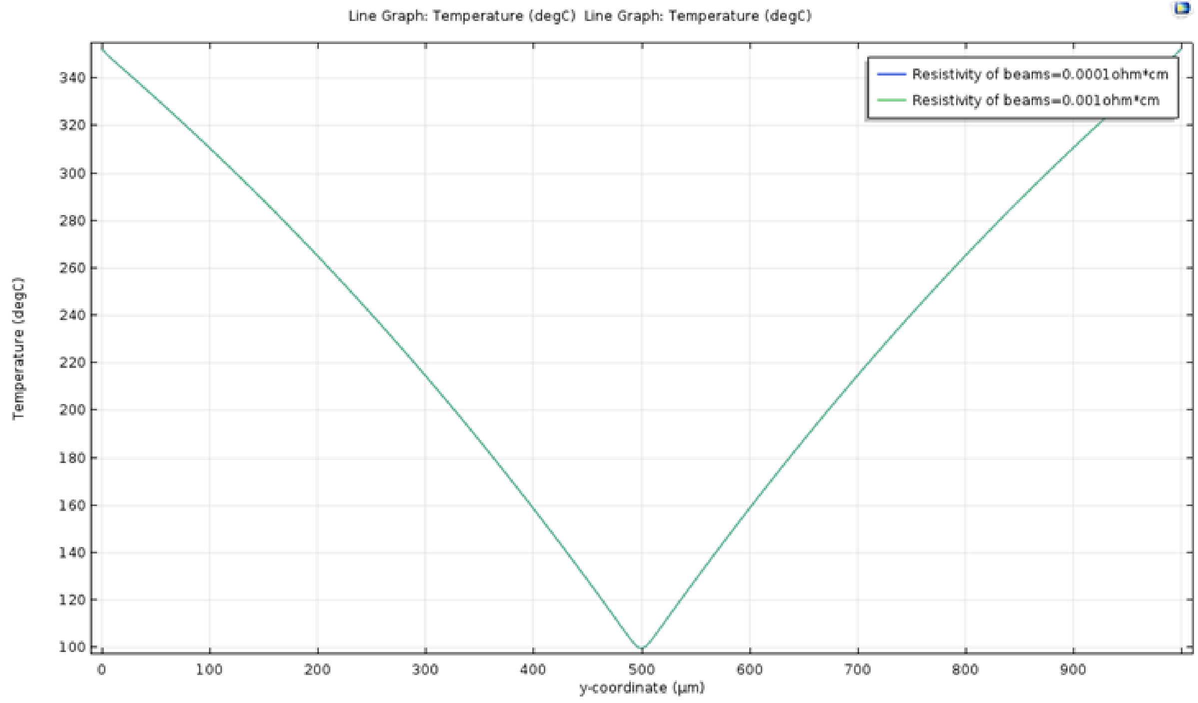

Figure 2.47: The effect of resistivity of lateral beams

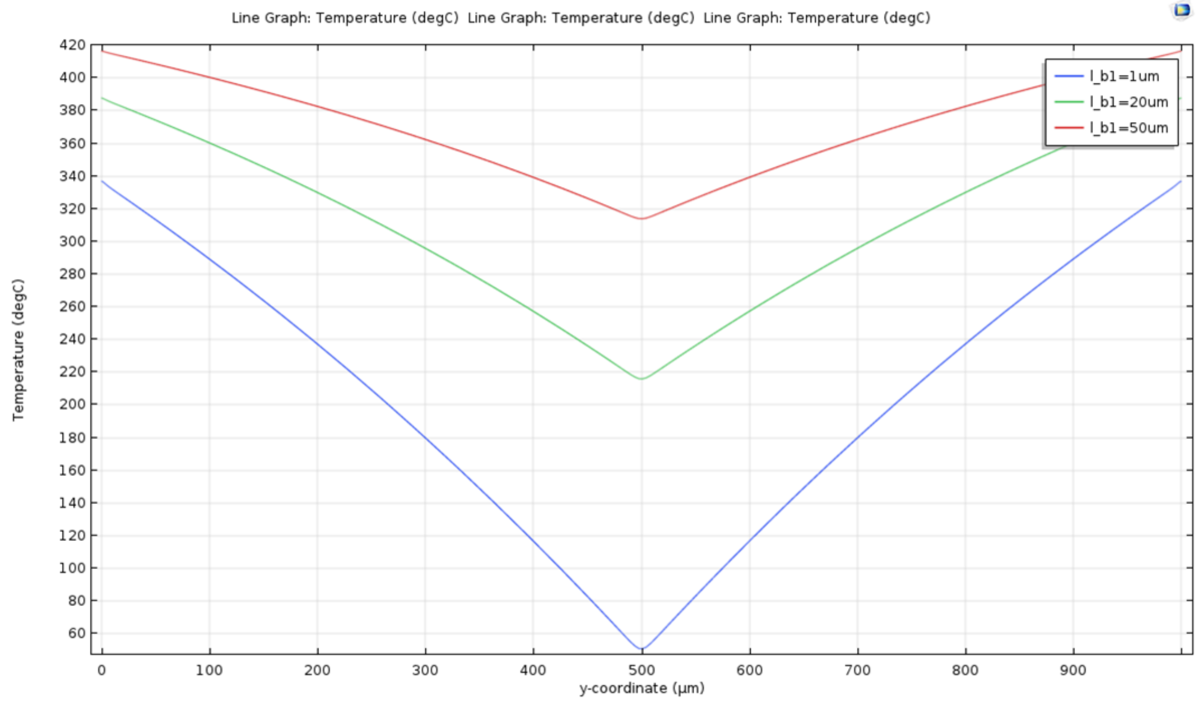

Figure 2.48: The effect of length of lateral beams

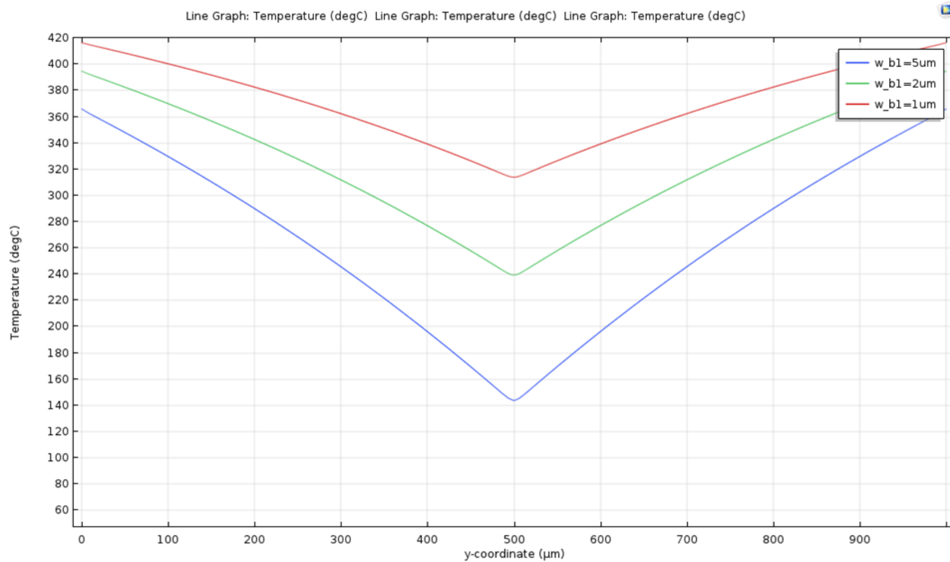

Figure 2.49: The effect of width of lateral beams

From Figure 2.47, the change of resistivity has no use on temperature profile. Heat conduction to substrate is very strong here and the lateral beam is too small to compensate it by more heat generation by muc smaller resistivity.

The effect of length and width of lateral beams is so obvious that they are useful tools for temperature adjustment on hot wire based on same theories for beams at ends. However, width of beams determines both resistance and area of interface to substrate, and it is shown in Figure 2.49 that a smaller width tends to a better temperature distribution. As 1mm is the technical limit of fabrication, the width can not be further smaller. Therefore, the length of lateral beam is the main method. From the Figure 2.48, the longer the lateral beam is, the better its effect is.

2.9.4. Lateral meander bridges

To acquire a lateral beam as long as possible, a lateral meander bridge is used as Figure 2.50. By taking advantage of this shape, lateral bridges can extend to a much larger degree. Besides, the interspace in meander which is similar to a spring can be tolerant of more mechanical change and hold a more stable condition for hot wire.

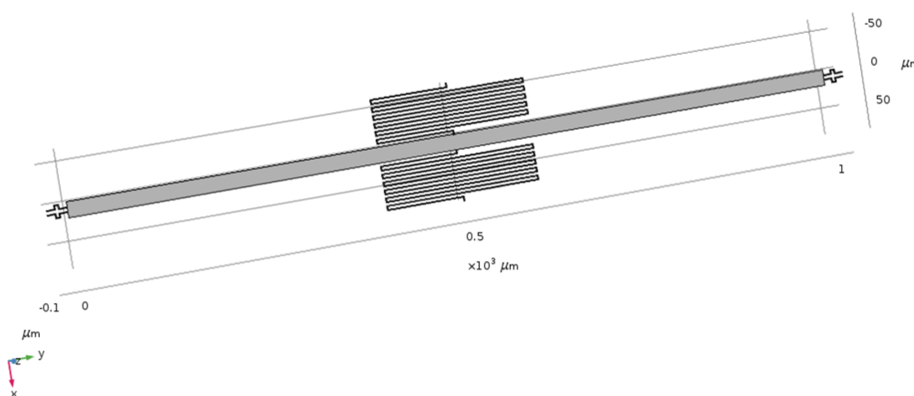

Figure 2.50: Hot wire with lateral meander bridge

Another conception is, whether an electrical source should be applied to the bridge. In Figure 2.51 is the comparison between with and without electrical source on lateral bridge.

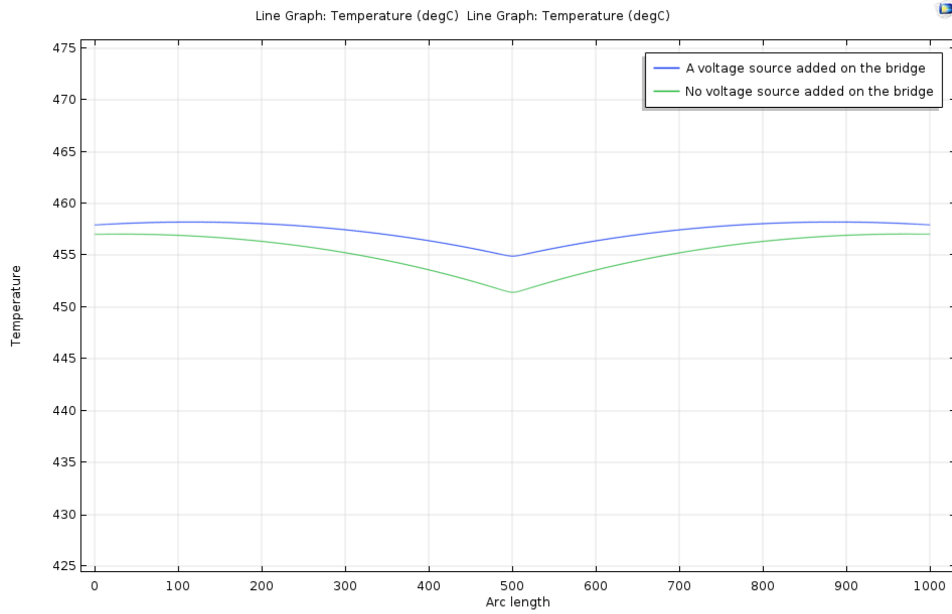

Figure 2.51: Voltage source on lateral bridges

One more voltage source does help to increase temperature in the middle by around 5°C. The new source of heat generation can compensate partial heat loss due to thermal conduction to substrate. In addition, the electrical model of hot wire can be abstracted to be as in Figure 2.52.

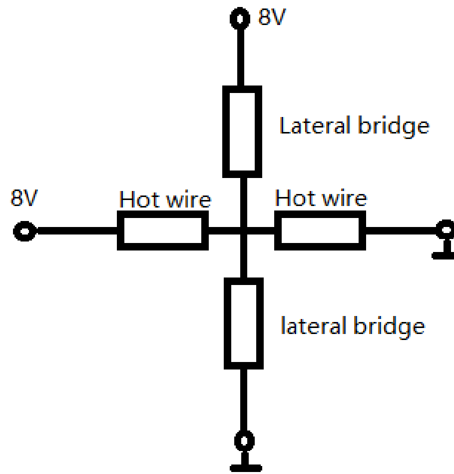

Figure 2.52: Equivalent diagram of resistor

The potential difference at each side from the center to ends is same. Thus, temperature uniformity between both sides is guaranteed. In the later simulation, a voltage source is added to lateral bridge.

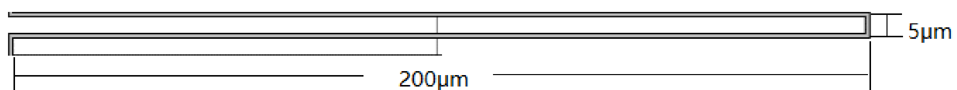

Figure 2.53: The unit of lateral bridges

Figure 2.53 is the unit of lateral bridges. The length can be controlled by the amount of units being used. The width of bridge is constant 1μm.

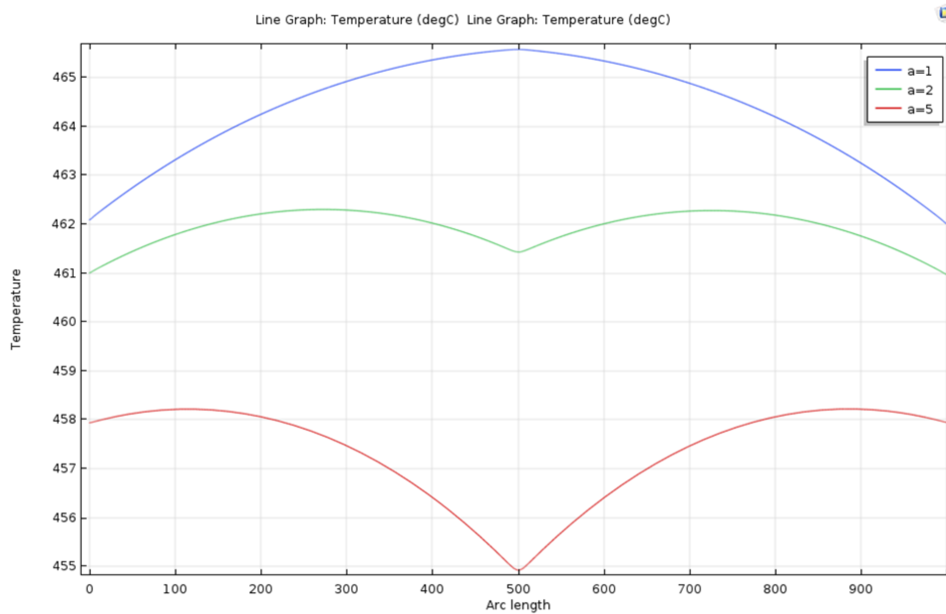

Figure 2.54: The amount of segments on bridges. a is the amount of segments.

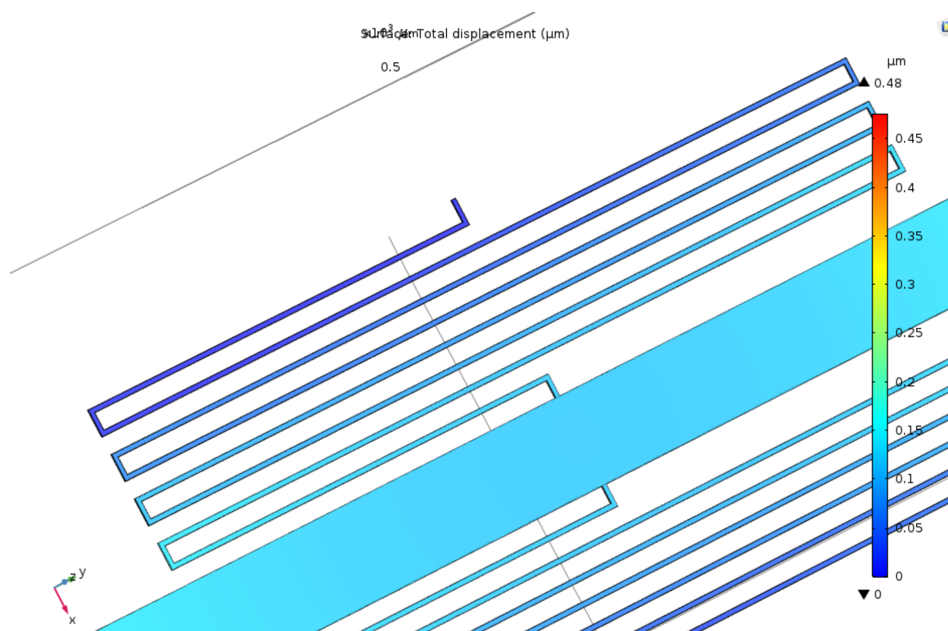

Figure 2.55: Displacement on lateral bridges when pressure exerting

In Figure 2.54, a is the amount of segments. The trend of change on temperature with longer bridges shows that, with more segments which is equivalent to longer middle bridge, its resistance is larger thus the the heat generation is less when voltage source is applied. It then can not compensate for heat conduction to substrate through middle bridge and the dip in temperature becomes larger. But if it's too short, it then becomes an opposite story. Thus, a=3 is relatively good and selected.

In order to test the function of lateral meanders, a body load exerts on hot wire. It equals to ρg N/m^3, where ρ is density of polysilicon which is 2329kg/m^3 and g is gravity acceleration

9.8m/s^2. It simulates a static suspending hot wire. Though it is tiny, the influence of gravity still exits. In Figure 2.55, it shows that the displacement on lateral bridges is 0.15µm due to gravity. It does help to maintain stable when gravity works.

2.9.5. 4 and 5mm hot wire with middle bridges

Since 3 segments are selected for middle bridges to deal with unforeseen outside interference on hot wire, the design on width of hot wire of 4 and 5mm is used to acquire a relative uniform temperature performance on hot wire. As mentioned before, the change of width leads to not only heat generation, but also thermal conduction to substrate. It is a powerful method for design of hot wire. As in Figure 2.56 and 2.57, both of them have quite good temperature distribution. For 4m hot wire, width is 16µm, and 17µm for 5mm hot wire. The maximum temperature is 469.2°C and 427.2°C with a deviation of 1.8°C and 2.8°C respectively.

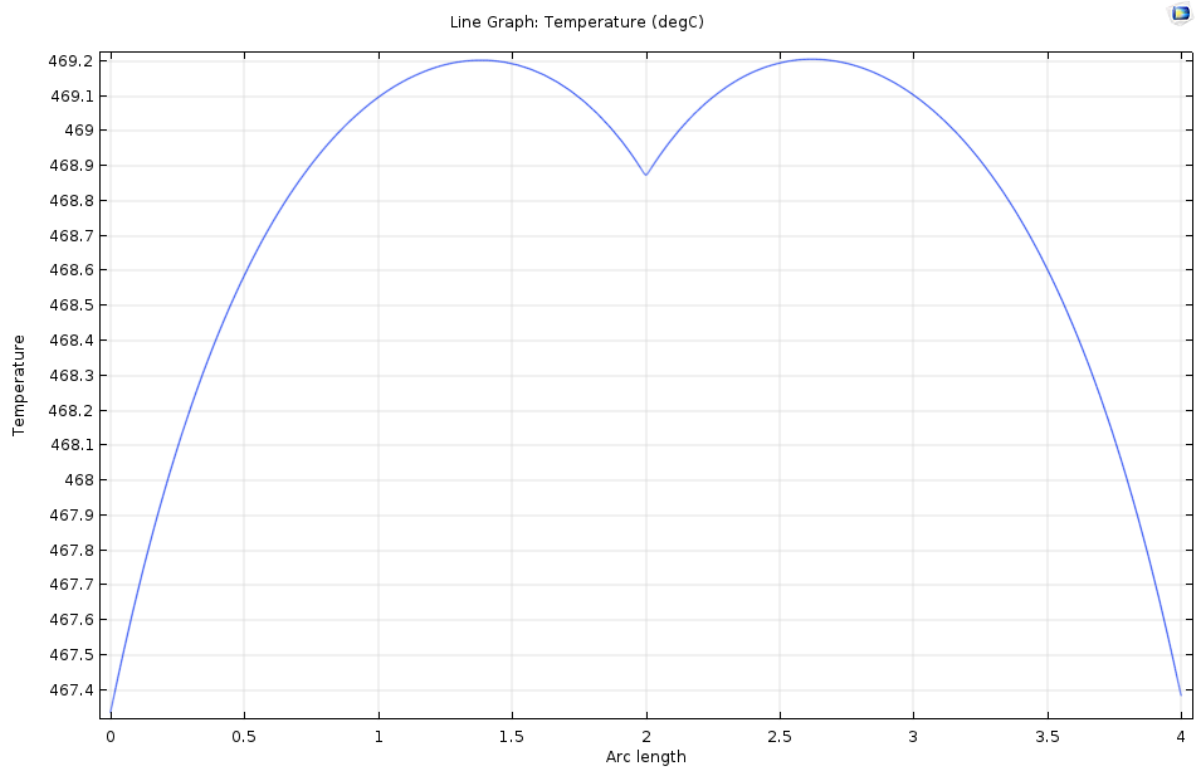

Figure 2.56: Temperature profile of 4mm hot wire with lateral bridges

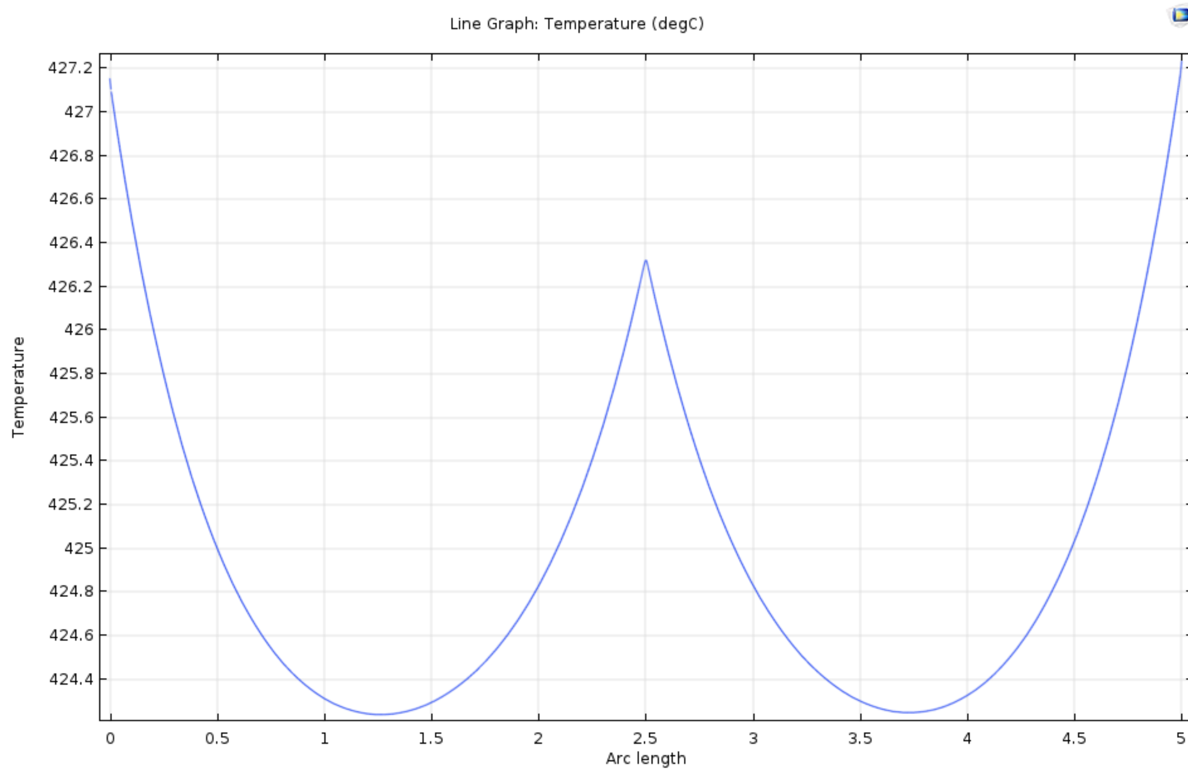

Figure 2.57: Temperature profile of 5mm hot wire with lateral bridges

2.9.6. All designs of hot wire

For 1mm hot wire,

With 2 straight beams at ends, 9V

Number	Width of hot wire[μm]	Length of beams[μm]	Width of beams[μm]
1	20	50	3
2	20	34	2
3	20	50	20
4	20	32	20

With 4 meander beams at ends, 9V

Number	width of hot wire[μm]	$l_b m1$[μm]	$l_b m2$[μm]
1	20	4	32
2	20	5	32
3	20	3	32
4	19	4	32
5	21	4	32

With 2 lateral meander beams, 9V

Number	width of hot wire[μm]	$l_b m1$[μm]	$l_b m2$[μm]	a
1	20	4	32	3
2	20	5	32	3
3	20	3	32	3
4	19	4	32	3
5	21	4	32	3
6	20	4	32	2
7	20	4	32	4
8	20	4	32	5

For 2mm hot wire,

With 4 meander beams at ends, 10V

Number	width of hot wire[μm]	$l_b m1$[μm]	$l_b m2$[μm]
1	20	3	34
2	20	4	34
3	20	2	34
4	19	3	34
5	21	3	34

With 2 lateral meander beams, 10V

Number	width of hot wire[μm]	$l_b m1$[μm]	$l_b m2$[μm]	a
1	20	3	34	3
2	20	4	34	3
3	20	2	34	3
4	19	3	34	3
5	21	3	34	3
6	20	3	34	2
7	20	3	34	4

For 4mm hot wire,

With 4 meander beams at ends, 13V

Number	width of hot wire[μm]	$l_b m1$[μm]	$l_b m2$[μm]
1	16	5	40
2	16	6	40
3	16	4	40
4	15	5	40
5	20	5	40
6	40	5	40

With 2 lateral meander beams, 13V

Number	width of hot wire[μm]	$l_b m1$[μm]	$l_b m2$[μm]	a
1	16	3	40	3
2	16	4	40	3
3	16	2	40	3
4	16	3	40	2
5	16	3	40	4
6	15	3	40	3
7	20	3	40	3
8	40	3	40	3

For 4mm hot wire, there is a special design that 4mm can be composed of an array of 0.5mm hot wire.

Combination of 0.5mm hot wire, 8.5V

Number	Amount of 0.5mm hot wire
1	200

For 5mm hot wire,

With 4 meander beams at ends, 13V

Number	width of hot wire[µm]	$l_b m1$[µm]	$l_b m2$[µm]
1	17	6	40
2	17	5	40
3	17	4	40
4	16	6	40
5	20	6	40
6	50	6	40

With 2 lateral meander beams, 13V

Number	width of hot wire[µm]	$l_b m1$[µm]	$l_b m2$[µm]	a
1	17	6	40	3
2	17	6	40	2
3	17	5	40	4
4	17	5	40	3
5	17	4	40	3
6	16	6	16	3
7	20	6	40	3
8	50	6	40	3

For 5mm hot wire, same as 4mm hot wire that it can be composed of an array of 0.5mm hot wire.

Combination of 0.5mm hot wire, 8.5V

Number	Amount of 0.5mm hot wire
1	250

3

Optical design of a linear variable optical filter (LVOF)

The interference filters have applications in many field such as spectroscopy, chemistry, and astronomy [28]. An interference filter is an optical structure operating based on interference of light in thin layers of optical materials. A common type of optical filter is an Fabry-Perot (FP) filter which composed of two mirrors separated by an optical resonator. When a monochromatic light enters an FP filter, it is reflected in the resonator for multiple times. At each reflection, the beam is divided into two parts, reflected beam and transmitted beam. As the transverse distribution of amplitude of those transmitted beams obeys Gaussian function, the multiple reflected and transmitted beams are superimposed.

As these beams come from the same source, they share same frequency and initial phase. But the difference of optical path in each reflected beam between the mirrors introduces an optical phases difference between them. Therefore, if the phase difference is constant over time, the interference occurs and an interference pattern is thereby generated. The interference pattern is actually the characterization for the resultant intensity of superposition of these transmitted beams and the phase difference between multiple reflections. The phase difference between the adjacent beams is determined by difference in optical path, which means the thickness of the resonator layer in an optical filter and the wavelength of the light [29].

At the interference, the resulting total amplitude is equal to the vector sum of complex amplitude of each individual beam. Consequently, when the phase difference is an even multiple of π ($2n\pi$) the beams reinforce each other thereby lead to maximum values on intensity, which is called constructive interference. Similarly destructive interference occurs when the phase difference is equal to odd multiples of π and the beams cancel each other.

An optical filter can thereby be used to identify the component of wavelength in original source. Most importantly, those maximum values on interference can be regarded as high transmittance of the original incident light at certain point. By choosing carefully the specific range of thickness of resonator layer and length of device, the position of those maximum transmittance for certain wavelength can be manipulated. Only the selected wavelength can have a high transmittance with the shown length of device while others not. For optical filter, it means part of the wavelength range is filtered while only selected wavelength can go through.

As mentioned before, the microspectrometer based on interference filter is a good way of miniaturization of spectrometer. In order to achieve wide-band high-resolution operation which is the important requirement for spectroscopy, whether an array of fixed resonators with different thickness such as FP filters array [30, 31] or mechanically moving one of the flat mirror such as tunable FP filter [32, 33] can be used. But both of them have unavoidable defects that FP filter array have limited operating spectral channels and tunable FP filter can not fully guarantee the parallelism of two reflective mirrors. A better structure called linear

variable optical filter (LVOF) which has advantages of both configurations mentioned above but without their defects is proposed.

It is a type of FP filter composed of two highly reflective mirrors with a tapered resonator inside. One mirror is slightly tilted and the linearly changing thickness of resonator along its length leads to unlimited amount of spectral channels which thereby depends on the number of detectors. Thus, LVOF can achieve the high-resolution for a comparatively wide-band operation. An LVOF can be compared to a large array of FP filters placed adjacent to each other. The thickness of resonators of neighboring FP filters are stepwise increased.

More accurately, an LVOF is a type of Fizeau interferometer, also called wedged filter. In this thesis and for the sake of simplicity, FP filter analogy is used.

Both COMSOL and ZEMAX allow an advanced optical system design. Nevertheless, ZEMAX an geometric optic based software that it can simulate the trajectory of multiple reflected beams inside resonator but not interference referring to wave optics. COMSOL multiphysics is based on finite element method and has the module of wave optics, but computation with it will take huge computational resource and power and takes much longer time. To acquire a relatively accurate results, the rule of thumb is that the element size (mesh) must be at least 6 times smaller than the wavelength. Therefore, simulation of an LVOF which is typically more than 1000x longer than a wavelength using COMSOL (or any other finite element tool) is computationally intensive.

Although the geometric optics module can achieve such simulation even exhibit the feature of optical filter in Bragg-mirror model which can be regarded as two highly reflective mirrors in filter, it is not adapted to the structure needed. Moreover, it can not calculate the deposited power, which means the resultant intensity of interference of reflected beams, on one side of the optical system in a customized model. Neither of them can be used to conduct simulation of LVOF in both geometric and wave optics. Hence, the analysis and design of LVOF has to be calculated numerically in Matlab according to equations of phase difference in FP filter as well as Fizeau filter.

3.1. Theoretical background

3.1.1. Bragg Reflector

As mentioned before, interference filter has two flat highly reflective mirrors. They are normally Bragg reflectors which belong to multi-layered dielectric mirrors made of non-absorbing material [34, 35]. A pair of layers of high refractive index n_1 and low refractive index n_2 respectively used as the unit, it stacks for N times and each layer has one quarter wavelength optical thickness (QWOT) which is,

$$QWOT = \frac{\lambda_0}{4n} \tag{3.1}$$

Where λ_0 is the reference wavelength which is typically the center wavelength of the spectrum involved in incident light. n is the refractive index at λ_0. The whole structure is as Figure 3.1,

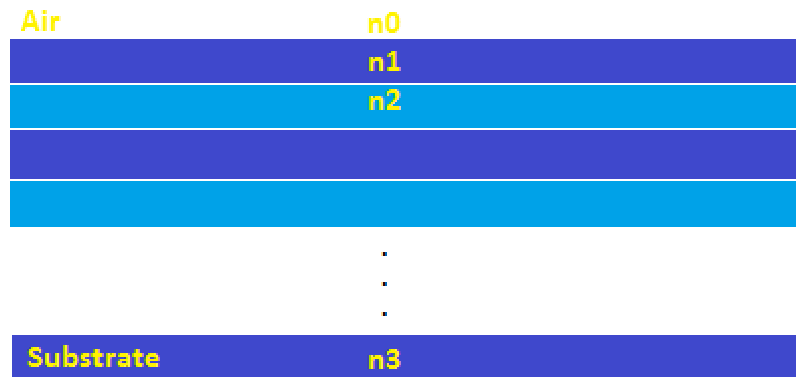

Figure 3.1: The structure of Bragg mirror.

The working principle is that, each time when the beam reaches the high n layer from the low n layer, it will have π shift on phase different which is equivalent to half wavelength. Whereas, there is no phase difference when it goes through high n layer to low n layer. Coherence occurs when the phase difference between two reflected beams is multiple of 2π.

To get the mirror with high reflectivity that satisfies the requirement of optical filter, another layer of high refractive index n_1 can added to be the last layer of the structure. In addition, it can be dramatically increased by more stacks of the pair of dielectric layers which means a larger N. The resulting reflectively can be calculated as [36],

$$R = \frac{n_0 n_2^{2N} - n_3 n_1^{2N}}{n_0 n_2^{2N} + n_3 n_1^{2N}} \tag{3.2}$$

The bandwidth of the mirror $\Delta\lambda$ is characterized mainly by the refractive index difference of the comprising layers 3.3.

$$\frac{\Delta\lambda}{\lambda_0} = \frac{4}{\pi} Arcsin(\frac{n_2 - n_1}{n_2 + n_1}) \tag{3.3}$$

Accordingly a Bragg reflector is designed for mid-infrared application. The reference wavelength used is 1.9µm, n_1=2.32 and n_2=1.38. The simulation result of transmittance of Bragg reflector with such refractive index is shown in Figure 3.2. It compares the effect of different amount of stacked layers.

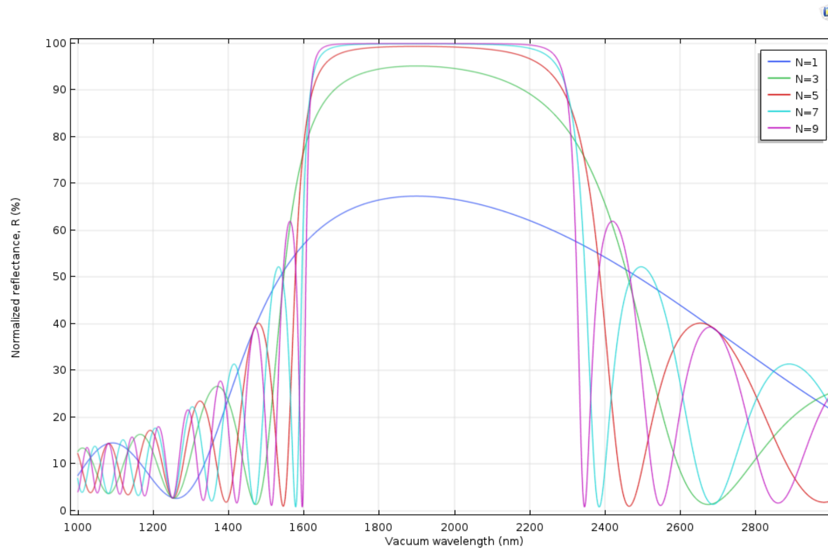

Figure 3.2: The spectral response of Bragg mirror for different stacked layers N.

In Figure 3.2, with a higher number stacked layers, the reflection quickly approaches 100 percentage, meanwhile the bandwidth of the mirror $\Delta\lambda$ does not change with the number of the layers.

From the equation 3.3, it is clear that with the larger difference between the two refractive index of two dielectric layer in the repeating unit, the rejection range turns to larger. Besides, the larger reference wavelength has same effect. Figure 3.3 shows the effect of refractive index difference on the bandwidth of a Bragg reflector.

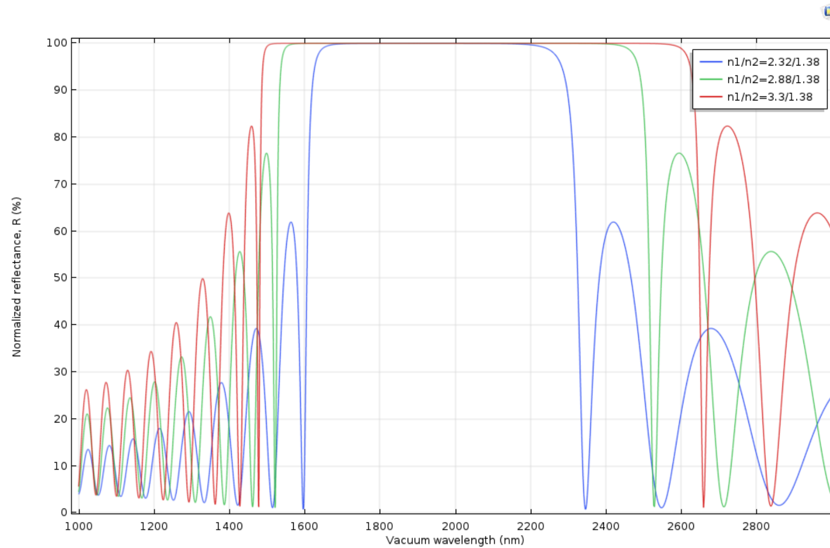

Figure 3.3: The spectral response of Bragg mirror for different n_1/n_2.

3.1.2. Schematics of FP filter

Since the phase difference of multiple reflected beams in resonator determines the interference pattern which refers to the transmittance of incident light in optical filter, calculating the phase difference is the major numerical method for analysis of the optical filter. The phase difference of each two reflected beams is computed then all of them is added up to measure the overall effect. The basic theory of FP filter is mainly referred to [40].

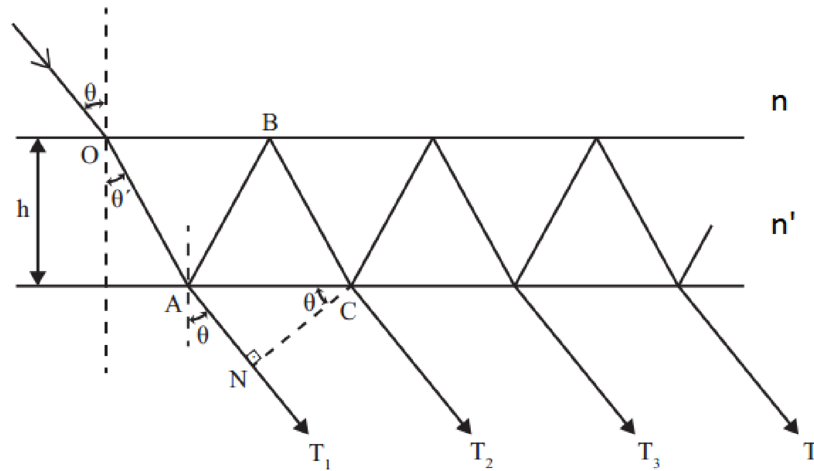

Figure 3.4: The schematics of FP filter [40].

In Figure 3.4 it is the schematic diagram of FP filter presenting its working principle [37]. Two mirrors in FP filter has reflectivity R and transmissivity T, absorption effect of optical medium in resonator is neglected in this case. The resonator with thickness of h has refractive index n' while it is n in surroundings which is most probably air.

The incident collimated monochromatic light gets into FP filter with angle θ at point O on upper side. It hits the second lower surface at point A with the incident angle is θ'. According to Snell's law, they have the relation that,

$$nsin\theta = n'sin\theta' \tag{3.4}$$

The beam is then split into two that one with lower intensity T_1 is transmitted through filter, while the other one is reflected to the upper surface at point B and later gets to the

lower surface again at point C where it gives rise to transmitted beam T_2 and repeats the previous process. Since two flat mirrors are parallel in FP filter, all transmitted beams are parallel as well with the refractive angle θ. After 2p successive reflection, the transmitted beam is T_p.

The optical path between T_1 and T_p is [40],

$$\Delta S_p = (n'(AB + BC) - nAN)(p - 1) \tag{3.5}$$

The optical path is defined as the path along which the beam traverses the optical medium. It is the multiplication of length of actual path and refractive index. Hence, n'(AB+BC)-nAN in equation represents the optical path difference of two neighboring transmitted beam such as T_1 and T_2, while it is multiplied by p-1 when calculating the optical path difference between the first and pth transmitted beam.

From the diagram, AB=BC=h/cosθ' and AN=ACsinθ=2htanθ'sinθ, the optical path can be written as [40],

$$\Delta S_p = (\frac{2n'h}{cos\theta'} - \frac{2nhsin\theta' sin\theta}{cos\theta'})(p - 1) = 2n'hcos\theta'(p - 1) \tag{3.6}$$

Since optical path difference has a direct relation with phase difference, the transformation between can be described as,

$$\Delta\phi_p = \frac{2\pi}{\lambda_0}\Delta S_p \tag{3.7}$$

Where λ_0 is the reference wavelength of incident light.

Thus, the phase difference between the 1st and pth transmitted beam is [40],

$$\phi_p = \frac{4\pi}{\lambda_0}n'hcos\theta'(p - 1) \tag{3.8}$$

In addition, when it is normal incident which means θ=0°and 1st and 2nd beam are coherent with the phase difference between them is the multiple of 2π. Meanwhile the intensity of interference is measured just at one side of the optical filter which means z=0. If only focusing on the difference of first and second order of interference, the direct relation between the order of coherence and thickness of resonator layer can be simplified to,

$$2n'h = m\lambda_0 \tag{3.9}$$

3.1.3. Schematics of wedged FP filter

The wedged FP filter which is also called Fizeau filter works in the principle of multiple beam interference [38]. It is composed of one tilted mirror and one flat mirror. Both are highly reflective for the high sharpness and intensity of fringes on interference pattern. The thickness of resonant cavity in-between determines the selected wavelength that can travel through as well as the position of fringe. Fizeau filter is often applied to do precision measurement of flatness of optical surface [39]. While the basic theory of LVOF explained in this section is referred to The basic theory of FP filter is mainly referred to [40].

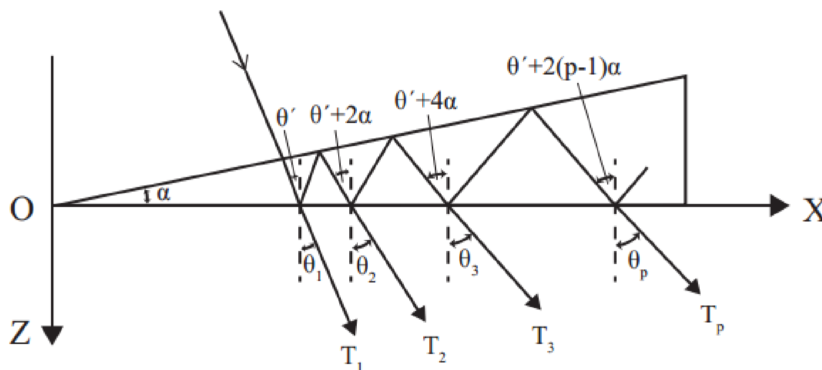

Figure 3.5: The schematics of Fizeau filter. [40]

Figure 3.5 describes the trajectory of multiple reflected beam inside Fizeau filter. The upper side of Fizeau filter is tilted in the angle α, its length depends on the inclined angle and the difference between minimum and maximum thickness. the refractive index of resonator is n' while that of surrounding material is n. One collimated monochromatic light impinges on the lower surface with the incident angle of θ'. It is a plane wave that all wavefronts go through the wedge apex. In addition, if θ' is positive, it is positive incidence otherwise it is negative incidence. In this figure, only positive incidence is presented [40].

When the incident beam hits the bottom side, part of light T_1 transmits through while the other part undergoes twice reflection, then reaches the lower surface again generating another transmitted beam T_2 and reflected beam. The incident angle after each reflection is increased by 2α which can be calculated according to triangular geometry. This process is repeated as the beam walks away from the wedge apex, until it travels out of the filter or the intensity of beam is too weak to be reflected. The refractive angle is θ_1, θ_2 to θ_p. The relation between the incident angle and refractive angle can be described according to Snell's law:

$$n sin\theta_p = n' sin(\theta' + 2(p-1)\alpha) \tag{3.10}$$

Compared with FP filter, the largest difference is the traveling distance for each reflected beam in Fizeau filter is much longer than that in FP filter. It causes the number of available beams that can be taken account into overall interference effect is much less than FP filter because beam goes out of Fizeau filter is much faster than FP filter. This walk-off effect leads to the reduced transmittance of selected wavelength.

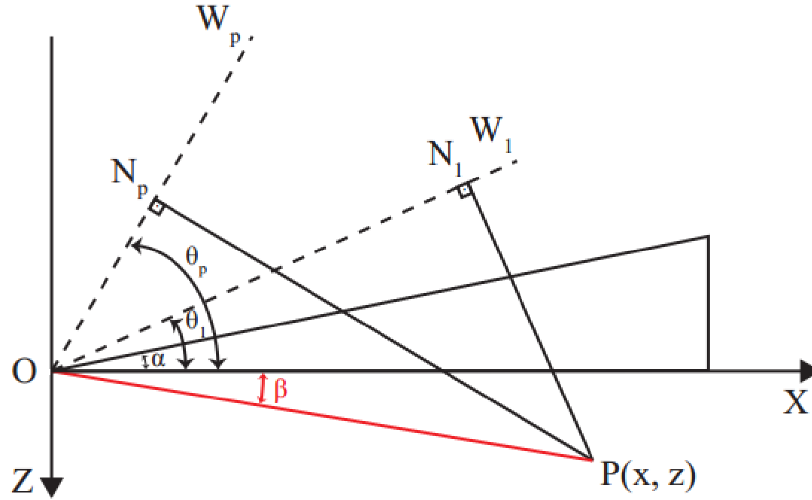

Figure 3.6: Optical path difference between the 1st and pth reflected beam [40].

Each reflected beam in Fizeau filter has the wavefront, W_1 to W_p in the figure, that all passing through wedge apex. They make the angle of θ_1 to θ_p away from x axis. They interfere at point P which is orthogonal with wavefronts at N_1 to N_p. OP is tilt from x axis by angle of β. The optical path therefore is [40],

$$\Delta S_p = n(PN_p - PN_1) \tag{3.11}$$

Applying triangle geometry,

$$PN_1 = OP(sin(\theta_1 + \beta)) = OP(sin\theta_1 cos\beta + sin\beta cos\theta_1) \tag{3.12}$$

$$PN_p = OP(sin(\theta_p + \beta)) = OP(sin\theta_p cos\beta + sin\beta cos\theta_p) \tag{3.13}$$

And

$$OP cos\beta = x, OP sin\beta = z \tag{3.14}$$

Combining with Snell's law, the optical path difference can be written as,

$$\Delta S_p = n'x(sin(\theta'+2(p-1)\alpha)-n'sin\theta')+z(\sqrt{n^2-[n'sin(\theta+2(p-1)\alpha)]^2}-\sqrt{n^2-(n'sin\theta')^2}) \quad (3.15)$$

Assuming both resonator and surrounding is air, which means n=n'=1, then

$$\Delta S_p = x[sin(\theta'+2(p-1)\alpha)-sin\theta']+z[cos(\theta'+2(p-1)\alpha)-cos\theta'] \quad (3.16)$$

Then the corresponding phase difference between 1st and pth beam can be obtained according to 3.7,

$$\phi_p = \frac{2\pi}{\lambda}x[sin(\theta'+2(p-1)\alpha)-sin\theta']+z[cos(\theta'+2(p-1)\alpha)-cos\theta'] \quad (3.17)$$

When it is normal incident and transmission distribution is calculated along the flat side of LVOF which means z=0, and only the phase difference of first and second transmitted beams is considered, the relation between the order of coherence and thickness of resonator layer can be simplified as,

$$2hcos^2\alpha = m\lambda_0 \quad (3.18)$$

Since $cos^2\alpha \approx 1-sin^2\alpha \approx 1-\alpha^2 \approx 1$, it can be further simplified to

$$2h = m\lambda_0 \quad (3.19)$$

The corresponding x position is,

$$x = \frac{m\lambda_0}{2tan\alpha} \quad (3.20)$$

As for negative incident, it is manifested that same formula 3.16, 3.17 and 3.20 are also applicable only with small changes in deduction process.

Filter transmission

The amplitude of resultant interference pattern which also means transmittance in optical filter can be calculated. Firstly, the amplitude of each transmitted beam is [40],

$$tt'r'^{2(p-1)}A_ie^{i\phi_p} \quad (3.21)$$

Where t and t' are transmission coefficient. t is for light traveling from surroundings to resonator while the other one is for the opposing situation. r' is the reflection coefficient. For each transmitted beam T_p, it has undergone two transmissions (from surroundings to resonator and from resonator to surroundings) and 2(p-1) reflections inside resonator. A_i is the amplitude of incident light. $e^i\phi_p$ represents the exponential form of plane wave that make amplitude be complex number. The main reason is that complex exponential is algebraically easier to handle than trigonometric sin and cos. The actual amplitude can be got from its real part.

Then the total amplitude of interference at point P after p transmitted beams are superimposed can be described as [40],

$$A_t = A_iT\sum_{p=1}^{\infty}R^{(p-1)}e^{i\phi_p} \quad (3.22)$$

Where T and R is the transmissivity and reflectivity of mirrors that is equal to tt' and rr', respectively.

The intensity of interference at point P can be calculated as [40],

$$I_t = A_i^2T^2\left|\sum_{p=1}^{\infty}R^{(p-1)}e^{i\phi_p}\right|^2 \quad (3.23)$$

To obtain the transmittance along the length of Fizeau filter for certain wavelength, x in 3.20 should be scanned from original point to the required position, which is defined by h and α, with monochromatic incident light. Besides, the spectral response at one certain point can be obtained by sweeping the spectrum in λ.

As for the selection of p, there is actually an inherent error in the final result of calculation that comes from the replacement of infinite involved beams for interference by a finite number p. This truncation of infinite summation after p terms can be estimated according to the assumption that, all terms that left out of interference are in phase with each other which is the worst situation for the error. It then can be expressed by the difference between an infinite series starting from 1 and a finite series starting from 1 and ending at p. This intensity error is then be described as [41],

$$\Delta I_t = \frac{T}{1-R} R^{2n+2} \tag{3.24}$$

Ignoring the effect of absorption which means $T^2/(1-R)^2$, the number of beams required fr certain accuracy can be described as,

$$p = \frac{log(\Delta I_t)}{2log(R) - 1} \tag{3.25}$$

So far, the absorption effect of resonator medium is ignored. In fact, when light travels through the resonator, the amplitude will be attenuated if the resonator medium is not air and can absorb the light. The effect can be described by adding $e^{-\gamma z}$ to the exponential term, where γ is the absorption coefficient per unit optical path length and z is the length of optical path. However, in this thesis, it works in the vacuum environment or with little air inside. The absorption effect can be neglected.

3.2. Characterization of LVOF

3.2.1. FSR, FWHM and finesses

To quantifies the quality of a LVOF based microspectrometer, maximum free spectral range (FSR) and full width half maximum (FWHM) are two necessary aspects that have to be discussed. By definition, FSR refers to the difference between the wavelength of two neighboring operating order at same position along the length of LVOF which is equivalent to corresponding length of cavity. It can be calculated according to 3.19 for normal incidence,

$$FSR_m = \frac{2n'h}{m(m+1)} \tag{3.26}$$

It should be as larger as better so that the device will operate at only one interference order over the required incident spectrum thereby one transmission peak existing. However, it will decrease with larger order m which is determined by 3.19, as shown in Figure 3.7.

The designed LVOF has the inclination angle of 0.001rad which is approximately 0.057°. The spectral response is calculated on the flat surface of LVOF which means z=0, it is also regarded as the reference x axis. The selected position is 5mm away from the wedge apex on x axis which corresponds to 5µm thickness of resonant cavity, according to $x = \frac{h}{tan\alpha}$. The reflectivity R=0.96. Assuming n'=1 and normal incident with the spectral range from 1.9 to 10.9µm, θ' in 3.17 thereby is 0.

In accordance with 3.19, 5 order of interference at shown wavelength can be involved in the spectral range of incident light. It is clearly to see the FSR decreases from 5µm to 0.5 µm with higher interference order , while FWHM, which is defined as the difference between two wavelength of half maximum transmission, decreases slightly as well leading to a sharper transmission fringe and higher resolution. Actually, the conflict exits between the design of FWHM and FSR that high resolving power must be bound to small operating bandwidth.

A necessary characterization for resolution is finesses which is defined as the ratio of FSR and FWHM. A large finesses means large operating bandwidth and sharper fringe thereby high resolution of interferometer. The finesses of LVOF is usually smaller than FP filter which means FP filter is more suitable for broad-band operation but LVOF has the absolute advantage on the number of spectral channels and robustness of two highly reflective dielectric multi-layered mirrors.

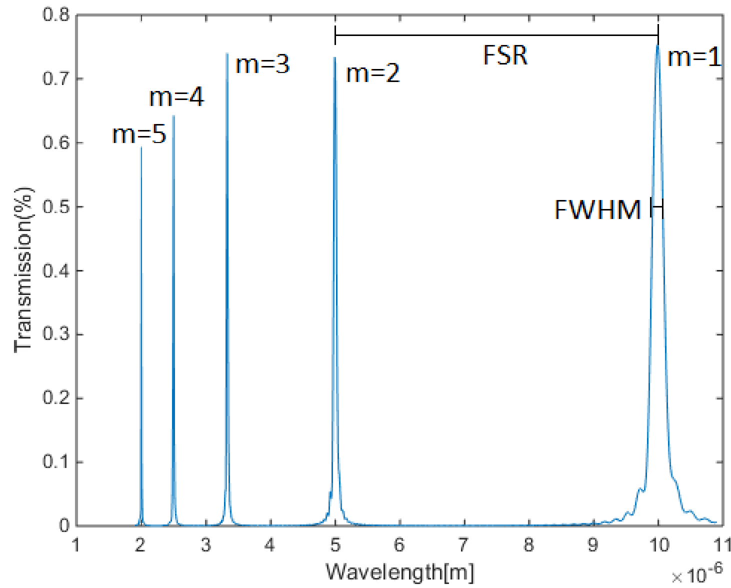

Figure 3.7: The spectral response of LVOF.

3.2.2. Reflectivity of two mirrors

Reflectivity of the mirrors have crucial impact on the resolution of LVOF. It is simulated in Figure 3.8 that the transmittance of LVOF changes with reflectance R of mirrors.

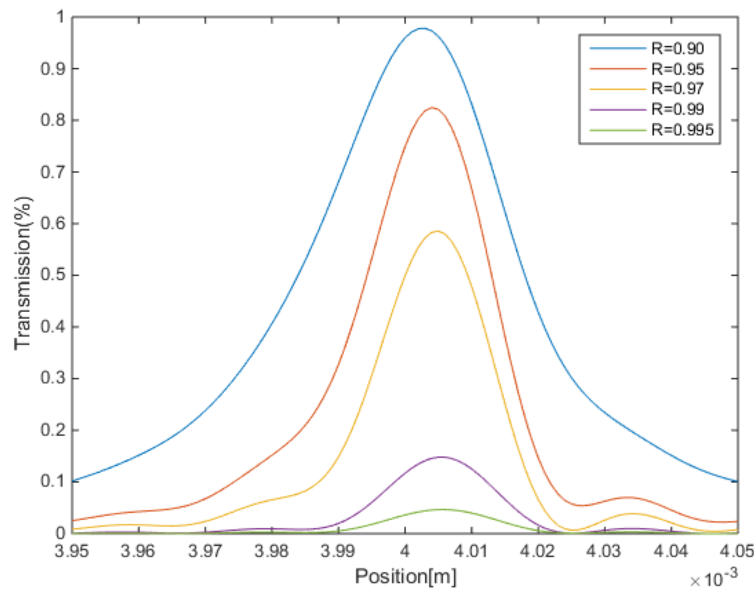

Figure 3.8: The impact of reflectivity of mirrors.

The LVOF is designed to with 1/1000rad tapering angle and 5mm in length which corresponds to 5µm of cavity length, which contains 5 order of interference. Assuming n'=1 and the incident light is normal with 2µm reference wavelength.

In Figure 3.8, peak transmission of LVOF reduces substantially from nearly 1 to 0.045 when reflectivity increases from 0.9 to 0.99, while the resolution increased a lot on the contrary. Besides, the position where peak transmission should occur shifts to right slightly. The transmission curve shows asymmetric broadening around 4µm and side peaks appear.

It can be explained by the walk-off effect of beams traveling inside the resonant cavity.

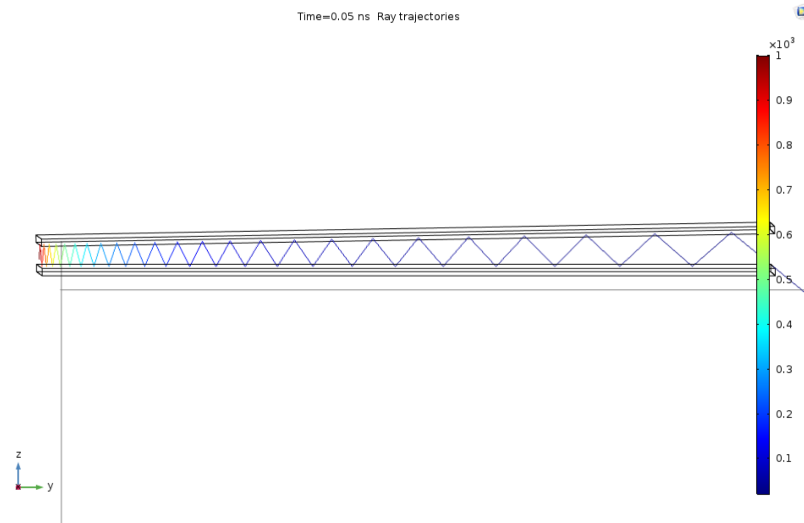

Figure 3.9: The walk-off effect.

The walk-off effect can be attributed to the fact the incident lights shifts laterally at every reflection in a wedged structure. By comparison with the parallel FP filter, only limited number of beams can interfere with each other before they goes out of the resonant cavity [42]. High reflectivity of mirrors intensifies the effect and causes the huge decrease of transmission. Moreover, the formula for the position where peak transmission occurs can be expressed in another way according to [43]. It uses a similar method but reveals the relation between the x position and propagation angle more clearly.

$$x = -\frac{\lambda}{S}(1 - \frac{{\theta_N}^2}{2n^2}) + \frac{m\lambda}{2n'\alpha} \tag{3.27}$$

Where S is the wavelength slope $S = d\lambda/dx = \alpha\lambda/h$, $theta_N$ is the propagation angle which is resulted from the multiple reflection of beams on the flat side of LVOF. Since the angle increases by 2α each time, it leads to the position shift according to the quadratic relation between x position and propagation angle in formula. That is the reason for the asymmetric broadening.

3.2.3. The number of reflections (p)

Figure 3.10 shows the transmission distribution along the length of LVOF with various p. Since the simulation about the performance of LVOF is based on numerical calculation, the meaning of larger p is that the calculation result is more accurate. It can be observed from the figure that when p is larger than 100, the calculation results tend to maintain stable, without much change. On the other hand, physically larger p means that the beam is reflected more times which is equivalent to higher reflectivity of two mirrors. Thus, intuitively the result should decrease as less beams can travel through.

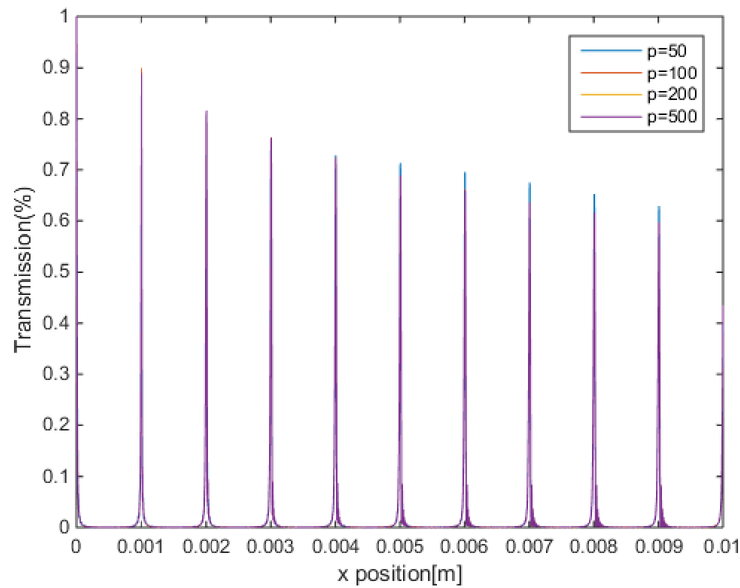

Figure 3.10: The number of multiple reflection p

3.2.4. The thickness and tapering angle of resonant cavity

The thickness of resonant cavity directly determines the wavelength that can pass through the optical filter and the position where the peak transmission occurs. With same length, various change of thickness along the length of LVOF can be obtained by using different tapering angle as shown in Figure 3.11.

Assuming normal incidence with the reference wavelength of 2μm, n'=1 and reflectivity of mirrors is 0.96. The p is selected to be 50. Another thing needed to pay attention to is that, the formula calculating transmission distribution of LVOF which has some thickness at starting point is a bit different from the one which is already given. z in 3.17 should be replaced by (z+initial thickness of LVOF) to show that it not start from wedge apex.

Comparing a and b which shows the first 10 order of interference, the transmission peak for the thinner LVOF is higher than thicker one. That makes sense because beams in resonant cavity of thicker LVOF shift laterally more than in thinner one at each reflection, which strengthens the walk-off effect that beams travels out of LVOF faster. Furthermore, Figure c and d shows the first order of interference with tapering angle of 1/10000rad which is 10 times larger than before. It is easily found that the distance between the x position where the neighboring order of interference occurs is extended by 10 times as well, which represents the corresponding length of resonant cavity for first order remains same. It is consistent with the results of 3.17 and 3.19. Besides, the resolution in a is better than in b due to similar reason to last case. The tapering resonant cavity in b is much sharper than in a, when beams travels in it they are easier to be reflected which leads to stronger walk-off effect.

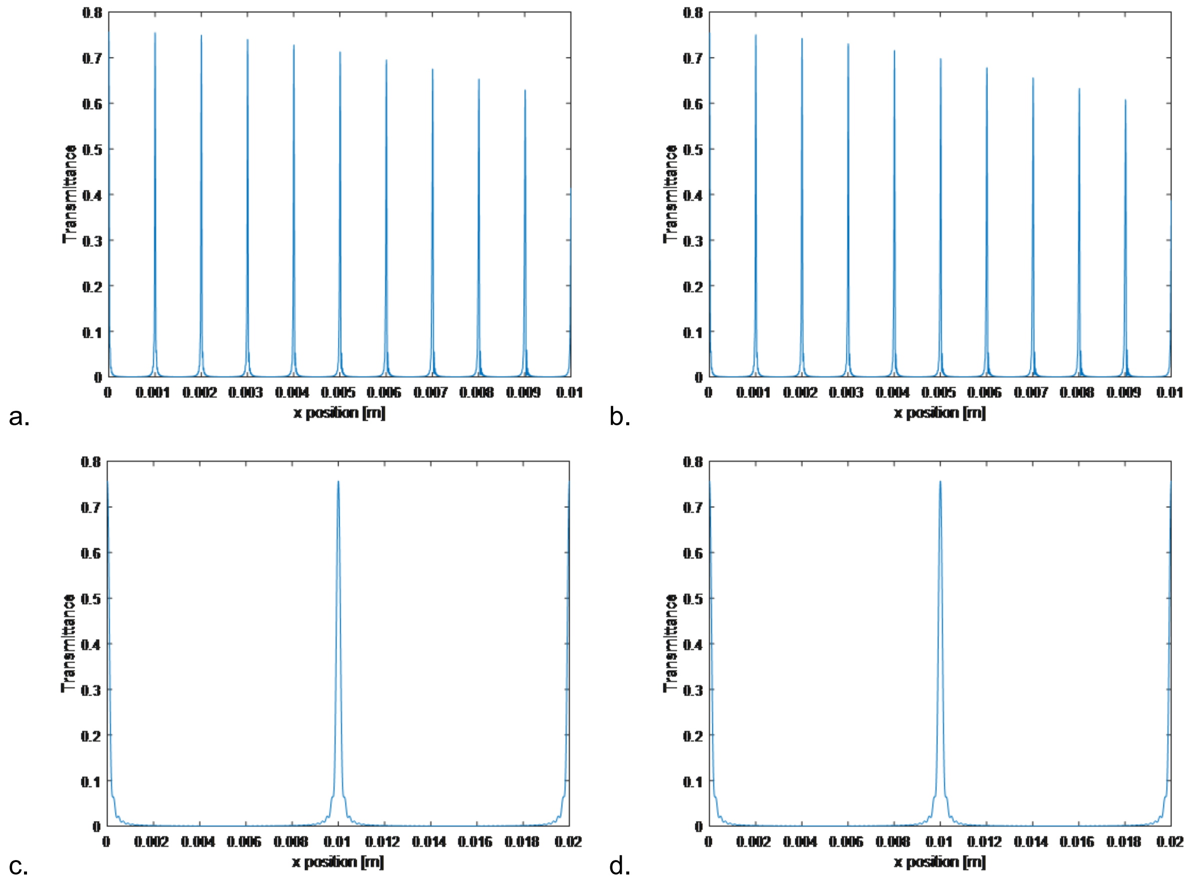

Figure 3.11: Transmission distribution along the length of LVOF with normal incidence. a. The thickness change along the LVOF is 0-10μm with 1/1000rad tapering angle and 10mm length. b. 40-50μm with 1/1000rad tapering angle and 10mm length. c. 0-2μm with 1/10000rad tapering angle and 20mm length. d. 4-6μm with 1/10000rad tapering angle and 20mm length.

3.2.5. Incident angle

In all previous numerical simulation results, it is assumed to be normal incidence. In fact, the resolution or, put it another way, the sharpness of fringe depends on the incident angle to a high degree. As mentioned above, beams traveling in the resonant cavity will be reflected multiple times and shift laterally due to the non-parallelism of two high reflective mirrors, and finally get out of LVOF. This is called walk-off effect and the positive incidence will actually strengthen it and weaken the performance of LVOF. Since the propagation angle is increased by 2α at each reflection, a positive incident angle as well as the normal incidence will push beams away from the wedge apex fast from the very beginning. Comparing Figure 3.12 with case of normal incidence shown above, the peak transmission decreases by maximum more than 25 percentage and drops down very quickly, which is an obvious proof.

On the contrary, a negative incidence angle will push beams close to wedge apex and cancel the walf-off effect. Thus, the optimum incidence angle must be negative. Nevertheless, after several times reflection, the negative angle is increased by multiple 2α and becomes positive again. A more negative angle will even have similar effect to small positive angle, as shown in Figure 3.13.

For positive incidence from normal to 5°, not surprisingly the transmission peak keeps decreasing from nearly 0.75 to 0.58 and FWHM becomes wider. However, for negative incidence from normal to -5°, the transmission peak firstly increases slightly and then backs to the value of normal incidence with almost no change in FWHM. The maximum transmission peak occurs when it is -2°. It then tends to decreasing and FWHM again becoming wider which is similar to the effect of a positive incidence angle. Comparing the case of -5°and 10°, it can be found that the asymmetric broadening is towards to opposite direction.

In this thesis, the IR source is a long and thin hot wire that put underneath the LVOF, which means the incidence angle of lights that impinging into LVOF can be any possible values. The largest incidence angle comes between one end point of hot wire and the other opposing end point of LVOF. it can be positive or negative.

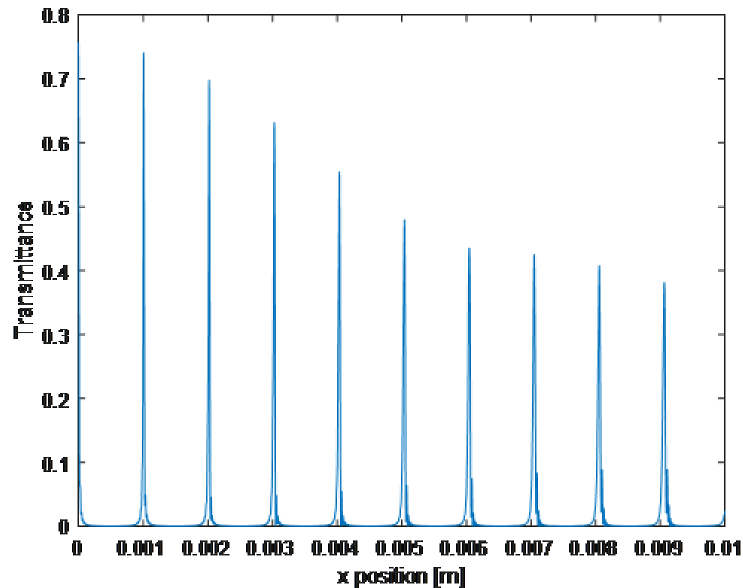

Figure 3.12: Transmission distribution along the length of LVOF with 5°incidence. The thickness change along the LVOF is 0-10μm with 1/1000rad tapering angle and 10mm length.

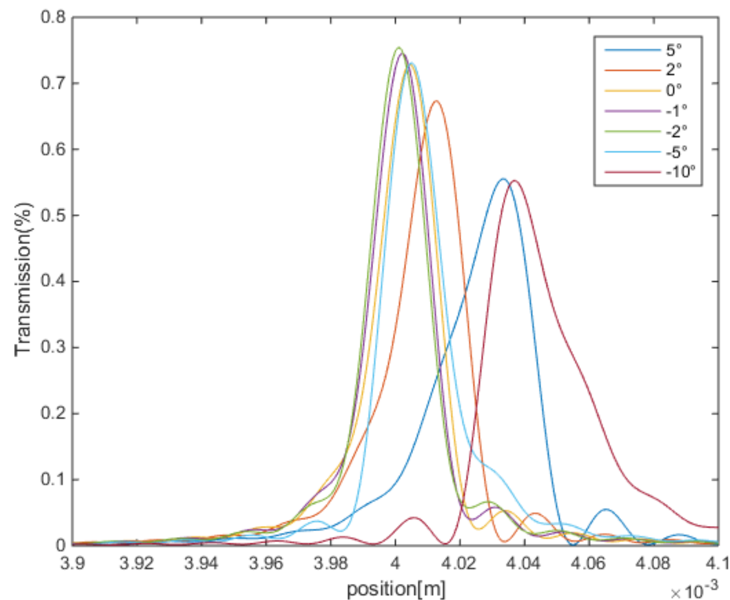

Figure 3.13: The forth order transmission peak with multiple incidence angle.

3.2.6. Cone angle

So far it is assumed that the incident light is fully collimated and only has one incident angle when it impinges into LVOF each time. However, limited by the condition in practice, the incident beam always diverges into a small range of angle which is the cone angle. The

power involved in original beam is equally distributed to each component beam with different angle. It is a bit similar to the case of multiple incident angle, but one of the biggest difference is each beam of different incident angle has equal and independent power that they do not share the energy from common single beam of light source. So if the incident beam has the cone angle β, which can be divided into several beams with 0.1°step in incident angle as shown in Figure 3.14. The effect of cone angle can be simulated. The result is shown in Figure 3.15.

Except the one mentioned before, there are more differences between cone angle and incident angle in terms of interference. For beams with different incident angle, they can not interfere with each other. It is assumed that they come from different spot sources that far away from each other. From the view of basic theory of interference, they don't have constant phase difference that required by interference. While for cone angle, it is assumed that beams within the cone angle come from one spot source or two adjacent source that have constant phase difference, so that they can interfere with each other.

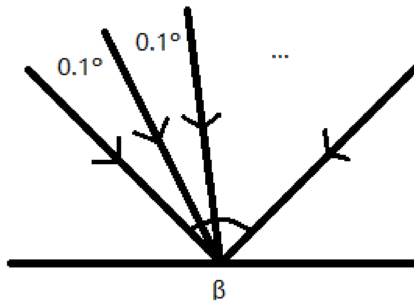

Figure 3.14: Cone angle

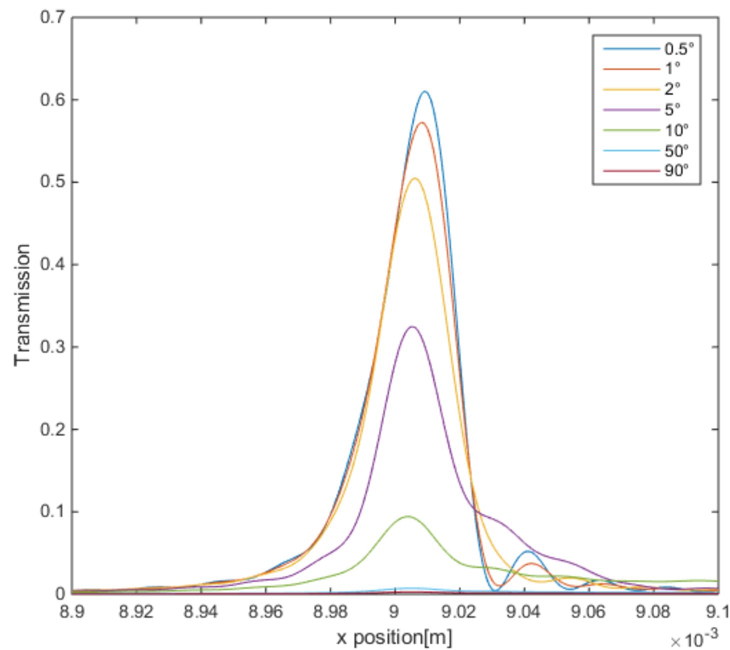

Figure 3.15: The effect of cone angle at 9th transmission peak.

In this simulation in 3.15, cone angle is set to 0.5°, 1°, 2°, 5°, 10°, 50°and 90°. With larger cone angle, the transmission decreases more, which is consistent with the conclusion before. Since LVOF is nonparallel structure, beam component with larger incident angle promotes

travel effect which pushes light beam going to one side of the structure. That reduces the transmittance.

3.2.7. Separation between LVOF and detector

The phase difference between transmitted beams varies not only along the x axis, but also z direction which represents the distance between LVOF and detector array. It comes from the last half of formula 3.17 for calculation of phase difference. The result is shown in Figure 3.16.

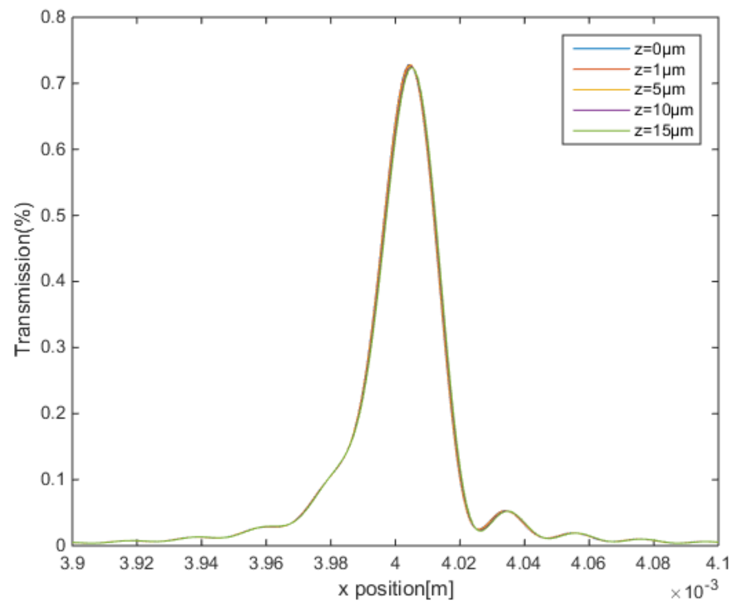

Figure 3.16: The forth order transmission peak with multiple separation between LVOF and detector.

There is indeed some variation in transmission peak for multiple separation, but it is too small to be considered about. The reason for it is that the change of separation is in order of micro meter which is very tiny to induce large deviation on transmission peaks. When the separation is increased to the order of millimeter, the effect will become apparent and has to be taken into account. By then, the separation between the LVOF and detector array also depends on the incident angle which is not discussed in detail in this thesis.

3.3. LVOF with hot wire light source

In the most simulation above (except for the cone angle one), the light is assumed to be well collimated that beams are almost parallel when hitting the surface of LVOF. Thus, each x position on the side has same initial incident angle. However, the situation is changed when the hot wire is used as the IR light source.

Since hot wire is the long rectangle light source that placed just underneath LVOF, which means every point on it can be regarded as an independent spot source. Thus, each x position on the surface of LVOF can accept the IR light from them with different incident angle which depends on the relative position between the x position on LVOF and the interested spot source on hot wire. Furthermore, as mentioned before, each incident beam also has its own cone angle effect. Therefore, two aspects has to be taken care of when focusing on the incident IR intensity at one x position on LVOF. One is the multiple incident beams from each spot on hot wire. They have same and independent intensity and do not interfere with each other, which means the resultant total incident intensity can be simply obtained by adding them up. Moreover, since the hot wire has limited length, the range of incident angle on one x can be easily calculated. The other aspect is cone angle effect. As mentioned before, every

step in one cone angle share same original incident intensity. It can cause the decrease on transmittance due to travel effect when cone angel is large.

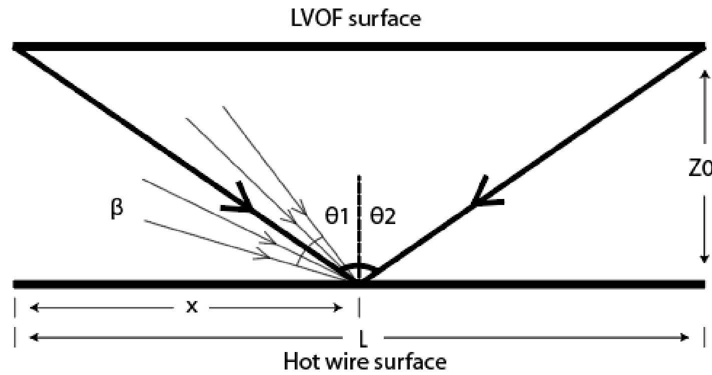

Figure 3.17: The calculation schematics of transmittance on LVOF with hot wire light source.

Compared to the collimated incident light with single incident angle, the situation now becomes much complicated. The θ' in 3.17 that represents incident angle has to sweep over multiple incident angles and cone angle of each of them. As shown in Figure 3.17, the hot wire is designed to be at same length as LVOF and aligned with it. At x position, the first sweep is for multiple incident beams within two ends on hot wire. θ_1 and θ_2 is the left and right bound. It can be easily got from,

$$\theta_1 = atan(\frac{x}{z_0}), \theta_2 = atan(\frac{L-x}{z_0}) \tag{3.28}$$

The second sweep is for cone angle β. It's usually a very small number to get higher transmittance. As mentioned before, the cone angle can not be too large to interfere. In this simulation, cone angle is set to 0.5°with step of 0.1°while incident angle has the increment of 1°from θ_1 to -θ_2.

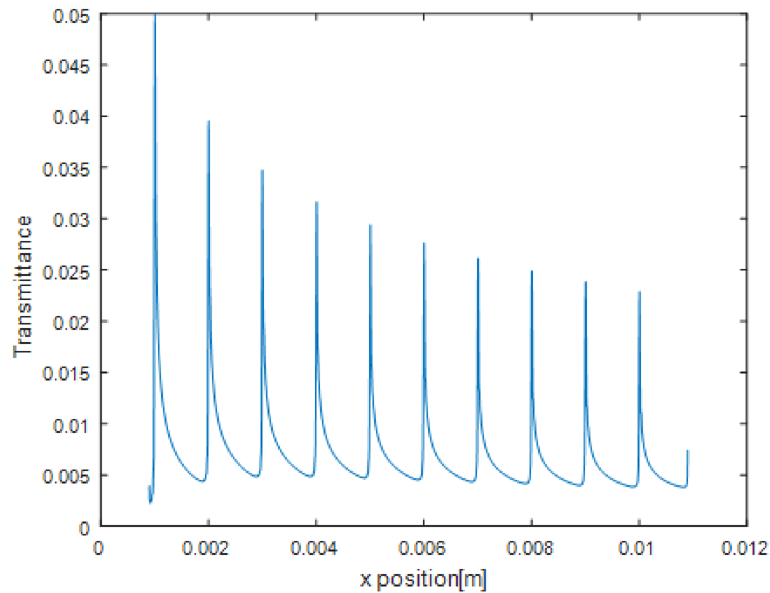

Figure 3.18: The transmittance of LVOF with hot wire light source. α=1/1000, length =10mm, rising from 0.9μm thick to 10.9μm thick. R=0.96 while T=0.04.

The simulation result is shown in Figure 3.18. The spacing between them is 5μm and cone

angle is 0.5°. For comparison, one FP filter of 1µm thick which is under the same condition as LVOF is also simulated and shown in Figure 3.19. Incident wavelength is 2µm.

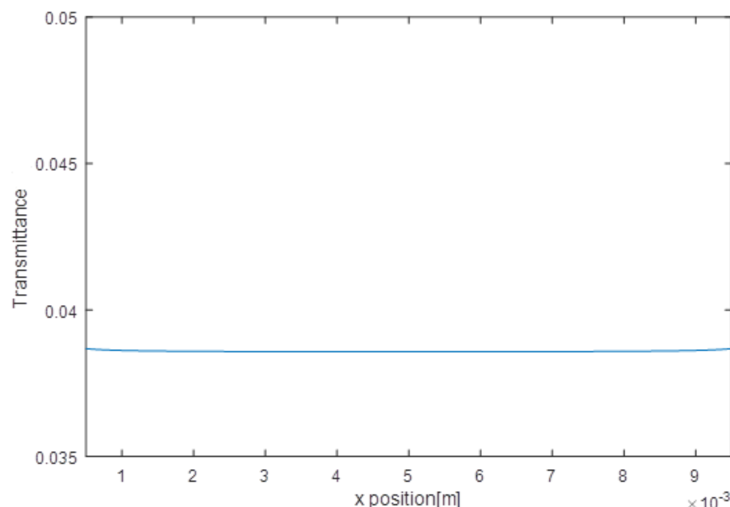

Figure 3.19: The transmittance of FP filter with hot wire light source. The thickness is 1µm.

The transmittance of LVOF in this case is much smaller than before. It is only 0.05 over 1 at first order of peak and 10 times larger than where the light should not pass, but the trend it changes along x position is similar to before that transmittance gradually decreases. Comparing to FP filter, it can be found that the highest transmittance in LVOF is 20% larger than in FP filter. The reason might be the gain effect in LVOF. The light beam that can not pass at one point on LVOF can keep traveling until where it can pass. It can collect more beams at that point which might slight increase the transmittance.

As for the extremely small transmittance, one possible reason is that, the range of incident angle is very large from one side of hot wire to the interested x position on LVOF. As mentioned before, a large incident angle can significantly intensify traveling effect that deduces transmittance. Since both hot wire and LVOF is long, the bound of incident angle at center point on LVOF is nearly 90°. Besides, the cone angle effect involved further makes it worse. Also, it might be some unknown mistakes in calculation. That is not certain yet.

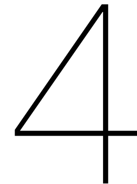

Layout design and fabrication of Polysilicon hot wire emitter

The planar process is the basic fabrication technology of IC and MEMS devices. It allows two-dimensional fabrication of structures on the silicon substrate with the application of photolithography, and additive and subtractive steps such as deposition, etching, and doping [44]. In this chapter, the fabrication flow of hot wires and LVOFs is introduced. Firstly, The layout design of masks used for hot wires is presented. Next, the detailed explanation of the fabrication of hot wire and LVOF is presented. Thirdly, the wire-bonding on the chip, which connects hot wires to power supply outside is discussed.

4.1. Layout design

One important step in fabrication flow is pattern transfer. By applying photolithography technology, pattern is transferred through masks to the wafer and designed structures are then formed by following few steps. The fabrication of polysilicon hot wire is based on four masks, which are combined and shown in the Figure 4.1. These are polysilicon mask (brown areas), doping mask (pink areas), interconnect mask (black areas) and SiN mask (yellow areas) which is used as the spacer between the hot wire and LVOF that put above. The chip area is selected to be 10 mm x 10 mm.

The printed polarity of masks including bright-field and dark-field must be selected. It decides that either the designed structure or its negative is performed on the mask. Besides, it is also related to the selection for polarity of photoresist and the following substractive and addictive processing [45]. In this case, positive photoresist is selected and the polarity of masks were chosen accordingly. Here the polysilicon mask and IC masks were dark-field (inverted) and the doping and SiN masks were bright-field. After the deposition of aimed material in the following addictive processing, all devices are thereby shaped in those areas.

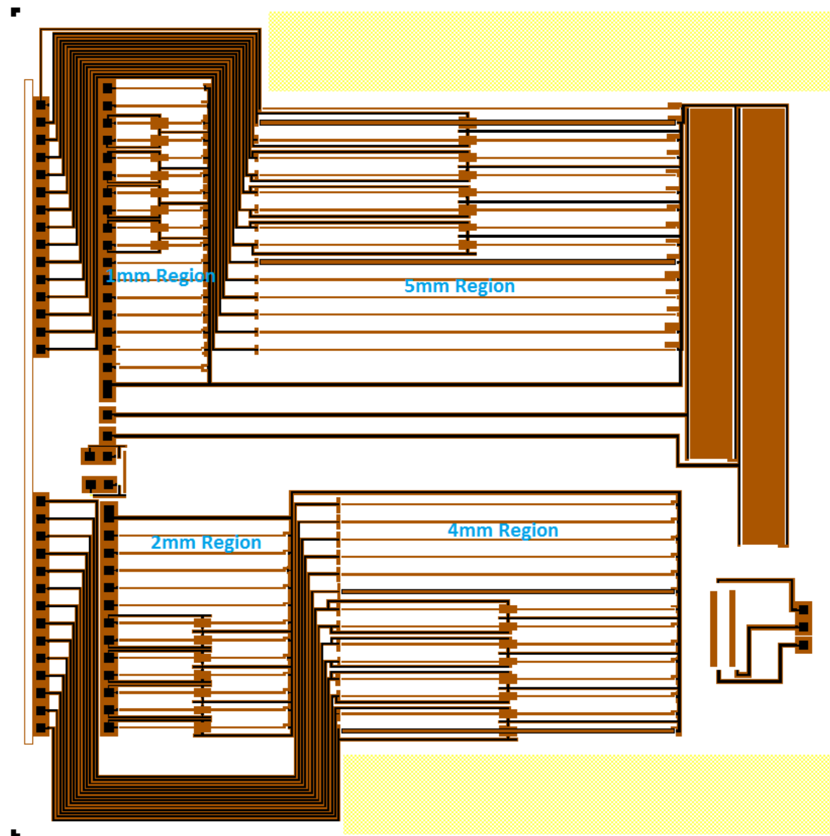

Figure 4.1: All four masks for fabrication of hot wire.

The polysilicon layer which lands on the SiO_2 layer is separated into 4 regions for 1mm, 2mm, 4mm and 5mm long wires respectively. All design plans of hot wire listed in the chapter 2 are involved. In the Figure 4.1, hot wires are thin and long polysilicon lines placed in sequence. Meanders at both ends and lateral sides connect them to the polysilicon layer. There is enough space between any of two devices so that they can work independently without any mutual effects. Specially, two distinct 4mm and 5mm hot wires are placed in the right side of the layout. They are comprised by 500µm hot wire arrays which are densely placed right next to each other as shown in Figure 4.2. It is regarded as no space between those 500µm hot wires and thereby making up much wider 4 and 5mm hot wires. Compared to the normal thin and long hot wires, it is more mechanically stable and thermally uniform since 500µm hot wire is relative shorter and can endure more mechanically uncertainties. For 4 and 5mm hot wire, there is 200 and 250 500µm hot wires in array respectively.

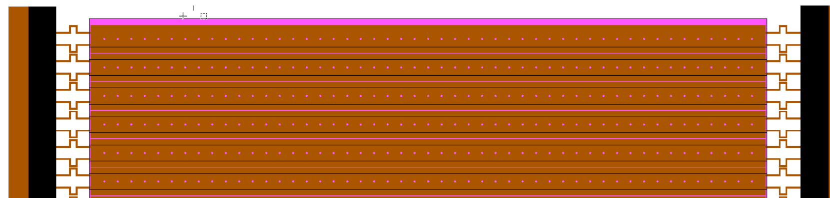

Figure 4.2: Hot wire comprised of array of 500μm hot wires.

In addition, since all hot wires are suspending above the SiO_2 layer, array of small holes are left on them to make the way for etching solution touching the underneath oxide layer and resolving it as shown in Figure 4.3. The radius of hole is 1µm and they are 10µm away from both neighboring holes and the edge of hot wire, to guarantee the level of under-etching on SiO_2 is uniform at all directions.

Except hot wires, polysilicon frames are used to sustain the IC lines on top of it. Similarly, the distance between those polysilicon frames is minimum 10µm to avoid mutual effects. Most importantly, to relief the effect of under-etching on polysilicon and make sure enough polysilicon support left after etching, it has to be 10 to 20µm wider than the IC lines, which is also shown in Figure 4.3. Thus, the polysilicon frame is 5µm wider than IC line on both sides.

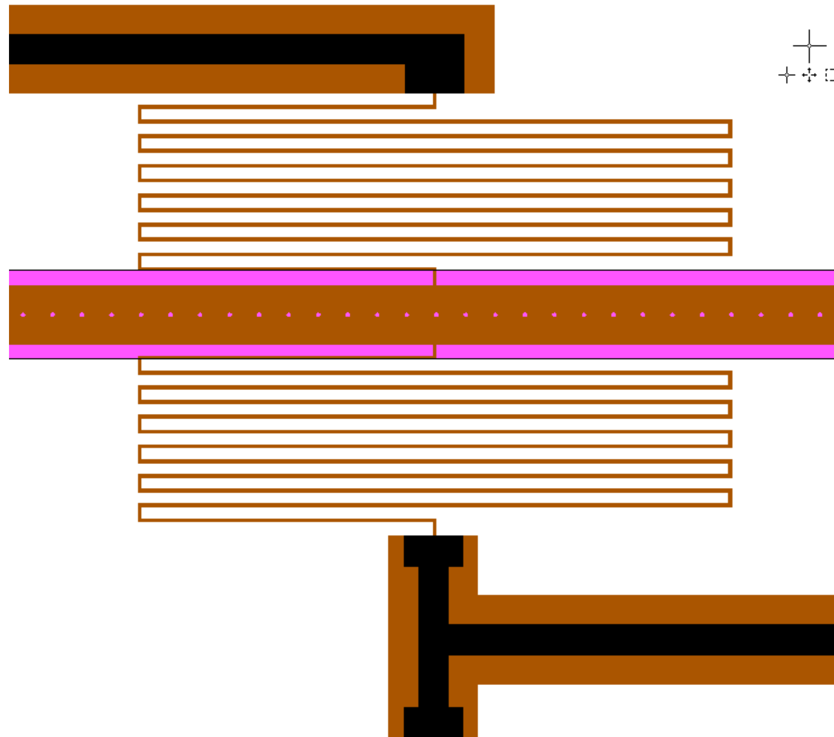

Figure 4.3: Holes on hot wire.

To satisfy the requirements of heat generation at different areas on hot wire, they have to be in different doping level. Thus, the resistivity varies across those regions. The mask for doping is represented in pink in Figure 4.3. It covers the whole hot wire and 5µm wider than it at both sides. In processing, dopant is implanted into hot wires through the photoresist layer which is modeled according to the doping mask. The resist layer is about 2µm and the implantation is performed at a small angle, which causes the shadow area on polysilicon layer which is just beside the resist layer that no dopant can reach it. Thus, the doping layer is necessarily larger than original hot wire which leaves enough area for doping.

At the lower right of the chip, there are two special configurations that the doping area is discrete with various size. That can lead to the linearly changed doping profile along the hot wire which the doping concentration decreases firstly to the minimum then increases again. It can be seen in the Figure 4.4 that the doping area is small and dense at ends of first hot wire which is for the high doping level section of the symmetric doping profile, while it is large and coarse tending to the center which is for lower doping level. The second one is for a non-symmetric doping profile based on same mechanics.

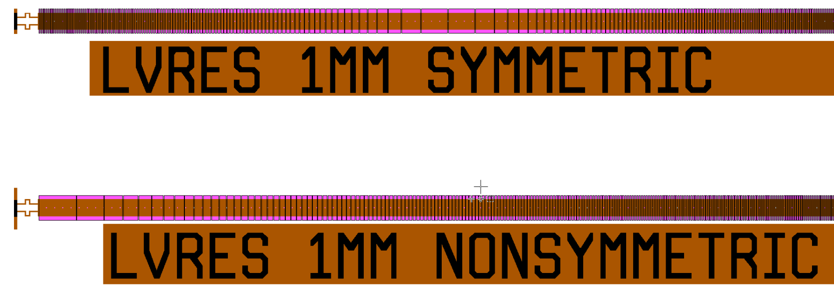

Figure 4.4: Mask for linearly changed doping profile.

As for IC lines, they are minimum 10µm black lines deposited on polysilicon frames that electrically connect hot wires to the outside power source through the bonding pad which is with the dimension of 100µm x 100µm. IC lines also connect plenty of ends of hot wire together to one shared ground for saving areas. In addition, IC line has to be wider than normal case where they connect meander ends for compensation of over etching, which is also shown in Figure 4.3.

The mask for SiN spacers are yellow rectangles at top and bottom sides. It is approximately 300nm thick that separates hot wires away from LVOF.

4.2. Fabrication process

Compared to some complicated MEMS structure, the fabrication of hot wire is simple and straightforward, but still many fabrication technology involved. Basically, the fab flow includes: first, the formation of SiO_2 layer on silicon wafer by thermal oxidation. The alternative choice is SOI wafer. Second, it is the deposition, pattern and doping of polysilicon layer. LPCVD is applied for deposition, hot wires and poly framed are then etched by plasma etching. Next, it is the deposition, pattern and etching for IC lines. The metal used here is aluminum and the method applied is LPCVD and plasma etching. The final step is for spacer by using similar flow as above, which contains the layer of SiN and SiO_2. In this section, detailed introduction to each step is given.

4.2.1. Thermal oxidation

All hot wires in this thesis are designed to suspend above the substrate, which means the layer right underneath the hot wire has to be removed in the final step. The technology applied here is surface micromachining [46]. Generally, it includes subsequent steps such as deposition of the structural and sacrificial layer , patterning, selective removal of sacrificial layer. Thus, the left structural layer which is the hot wire here can be suspending and the downmost Si substrate remains unaffected.

SiO_2 is widely used sacrificial material. It can be easily etched by hydrofluoric acid (HF). In a high temperature (900°C-1000°C) environment, Si can be oxidized by either oxygen which is called dry oxidation, or water vapour which is called wet oxidation. Both of reactions occur at the interface between the oxidation layer and Si substrate at the cost of consumption of Si substrate. In this thesis, wet oxidation is employed, SiO_2 which is used for sacrificial layer is deposited for 2-5µm.

4.2.2. Polysilicon deposition

Except the thermal oxidation, SiO_2 can also be formed by method of chemical vapour deposition. It mainly has four ways based on different mechanics including epitaxy, low pressure chemical vapour deposition (LPCVD), plasma-enhanced chemical vapour deposition (PECVD) and physical vapour deposition (PVD) which is also called sputtering. In this thesis, LPCVD is selected to deposit polysilicon layer, while PECVD is applied for deposition of oxide spacer layer and SiN layer.

The polysilicon layer is deposited by LPCVD for 300nm at about 500°C. The heat initiates the reaction between source gas and reactive material. Under the condition of low pressure,

the possibility of undesired gas phase reaction is reduced and the uniformity of deposited layer is then improved [47]. On the other hand, the major problem for LPCVD is the residual stress due to thermal expansion. After cooling, the deposited thin polysilicon film may not be identical to the substrate and cause the failure.

4.2.3. Doping of hot wires and bridges

The third step in the whole fabrication flow is the doping of bridges and hot wires. By the implantation of Boron, the electrical properties at corresponding areas are changed and the different resistivity profile required for thermal processes and uniform temperature mentioned before can be acquired.

Generally, the doping process includes two primary stages: implantation and diffusion. Dopant atoms such as Boron are ionized and further accelerated to bombard into the surface of polysilicon film and then induces the concentration gradient of Boron inside. Under the environment of relative high temperature, the dopant solutes in polysilicon film and keeps diffusing to deeper depth until the concentration gradient becomes zero, which requires much time and energy.Since the final concentration profile of dopant inside polysilicon film depends on the ion energy and dose of dopant which is initially given, to achieve the resistivity of 0.01Ω□cm on bridges and 0.0001Ω□cm on hot wire, the dose for bridges is 6e14 ion/cm^2 and the energy is 50keV. While they are 1e16 ion/cm^2 and 50keV for hot wires.

After the step of photoresist coating and soft-bake, the complete PR layer of approximately 2.1μm covers the wafer and the doping pattern is then transferred to it through the doping mask. Under the shield of PR layer, the implantation of ion beam of boron is confined in the designated area at a small angle. Since the doping mask is designed to be a bit larger than required, the full implantation over the area can be guaranteed.

In addition, cleaning of wafer to remove the residual PR layer is the necessary before performing each step of coating, etching, deposition or furnace. For removal of implanted or plasma etched PR layer, Tepla stripper is employed. While for wafer has contact with metal such as Al (1% Si included) which is used as interconnect, solution of 99% HNO_3 (Al) is used.

4.2.4. Etching of polysilicon

After patterning the wafer with polysilicon mask, the polysilicon layer is then etched to the designated structure. Similar to doping, it is firstly patterned for hot wires, bridges and poly frame. The PR layer used is same 2.1μm thick. The etching method applied is plasma etching which is also called dry etching which is based on the establishment of glow discharge to create reactive ions in gas phase. The material to be etched is then exposed to the bombardment of those ion beams and the corresponding reaction occurs at aimed area. The resultant volatile product is then pumped away and this area is thereby dissolved.

Compared to wet etching, plasma etching is an anisotropic process that etches at different rate in directions. It is less selective and more expensive than wet etching. Nevertheless, it is more controllable and repeatable which makes it more suitable for defining a small size structure. The rate of plasma etching can be controlled by energy given to accelerate ion beams.

The final step of process of polysilicon layer is the drive in annealing. As mentioned before, doping in polysilicon includes implantation and following diffusion of dopant which happens during annealing in furnace. Dopant immigrates deeper into structure, some damage can be repaired in this step as well. The property of the structure is therefore further improved. Of course, the wafer has to be carefully cleaned before getting into furnace.

4.2.5. Interconnect

To establish the interconnects, the wafer is coated with 675nm aluminum layer containing 1% silicon on polysilicon layer. Si is added to prevent spiking. The layer is then patterned and etched by plasma etching to the thin lines that connect devices to power source.

After another cleaning, alloying is performed in N_2/H_2 environment at about 400°C. This step can not only improve the contact between Al and Si, but also passivate the Si/SiO_2 interface.

4.2.6. Spacer

The spacer that separates hot wires and the LVOF comprises of two layers. A silicon nitride mask of 300nm is deposited on top of SiO_2 spacer layer of 5-10μm. Since silicon nitride is stiff, thermally stable and hard to etching, it is used as the mask for wet etching to SiO_2, which is put the upmost.

The deposition method for both two layers is PECVD. PECVD can form dielectrics from gas state to the solid film conformally on the substrate by chemical reaction at relative lower temperature. The basic schematics is also glow discharge and plasma bombardment. The gas mixture required for the formation of oxide spacer layer and silicon nitride mask is SiH_4 and N_2O, NH_3 and SiH_4 respectively [48, 49]. Except the fast speed as mentioned above, thin film made by PECVD usually has smooth surface and good uniformity. Good reproducibility and processability are two of its advantages.

Silicon nitride mask is then patterned and etched by plasma etching to prepare for the wet etching to all SiO_2 layers.

4.2.7. Removal of SiO_2 layers

So far, totally two $SiO_@$ layers exist in the structure. One is used to support the thin polysilicon film, meanwhile as the insulator between poly layer and substrate. While the other one is used as the spacer layer which is defined by silion nitride mask above. By vapour HF (VHF) etching, both of SiO_2 can be removed.

Vapour etching is a process that uses vapour of HF to remove material of specific pattern. HF gas reaches the selected material and reacts with it which is then etched. Thus, it is quick, cost-efficient and well as easily implemented. In this case, The part of area of top SiO_2 that is protected by silicon nitride mask can survive, while the one underneath the polysilicon film can be etched by chemical solution through array of small holes that is intentionally etched on hot wires.

Generally, Wet/vapour etching is an isotropic process which means it has same etching rate in all directions. By choosing the etchant carefully, it also has a higher selectivity comparing with dry etching. For instance, it can only etch metal layer without influences on oxidation layer on bottom. However, it is hard to fully control and sometimes leads to a high defect on wafer, which makes it usually been used in uncritical processes.

4.3. Fabrication results

The devices fabricated on polysilicon film are presented in Figure 4.5. Comparing with design in chapter 1 and layout before, all design of hot wires, bridges and poly frames are basically consistent with the initial plan and fully achieved. Furthermore, it can be seen in c that the thin shadow under the edge of polysilicon frame for IC, which is the obvious present of underetching on SiO_2 layer. Besides, it is clear in d that there is 3.55μm shadow exhibiting under the hot wire. It shows the part of SiO_2 layer underneath is indeed etched away and the hot wire is suspending above.

However, as the result of limitation of equipment, operation environment and shipping,a bunch of typical fabrication failures happened on hot wires as shown in Figure 4.6.

Due to the fragile feature and long length of hot wires, they are easy to be broken during fabrication and shipping. Since only tiny bridges connect them to polysilicon film, the thermal expansion induced by high temperature in fabrication and small vibration in shipping can both cause the breakage. Some other influential factors exist as well. Besides, since the meander is as narrow as only 1μm but several tens of microns long, it is even much more fragile than hot wire and easier to be broken as shown in c. Fortunately, most of meanders are connected well and just tilt upwards. In addition, those broken debris may stay on the chip and cover IC as presented by black spots and lines in d. They are probably unknown particle or a scratch as well.

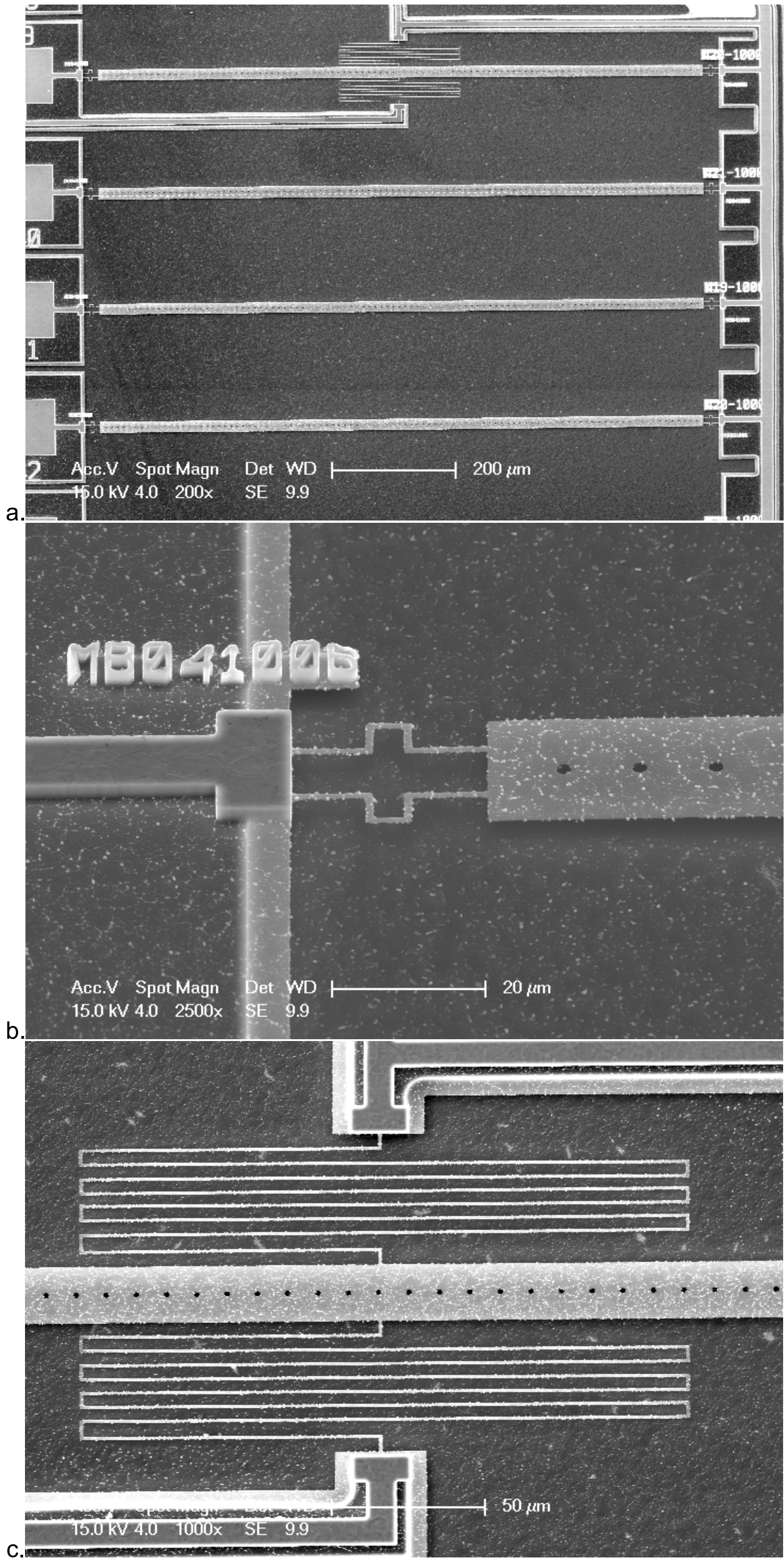
Acc.V Spot Magn Det WD 200 µm
15.0 kV 4.0 200x SE 9.9
a.
Acc.V Spot Magn Det WD 20 µm
15.0 kV 4.0 2500x SE 9.9
b.
50 µm
15.0 kV 4.0 1000x SE 9.9
c.

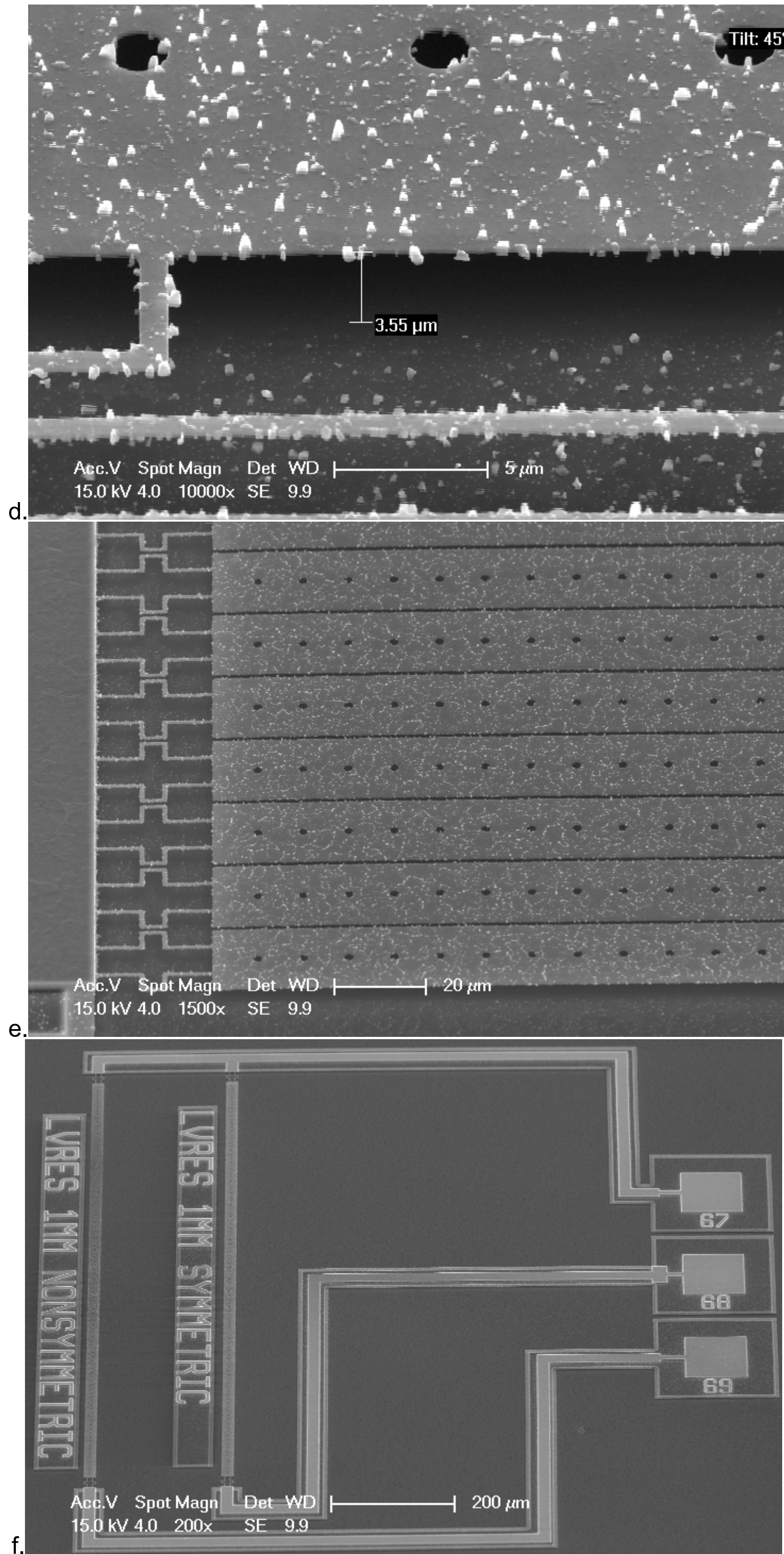

Figure 4.5: Fabrication results of hot wires on polysilicon film. a. 1mm hot wires. b. Bridge at end. c. Middle meanders. d. Under-etching on SiO_2 layer. e. 500μm hot wire array. f. two special hot wires with linearized resistivity profile.

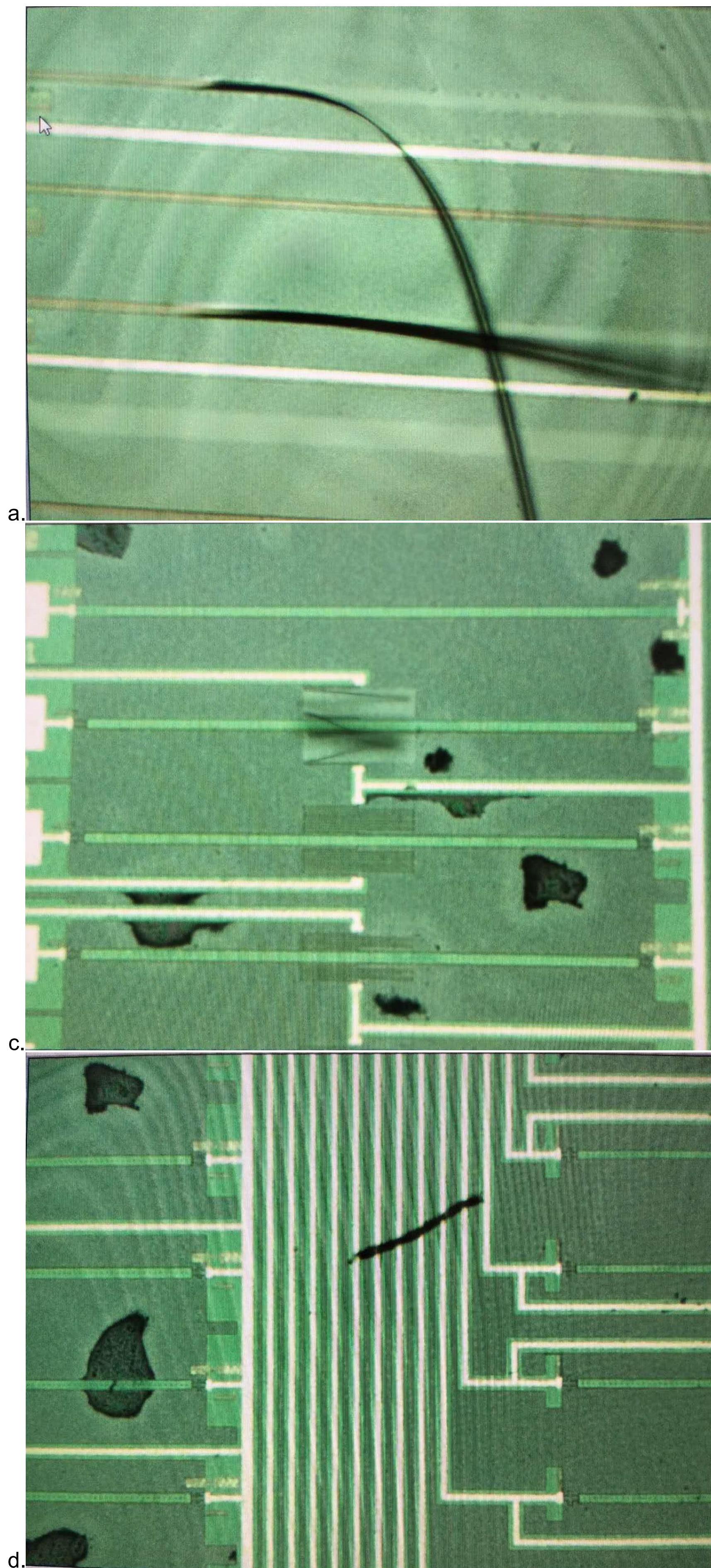

Figure 4.6: Fabrication failure of hot wires on polysilicon film. a,b. The breakage of hot wires c. The breakage of meanders. d. Impurities on IC.

4.4. Wire-bonding

The final step in the preparation for measurement is wire-bonding. The chip is stuck on the package with 40 pins. It connects devices to power supply by thin metal lead that stuck to the bonding pad at one end while the other one is stuck on the pin. The structure is shown in Figure 4.7. In order to avoid unexpected situations, few best-designed hot wires are connected repeatedly on different chips, while as many as possible different devices are connected as well. One important rule is the metal lead can not cross the hot wire which would affect IR measurement later.

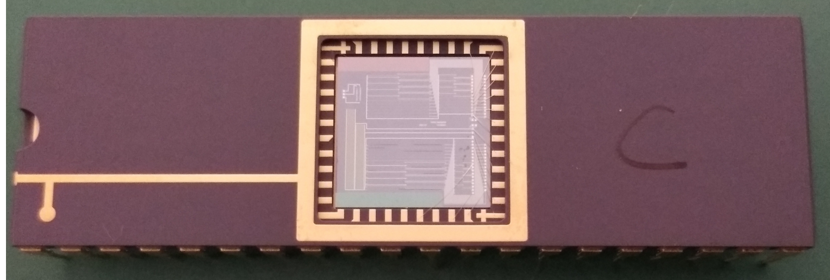

Figure 4.7: The complete package of chip.

5
Measurement and discussion

In this chapter, different measurement is exerted on devices to test their electrical and optical properties and performance. The measurement on the packaged chip is mainly divided into two sections: resistance and TCR of devices, and their IR emitting performance which they are designed for. First, the resistance of device is measured in room temperature and heated environment from which the real doping level, resistivity and TCR of device is acquired. Second, the intensity of IR they emit when electrically powered is measured under the condition of vacuum. By observing through an infrared camera (FLIR), the temperature distribution along the device can be obtained, which characterize its IR emitting performance. By comparing the results of simulation and measurement, the design of hot wires is verified, and all potential error sources which may cause the different between them are analyzed and discussed. Finally, the conclusion is drawn which will guide the future work.

5.1. Measurement on resistance

To get the specific and different heat generation of hot wire body and bridges required for a uniform temperature profile, the resistivity of these two parts is specially designed.

A resistivity of 0.01 Ω□cm for bridges and 0.001 Ω□cm for hot wire body, respectively were selected based on the simulation results. This resistivity can be easily achieved by implanting Boron into polysilicon. The relation between the doping level and resistivity is shown in Figure 5.1. Besides, the corresponding TCR can also be found according to experiment data in Figure 5.2.

The actual resistance of two devices were measured in the heated furnace. The 2 mm and 4 mm hot wires with meander bridges at ends were selected for this measurement. The test temperature rises from room temperature 25°C to 150°C with the step of 10°C and 20°C, respectively. The instrument used is Binder Oven FD53 and Keithley 2002 multimeter. The changed resistance of devices is collected and then fitted into curve in MATLAB, and the result is shown in Figure 5.3. Their resistance measured in room temperature is 39.692kΩ and 64.981kΩ. By applying equation 2.2, the actual resistivity can be calculated and the corresponding theoretical TCR can be found froom the figure.

From two fitting curves, it is obvious that the resistance of hot wire changes with temperature in the manner of quadratic polynomial. That is because the second order effect of TCR which is be presented in equation 5.1. Since the hot wire is in series with bridge, the summation of resistance of two parts is the total resistance. R_b and R_h are the reference resistance at 25°C. α represents the 1st TCR, while β in the equation represents the second order TCR effect that the resistance changes with square of temperature difference. Since hot wire is comprised by bridges and hot wire body which has independent resistance and resistivity, it has to be carefully dealt with.

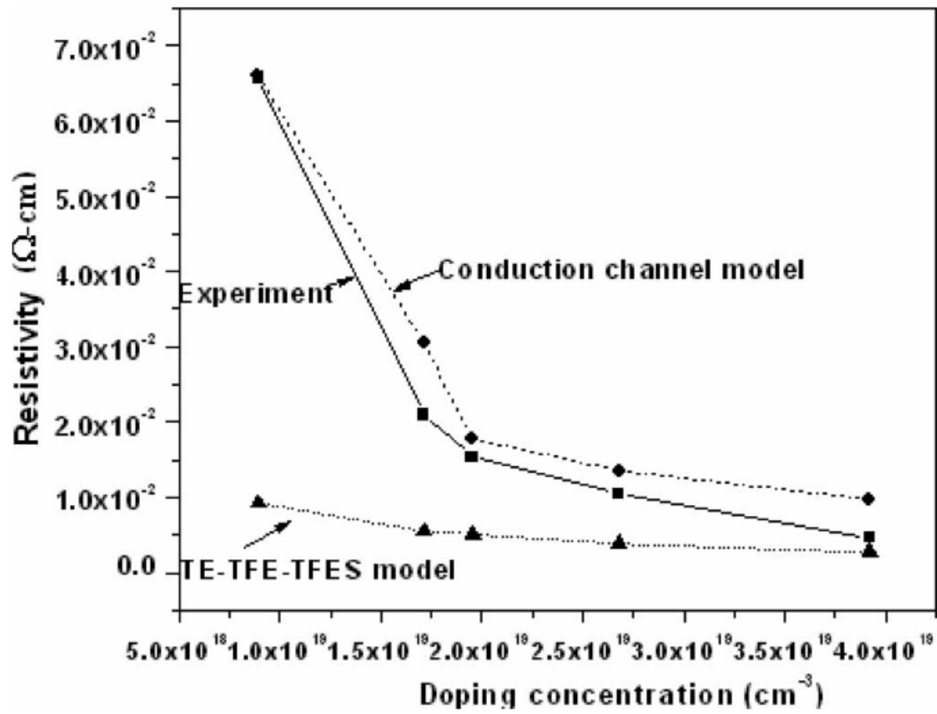

Figure 5.1: Resistivity versus impurity concentration for polysilicon [50].

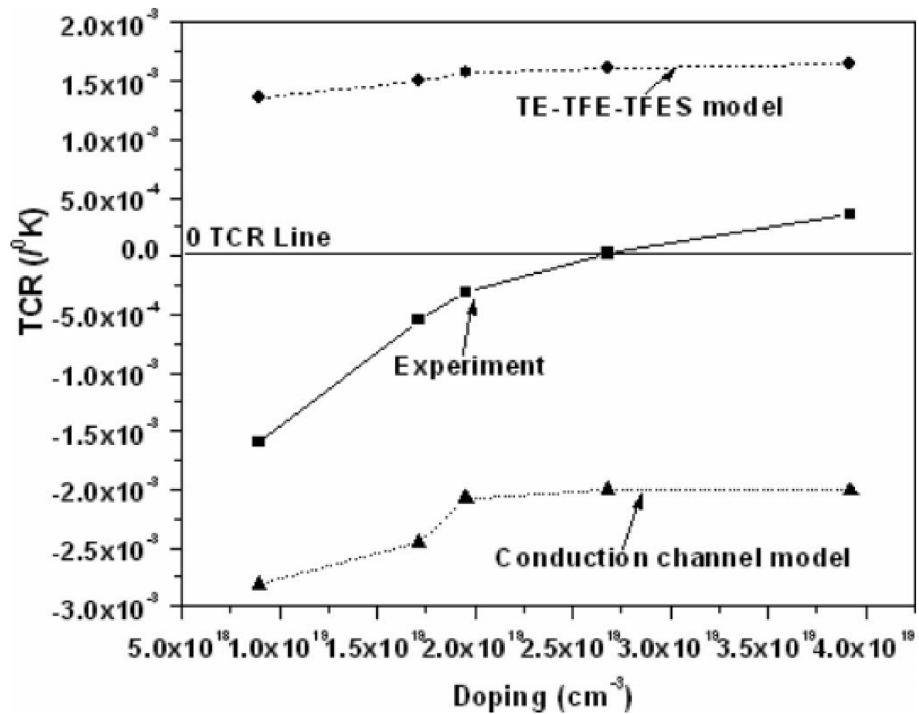

Figure 5.2: TCR verse impurity concentration for polysilicon [50].

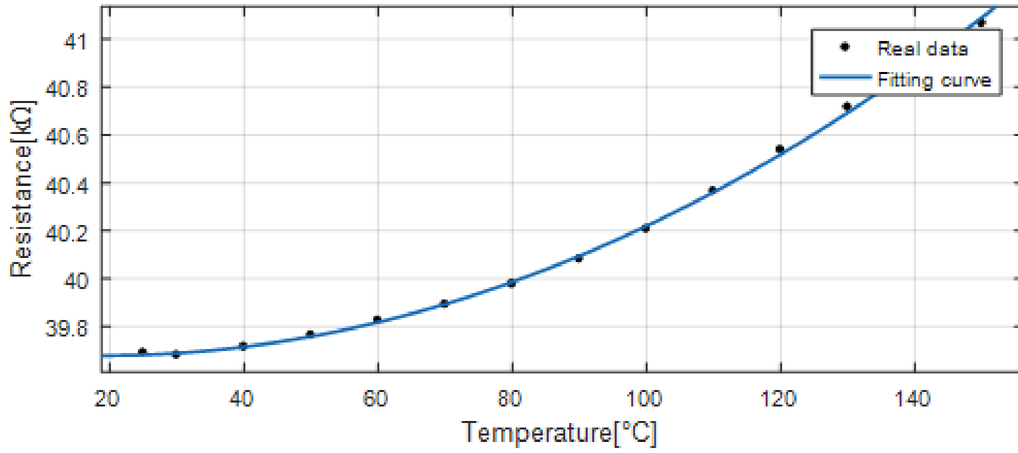

a.

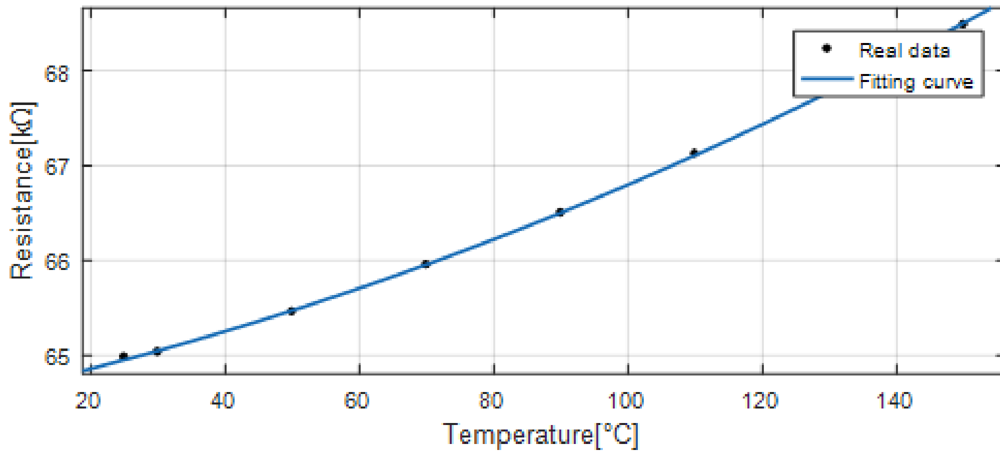

b.

Figure 5.3: The resistance changes with temperature. a. For 2mm hot wire. b. For 4mm hot wire.

$$
\begin{aligned}
R_{bridge} &= R_b(1 + \alpha_b \Delta T + \beta_b \Delta T^2) \\
R_{Horwire} &= R_h(1 + \alpha_h \Delta T + \beta_h \Delta T^2) \\
R_{total} &= (R_b + R_h) + (\alpha_b R_b + \alpha_h R_h)\Delta T + (\beta_b R_b + \beta_h R_h)\Delta T^2
\end{aligned} \tag{5.1}
$$

MATLAB can directly give the polynomial of fitting curve. By combining two equations and using 5.1, the first and second TCR of both bridge and hot wire body can be obtained. All results are shown in Tables 5.1 and 5.2.

Table 5.1: Measurement results on resistivity

	Resistivity designed[Ω·cm]	Resistivity measured at 298K[Ω·cm]
Bridge	0.01	0.0216
Hot wire body	0.001	0.0039

Table 5.2: Expected and measurement results of first and second order TCR

	Theoretical 1st TCR to measured resistivity[1/K]	Measured 1st TCR[1/K]	Measured 2nd TCR[1/K^2]
Bridge	-0.00053	-0.000666228	3.7614e-6
Hot wire body	0.00045	0.00113033	-1.41875e-6

According to Table 5.1, the actual resistivity for both bridge and hot wire body is 2 to 3 times larger than design. In fact, it happens to all devices. That makes sense that many unknown factors during fabrication can lead to insufficient implantation and diffusion, for instance short annealing time. But most important is the misuse of data for silicon, which is explained later.

On the other hand, the measured TCR of bridge has relatively good consistence with the theoretical value, while that of hot wire body has 2.5 times difference. That can be explained by the reading problem on extrapolation of experiment data. In the Figure 5.2, the TCR for the actual resistivity of hot wire body is beyond scale. What's more, the measurement result is not accurate enough. The error comes from inaccurate temperature (The accuracy of temperature shown on the screen of furnace depends on the position of thermal sensor and the time maintaining on it), data reading and so on. Actually, the drift is really a big problem on reading. The number keeps increasing or decreasing due to drift of multimeter (or maybe device itself), and intensively fluctuating due to noise. All of them might make the measurement result away from actual value. Besides, though the second order TCR is so small that it is even neglected in the first design consideration, it determines the changing trend of resistivity with temperature.

5.2. Measurement on IR emitting performance

5.2.1. Measurement set-up

The test on IR emitting from devices is conducted in the measurement set up shown in Figure 5.4. It is comprised of a vacuum chamber, vacuum pump, pressure gauge, electrical power source and a FILR IR camera. The chip is put into the chamber and then sealed. The air is then sucked by the vacuum pump that creates the vacuum environment. The pressure can be instantly observed by the pressure gauge. Thus, it can be controlled to some extent. A cable through a vacuum feedthrough connects the chip in the vacuum to the power source. On the other hand, IR camera is put right in front of the chamber's window, through which the temperature situation on devices can be photographed by the IR camera. The camera has to be focused and collimated before every use.

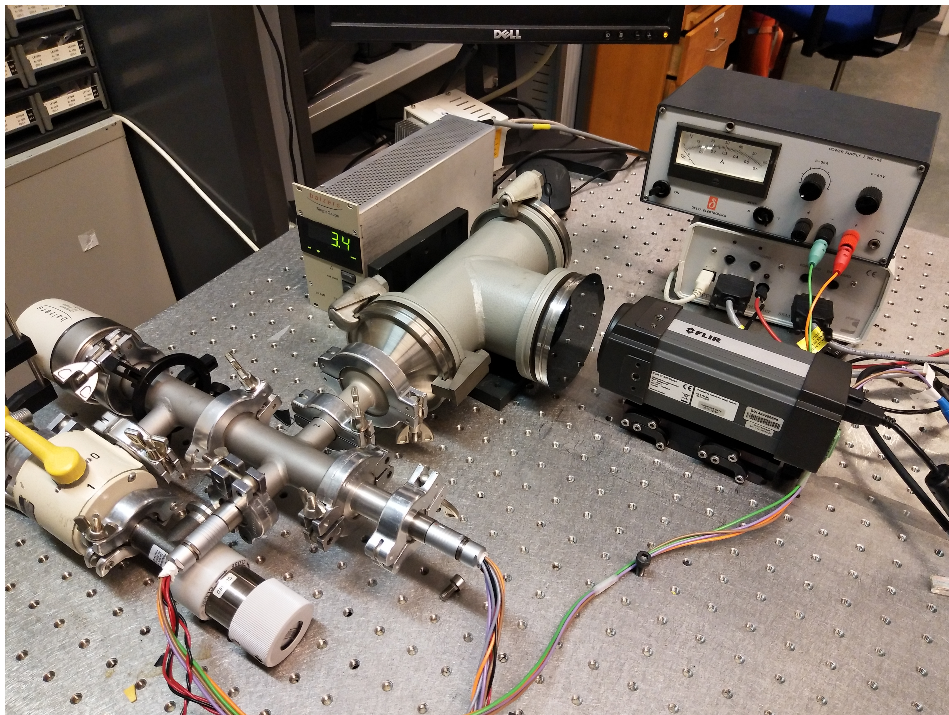

Figure 5.4: The measurement setup for IR emitting test.

One problem faced is the window on the cap. Originally, sapphire is used as seal on it. Unfortunately, nothing can be obtained on camera through it. Although the spectral transmittance of sapphire ranges up to 5µm which covers part of spectrum the device should emit, the camera is only sensitive from 7µm. Thus, a thin silicon window with a thickness of 525 /*mu*m is used which allows passing band from 1 to 10µm is used as the window. Since it is only about 0.525 millimeter thick, the attenuation of IR light in the window is negligible. However, it also leads to some potential danger while pumping down. The wafer might not survive from the sudden huge pressure difference between inside and outside and thereby break down.

As for instrument used, the vacuum pump is PFEIFFER D-35614 Asslar and the pressure gauge is BLAZERS compact full range gauge. It has broad range from 1bar to at least 0.01mbar. The FLIR IR camera is Thermalcam SC 3000. It is an advanced thermal imaging system that can capture, record and restore the thermal data on device at very high frequency up to 900Hz NTSC/750Hz PAL [53]. The quantum well infrared photodetector (QWIP) sensor in it has a image resolution of 320 x 240 pixels and thermal sensitivity of less than 20 mK at 30°C, which promises a high accuracy of data obtained.

5.2.2. The effect of pressure

The on-chip hotwire is initially designed as an IR source for the microspectrometers. Ideally, the temperature distribution on device should be as uniform as possible maintaining around 400°C based on simulation results. It means that a bright and thin line which has same color along its body should be observed through FILR IR camera. As mentioned before, in design stage in chapter 2, the heat conduction to surrounding air is not taken into account. All hot wires are designed under the condition of vacuum environment, and the heat transfer between device and remaining air is characterized by a heat flux boundary conditon, which only represents the heat convection to air.

However, heat conduction to air is in fact the most dominant factor that can determine the temperature magnitude and distribution on hot wire. At room pressure 1atm, air can absorb a large amount of thermal energy through it, the effect of heat convection is much less effective by comparison. Therefore, when device is heated and measured in air or relatively large pressure, only two bright spots at ends can be observed as shown in Figure 5.5.a.

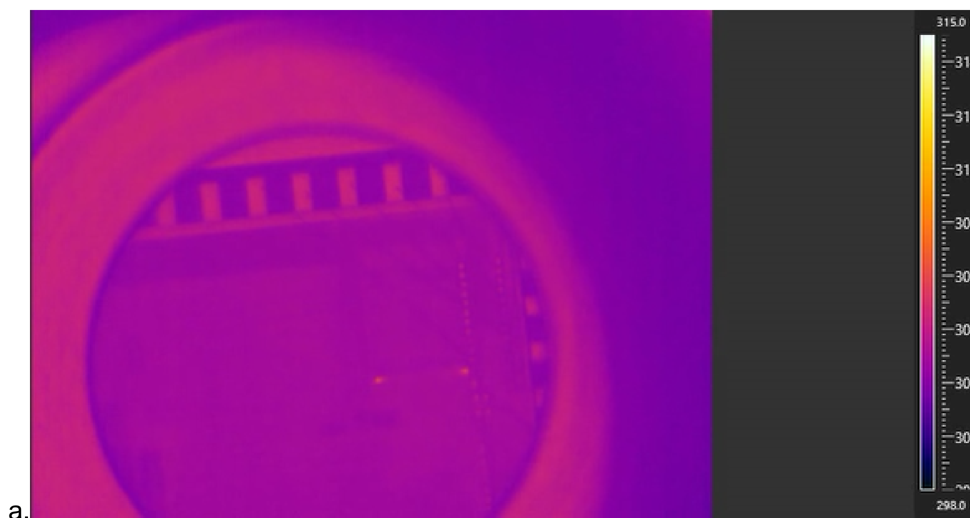

Figure 5.5: The change of temperature profile on hot wire with pressure from 1bar to 0.1mbar. The maximum temperature is fixed at 315K for better contrast. The hot wire used is 2mm long one with four meander bridges at two ends. Continued in next pages.

This is due to the fact that, although a large amount of thermal energy generated at the hot wire body and bridges, the heat is mainly conducted to air and cannot be maintained and transferred effectively to the body of hot wire.

By making the heat conductivity of air change with pressure, the effect of pressure can

be simulated. It is shown more clearly in simulation result in Figure 5.6.

At 1atm pressure environment, there is a large dip on temperature in middle due to heat conduction to air. The temperature is nearly room temperature and the max temperature at bridges is just 150°C. When it is more similar to vacuum (such as 0.001atm=1mbar), the temperature increases significantly and its temperature profile becomes more uniform.

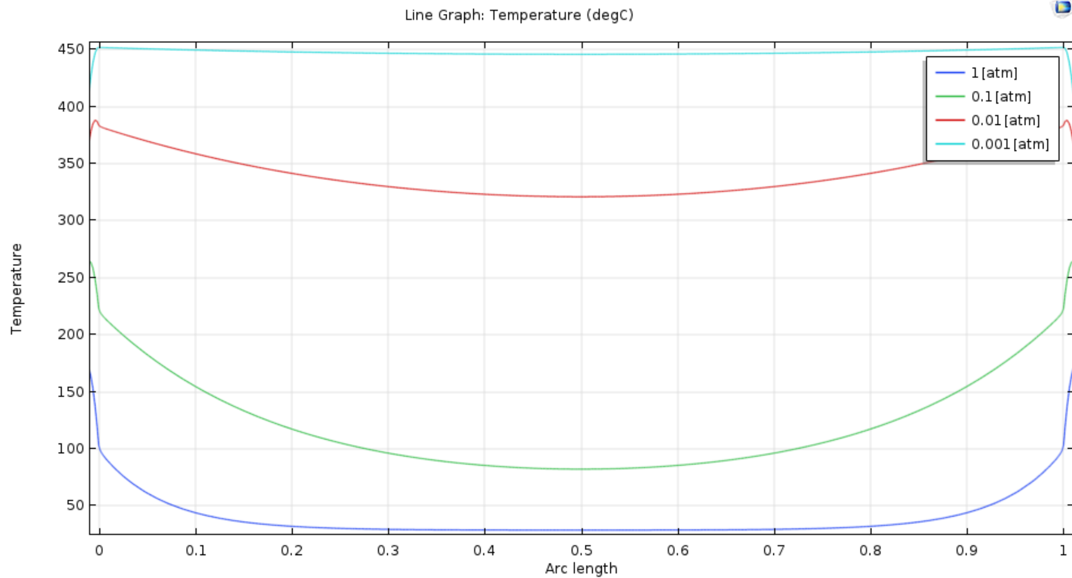

Figure 5.6: Simulation result of temperature change with pressure. The voltage used is 9V. Arc length means the y axis from 0 to 1mm.

Therefore, the device is initially designed to perform in vacuum environment that largely eases the heat conduction to air. Figure 5.5 and 5.7 show the temperature distribution on device change with pressure from 1bar (1atm) to 0.1mbar, which is equivalent from room pressure to vacuum. In the figure, it can be clearly seen the trend that hot wire gradually glows from ends to middle with lowering pressure, which means the thermal energy is transferred to the body of hot wire from where the power source is connected. Eventually, the whole hot wire starts to glow in relatively uniform way. Both simulation and measurement fully verify the effect of heat conduction to air.

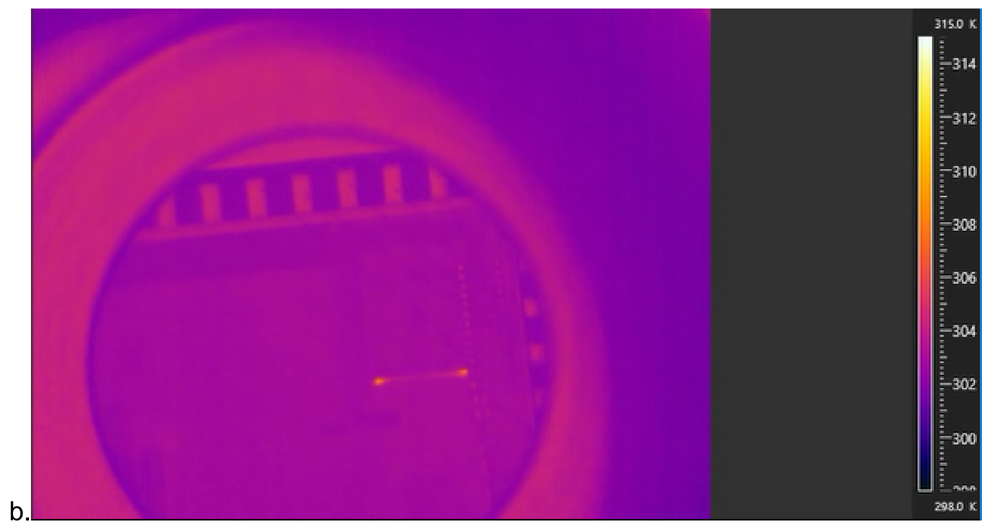

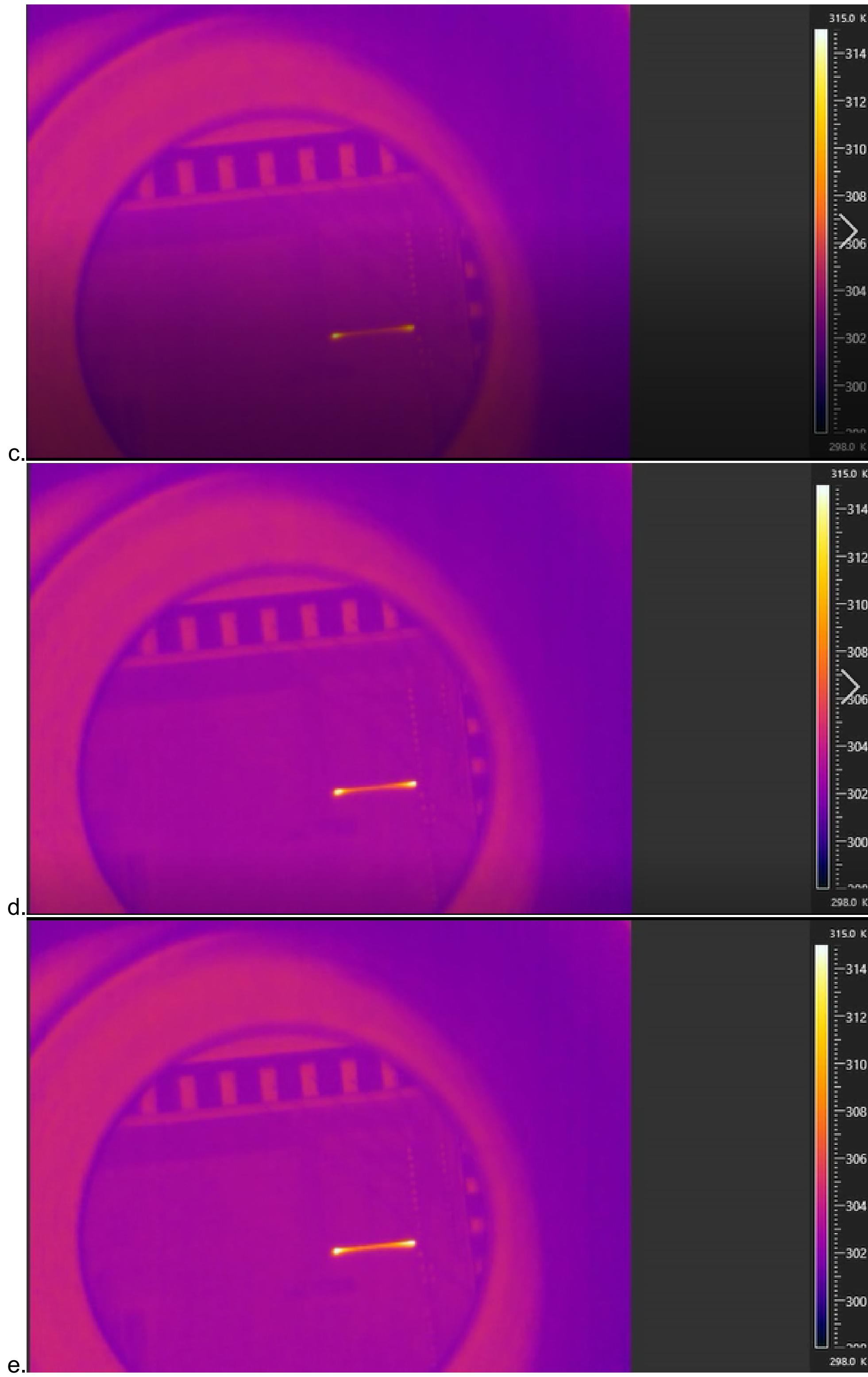
c.
315.0 K
314
312
310
308
306
304
302
300
298.0 K
d.
315.0 K
314
312
310
308
306
304
302
300
298.0 K
e.
315.0 K
314
312
310
308
306
304
302
300
298.0 K

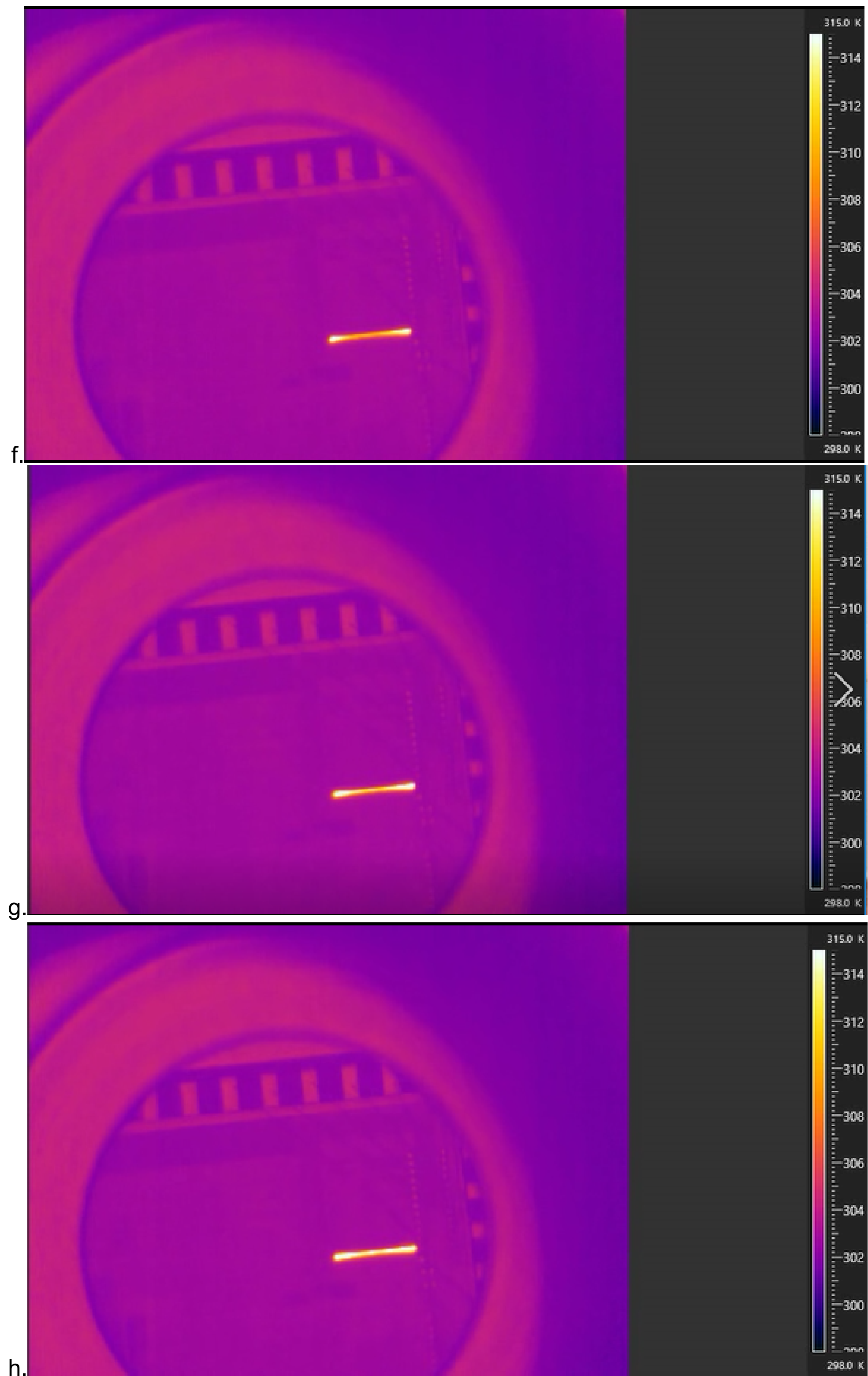

Figure 5.7: Continued. The change of temperature profile on hot wire with pressure from 1bar to 0.1mbar. The maximum temperature is fixed at 315K for better contrast. The hot wire used is 2mm long one with four meander bridges at two ends.

5.2.3. The effect of voltage source

Apart from the pressure, the increased voltage source is another way to enhance heat generation that might trade off the heat loss due to conduction to air. However, the measurement shows that there are still only two bright spots at ends when the pressure is 1atm, though much larger voltage than designed is provided. From the simulation shown in Figure 5.8, 15V indeed gives higher temperature at ends, but it remains low along the body of hot wire in middle. That explains the observation of two bright spots and manifests again the strength of conduction to air.

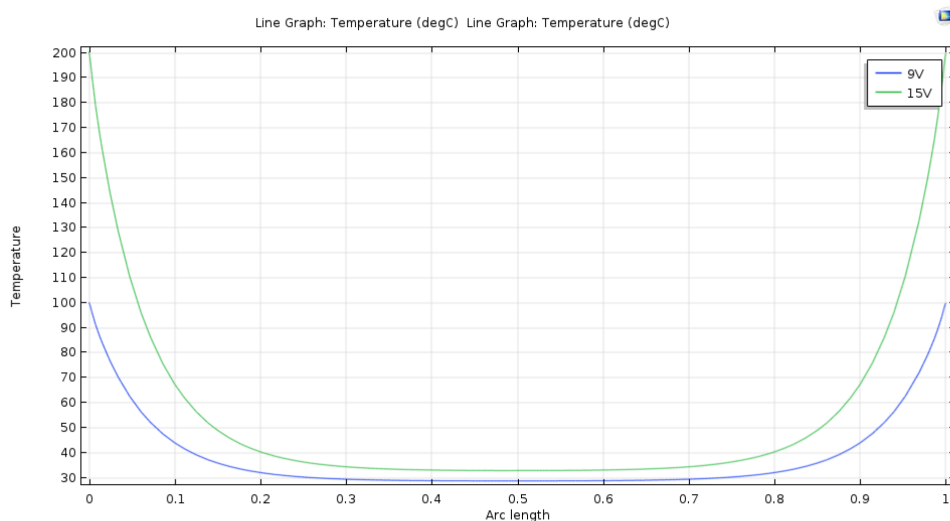

Figure 5.8: Simulation result of temperature change with voltage. The pressure is 1atm. Arc length means the y axis from 0 to 1mm.

On the other hand, when the hot wire works in the vacuum, larger voltage is the useful way to obtain higher temperature shown in Figure 5.9. It can be seen that in this case, temperature changes uniformly with voltage without the effect of heat conduction to air. It increases to 370K at 10V then burns. Theoretically, it should reach 400°C (673K) before burned, which is far away from the result obtained. Besides, the temperature distribution is not such uniform as designed. The reason is analyzed in next sections.

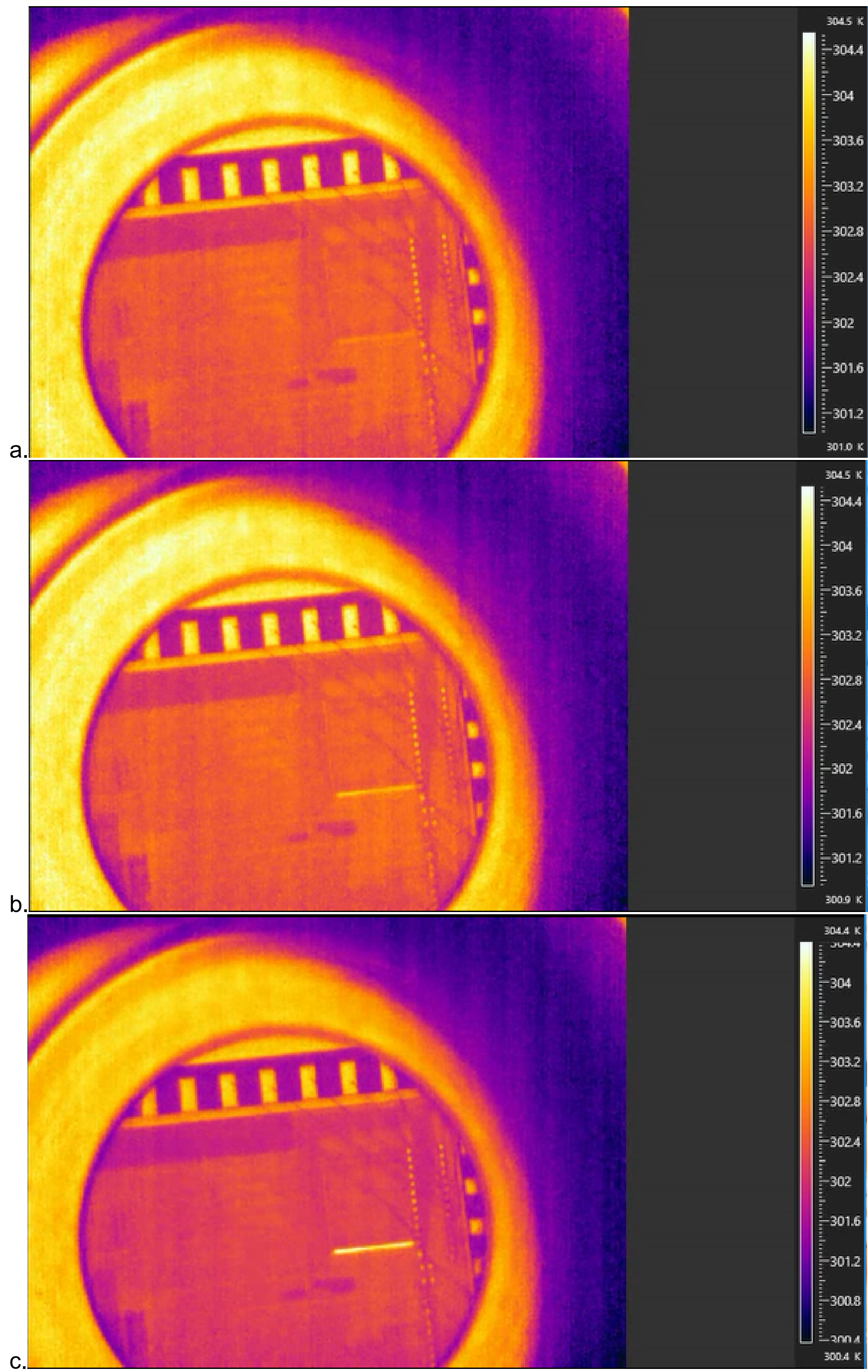
a.
304.5 K
304.4
304
303.6
303.2
302.8
302.4
302
301.6
301.2
301.0 K
b.
304.5 K
304.4
304
303.6
303.2
302.8
302.4
302
301.6
301.2
300.9 K
c.
304.4 K
304
303.6
303.2
302.8
302.4
302
301.6
301.2
300.8
300.4 K

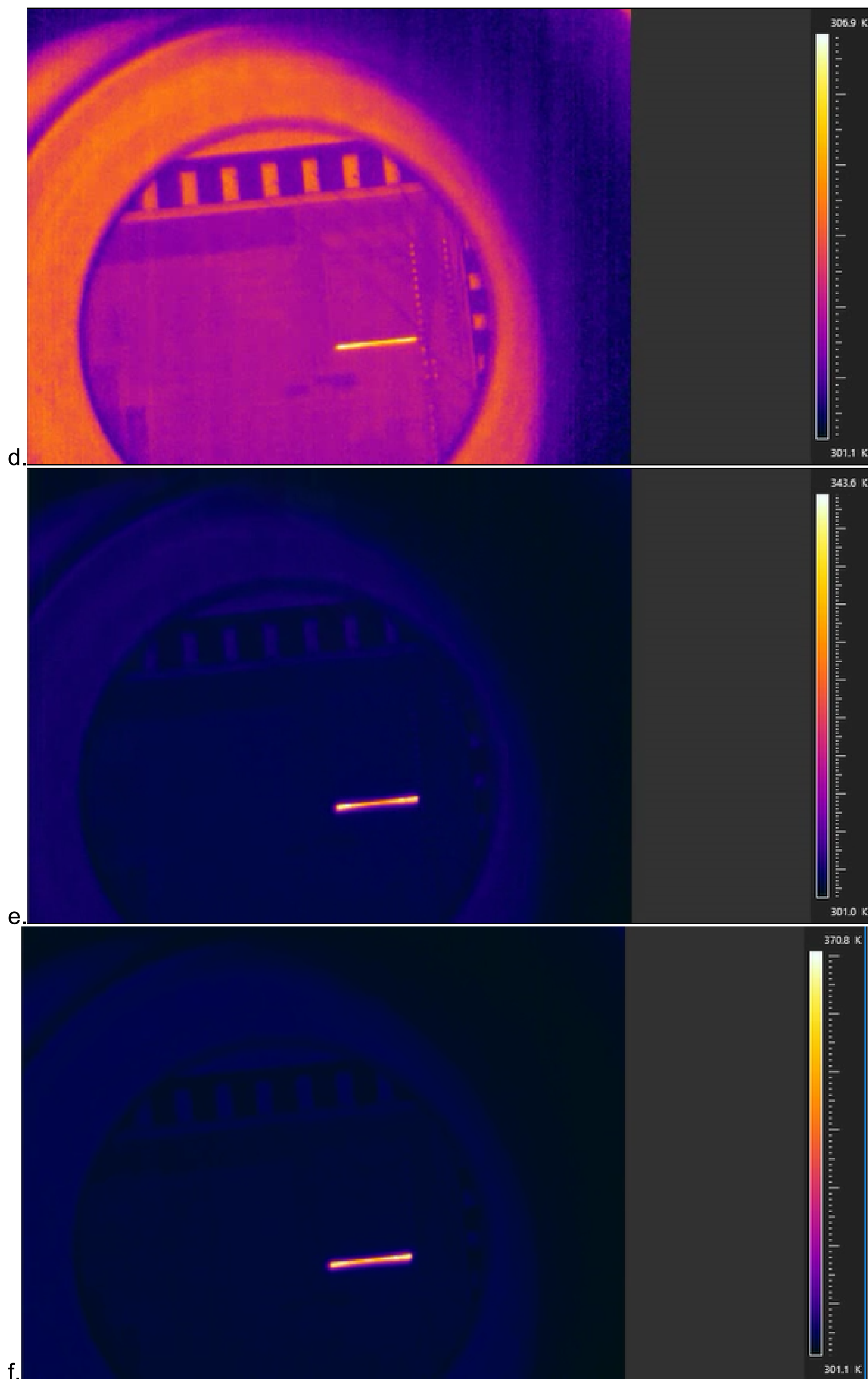

Figure 5.9: The change of temperature profile on hot wire with voltage from 1V to 10V. The hot wire used is 2mm long one with four meander bridges at two ends.

5.2.4. Hot wire array

As mentioned before, one special type of 4 and 5mm hot wire is comprised by 200 and 250 500μm hot wires. They form the hot wire array that is more mechanically stable and thermally uniform. The result is shown in Figure 5.10. Compared to the normal thin and long 2mm hot wire, it indeed has better temperature uniformity. Since the width of the array is 500μm, it has broader surface for IR emitting, the image is much clearer as well. Furthermore, since the length of each component is much shorter than before, the temperature is also higher with smaller voltage. Though it still not reach the desired 600K, the result gets much better.

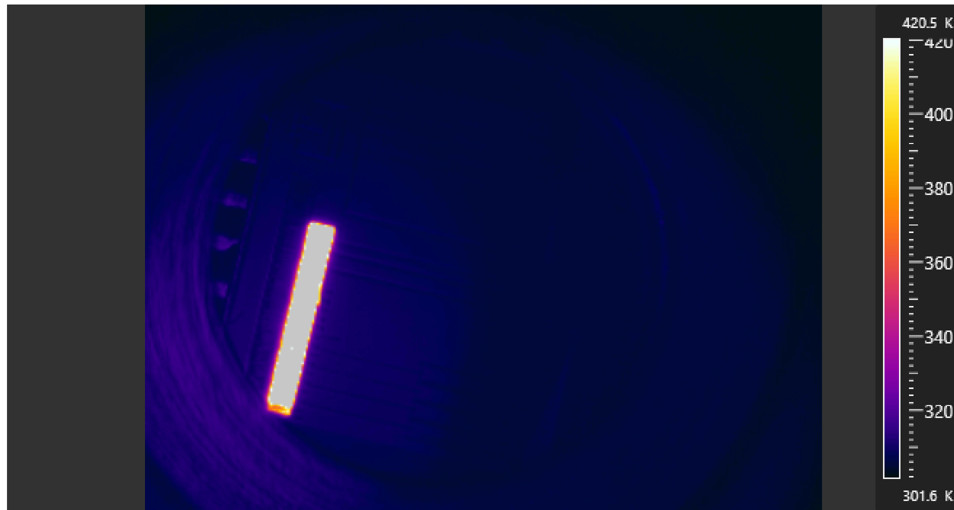

Figure 5.10: Measurement on hot wire array. There is 200 500μm hot wire to build the 4mm hot wire. The voltage is 5V.

5.2.5. Error source analysis

In the measurement above, it can be noticed that most of device can not reach the desired temperature. Some burns just at or before the designed voltage that only have relative low temperature. Others such as array one get higher temperature but still far away from expectation. Besides, the temperature distribution is not as uniform as designed. Always, only two hot spots can be seen at ends, though the voltage is large enough even burning the hot wire. There are many factors causing the problem.

Effect of silicon wafer and IR camera

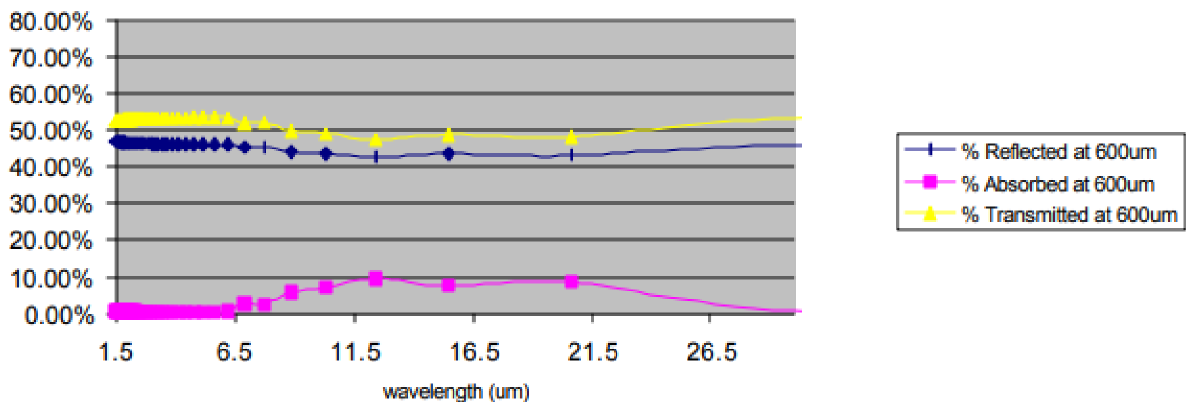

Figure 5.11: Spectral reflection, transmission and absorption of 600μm silicon film. [54].

Except the mechanical vulnerability of silicon wafer mentioned before, it can cause another big problem that the maximum temperature decreases a lot when it is photographed on IR camera. It is, to a large extent, because of the reflection on silicon wafer. Theoretically, the spectral transmission of thin silicon film over the band from 1 to 10μm is approximately only 50% according to Figure 5.11.

Even worse, the decrease becomes larger with higher maximum temperature on device as shown in Figure 5.12. A resistor is used to show the result clearer. By comparing a, b and c, d, the difference in temperature between without and with silicon wafer increases from 30°C to 50°C.

One possible reason here is IR camera. In order to show the temperature on hot wire, IR camera tries to collect the intensity at all corresponding related wavelength based on Wien's Law. For instance, when the peak wavelength of temperature on hot wire is 4μm, it has large portion of intensity that at wavelength longer than 4μm, 7μmfor instance. Silicon wafer might have absorption exactly at this range according to Figure 5.11. When temperature is higher, peak wavelength shifts to shorter value, which means the portion of intensity at the possible absorption range of silicon wafer also becomes larger. Thus, the temperature difference between actual value and that is shown on camera is larger. However, the exactly quantifiable relation between them is not certain yet.

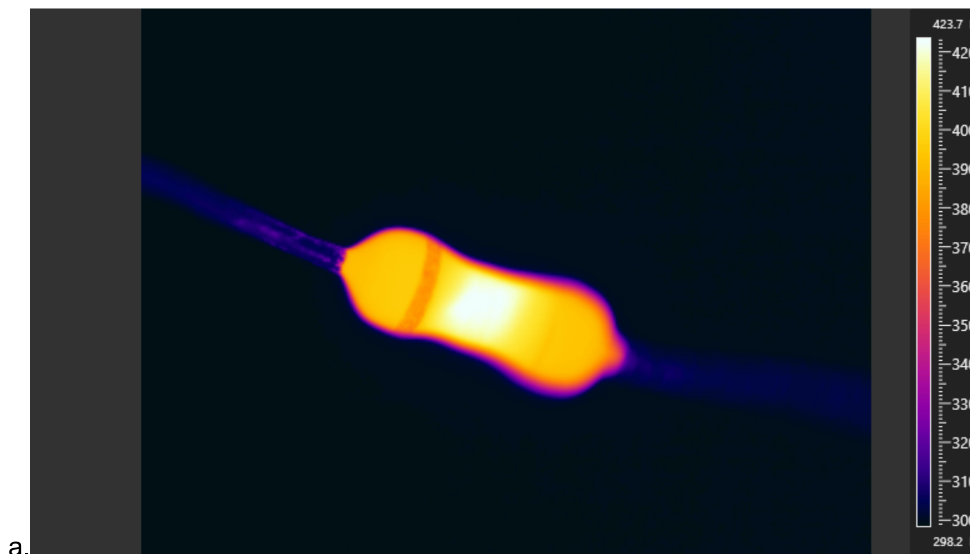

a.

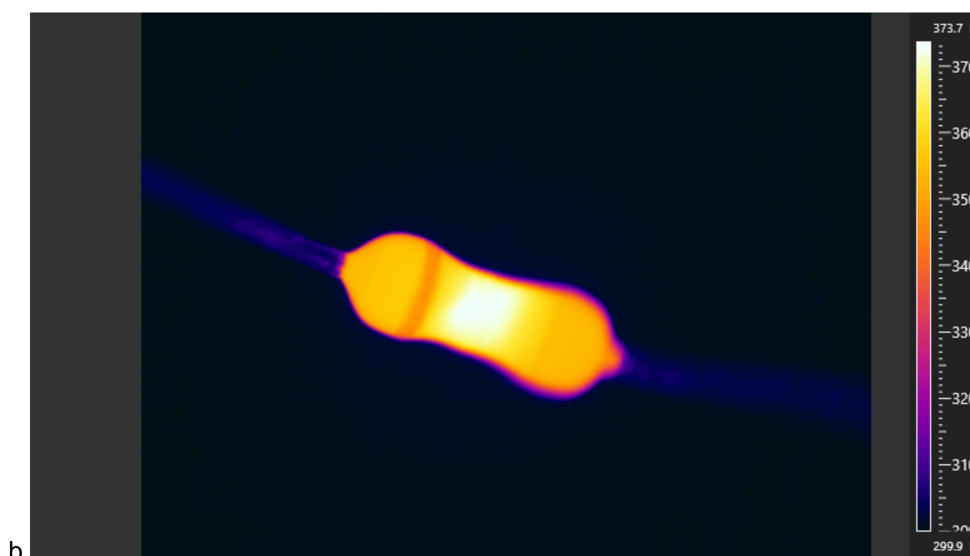

b.

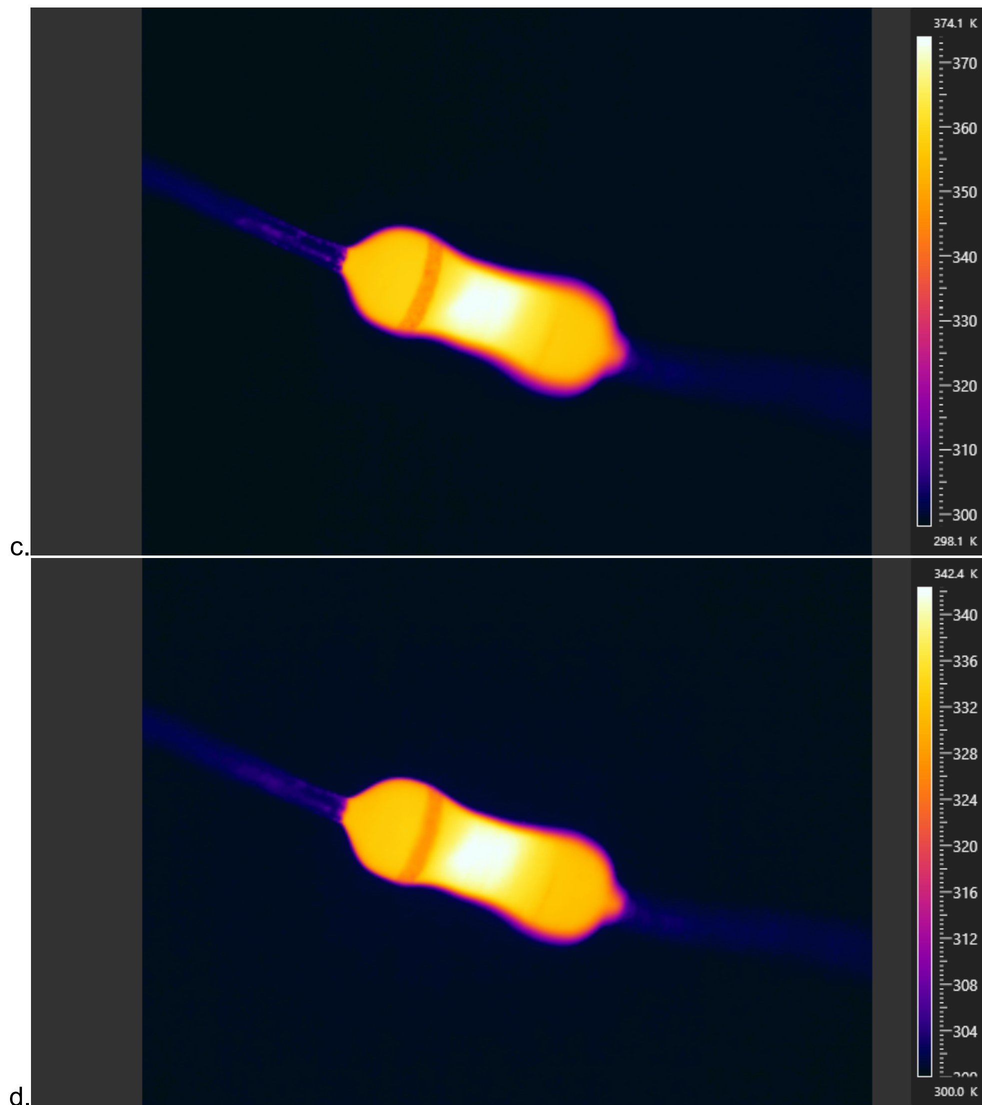

Figure 5.12: The absorption effect of silicon wafer on IR light. a, c shows the result without silicon wafer, while b, d with silicon wafer. The measurand used here is 10ohm resistor.

Difference between polysilicon and single crystalline silicon

In most of case, the expected temperature and its profile do not show up on the device. Usually, only two hot spots appear at ends of hot wire, they are heated and glowing bridges. That's might because the difference between polysilicon and single crystalline silicon on resistivity and TCR is large.

In the initial design, the figure of the relation of resistivity versus doping level is specifically for silicon but polysilicon. Silicon is normally referred to single crystalline silicon which is one single continuous crystal without grain boundary. While polysilicon is highly pured silicon that comprised of bunch of crystals [51]. Generally, the resistivity of polysilicon is larger than silicon [52]. It means doping level in polysilicon is usually larger than in silicon for same resistivity, which causes the mistake on TCR as well. Thus, the insufficient doping due to misuse of the data for silicon is also one important reason for the general 2 to 3 times larger resistance than expectation as mentioned before.

Therefore, the simulation for temperature distribution on hot wire is done again with right resistivity and TCR for polysiliconas shown in Figure 5.13. It can be seen that at the designed 9V for 1mm hot wire, the temperature becomes much higher than 400°C. Furthermore, the distribution is no longer uniform, but almost 100°C difference between the bridge and hot wire body. In association with the assumption that the temperature captured by FLIR camera

is much smaller than 50% of actual temperature, it is reasonable that only two hot spots can be observed since the temperature on hot wire body is nearly room temperature.

Besides, since the temperature is much higher, it is probably beyond the heat capacity of polysilicon. Especially for the 1µm thin bridge, it is very easy to burn.

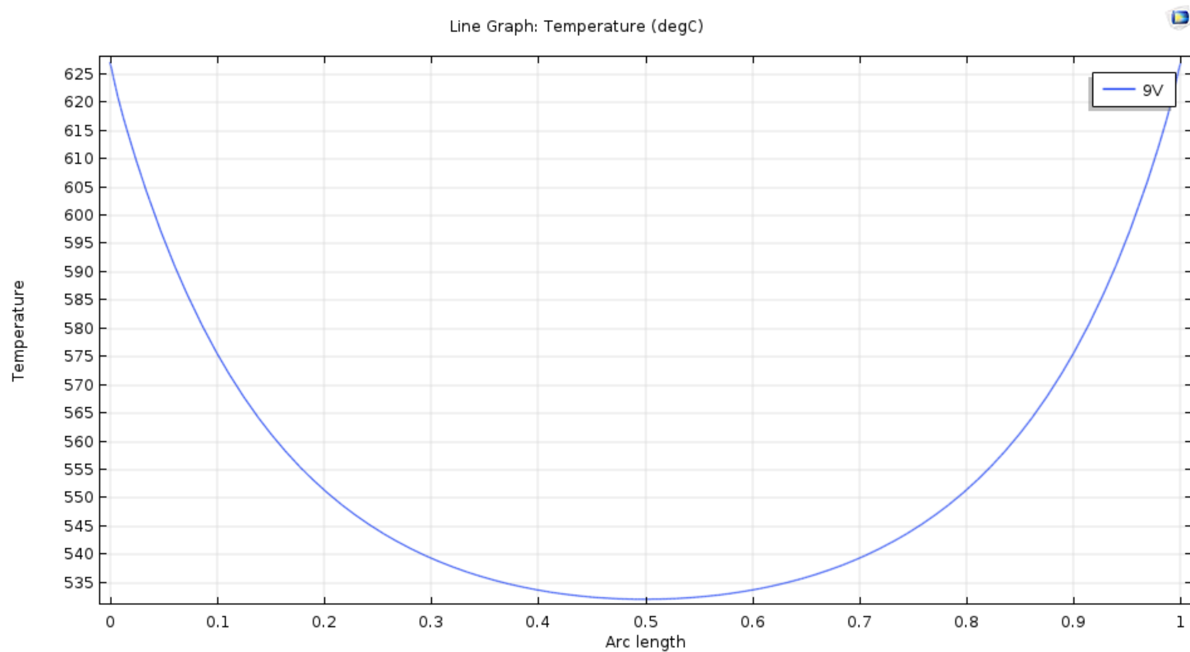

Figure 5.13: Temperature distribution on 1mm hot wire with resistivity and TCR of polysilicon.

6

Conclusion and future work

In this thesis, two essential parts of an IR microspectrometer are designed, fabricated and measured. Hot wire, which is used as the IR light source, is designed to have a constant temperature profile over its length for a uniform IR radiation. In order to achieve that, the thermal, electrical, and mechanical performance of the hot wire are fully studied. The heat transfer mechanics between the hot wire surface and surrounding air is also considered. Finally, a number of hot wires with various geometry and different resistivity profile and TCR are designed and fabricated based on simulation results in COMSOL.

Based on the black-body radiation, a resistor (i.e. hotwire) emits IR light at an specific spectrum when it is electrically heated by voltage and current source, according to the Joule heating effect. The generated heat can be modulated by resistivity and TCR of hot wire which can be changed by doping level. Therefore, to obtain a uniform IR emission, the temperature profile of the hotwire has to be as constant as possible.

For a micro-resistor, it was found that the thermal conduction is the major factor causing the non-uniformity of temperature distribution. It includes the heat conduction between substrate and hot wire body, and to surrounding air. While the heat convection has much less effect which can be almost neglected. The heat conduction to the surrounding air can also be avoided using vacuum packaging of the device.

Here, narrow and long bridge structures were used to separate the hotwires from the substrate. Since the bridge connects directly to substrate, the heat conduction through it reduces the temperature a lot where is close to the end of hot wire. To solve that, the ratio of the width of hot wire body and bridge has to be as large as possible. It can shrink the area of interface in between, then weaken the heat conduction. Besides, special resistivity profile can also be applied to generate more thermal energy that can compensate for the heat loss due to heat conduction. Moreover, TCR than can change resistivity with temperature has also certain effects. But it is proved that changing of resistivity works less well than that of interface area between hot wire body and substrate. Furthermore, bridge structures were designed to be meander-shaped to sustain the tensile force due to thermal expansion. Middle bridge is also added for stronger mechanical stability for longer hotwires. As mentioned earlier, strong heat conduction to surrounding air makes the temperature highly depend on air pressure. It leads to the huge temperature dip in the middle of hot wire. Thus, hot wires designed in this thesis needs to operate in vacuum environment.

The second focus of this thesis was on the optical design of the filter that is intended to spectrally select the output light along the length of the light source. LVOF is studied as an integrated filter for the filtering of output light. LVOF has been successfully implemented in microspectrometers as a dispersive element. In the case of hot wire as IR light source, which is different from collimated plane wave, the situation is more complicated. It has to combine multiple incident angle and the effect of large cone angle which might be the cause of extremely small transmittance. Basically, LVOF has slightly higher transmittance compared to FP filter due to the gain inside.

LVOF operating principle for a distributed light source was studied in depth and all possible factors affecting the performance of LVOF were investigated. Here the emphasis was put on the walk-off effect of light in the LVOF cavity. The coherency of the distributed light source (hotwire) was found to be a very interesting issue that has to be further researched. Finally, the performance of the LVOF is compared to a conventional Fabry-Perot.

The hot wires were fabricated through a flow of fabrication steps. Plenty of advanced fabrication technologies are involved. Eventually, the hot wire is measured for its electrical property and optical performance. To figure out the divergence between measurement result and initial design plan, all result are carefully analyzed and discussed. Although due to a few challenges, e.g. the effect of silicon wafer that is used as the window and the use of property of silicon rather than polysilicon, the final temperature distribution and magnitude on hot wire is not as expected, the basic working principle of the designed hot wire was proven.

Based on the result presented in this work, a number of aspects must be studied in the future work:

- Firstly, silicon carbide as alternative can replace polysilicon for hot wire. It has stronger heat capacity that can bear much higher temperature. IR emitter for broader band can thereby be designed. On the other hand, it is hard to implant and exert on other adjustments since it is extremely tough. It is a problem needed to be solved.
- Secondly, hot wire design needs to be further refined by using correct property of polysilicon rather than silicon. The heat conduction to air needs to be paid more attention.
- Thirdly, the simulation on LVOF for the case of hot wire as IR source needs to be further verified. The extent of the coherency of the light source must be further studied. Comparing the measurement results with light sources with different coherency can be used to find out the actual coherency of the distributed light source.
- Finally, an integrated IR light source with dedicated LVOF, i.e. an LVLS (Linearly variable light source) is designed, fabricated, and characterized.

Bibliography

[1] Barbara Stuart. *Infrared Spectroscopy*, pages 1–18. American Cancer Society, 2015. ISBN 9780471238966.

[2] VP Iordanov, GW Lubking, R Ishihara, RF Wolffenbuttel, PM Sarro, and MJ Vellekoop. Silicon thin-film uv filter for nadh fluorescence analysis. *Sensors and Actuators A: Physical*, 97:161–166, 2002.

[3] R F Wolffenbuttel. Mems-based optical mini- and microspectrometers for the visible and infrared spectral range. *Journal of Micromechanics and Microengineering*, 15(7): S145, 2005.

[4] BH Stuart. Infrared spectroscopy: fundamentals and applications wiley, 2004.

[5] James P. Smith. Product review: Spectrometers get small. *Analytical Chemistry*, 72(19): 653 A–658 A, 2000.

[6] RA Crocombe. Miniature optical spectrometers: There's plenty of room at the bottom part 1: Background and mid-infrared spectrometers. 2008 coupler in combination with a plano-convex lens. *Optics Express*, 14:4064, 2006.

[7] Erwin G Loewen and Evgeny Popov. *Diffraction gratings and applications*. CRC Press, 1997.

[8] SH Kong, DDL Wijngaards, and RF Wolffenbuttel. Infrared micro-spectrometer based on a diffraction grating. *Sensors and Actuators A: Physical*, 92(1-3):88–95, 2001.

[9] John P Coates. New microspectrometers. *Spectroscopy*, 15:21–27, 2000.

[10] Arvin Emadi, Huaiwen Wu, Ger de Graaf, and Reinoud Wolffenbuttel. Design and implementation of a sub-nm resolution microspectrometer based on a linear-variable optical filter. *Optics express*, 20(1):489–507, 2012.

[11] D Jung, S Bank, ML Lee, and D Wasserman. Next-generation mid-infrared sources. *Journal of Optics*, 19(12):123001, 2017.

[12] PK Gupta and SC Mehendale. Mid-infrared optically pumped molecular lasers. *Hyperfine Interactions*, 37(1-4):243–273, 1987.

[13] HH Bruun. Hot–wire anemometry, principles and signal processing, 1995.

[14] Charles G Lomas. *Fundamentals of hot wire anemometry*. Cambridge University Press, 2011.

[15] J. Chen and Chang Liu. Development and characterization of surface micromachined, out-of-plane hot-wire anemometer. *Journal of Microelectromechanical Systems*, 12(6): 979–988, Dec 2003. ISSN 1057-7157. doi: 10.1109/JMEMS.2003.820261.

[16] J.J. Healy, J.J. de Groot, and J. Kestin. The theory of the transient hot-wire method for measuring thermal conductivity. *Physica B+C*, 82(2):392 – 408, 1976. ISSN 0378-4363. doi: https://doi.org/10.1016/0378-4363(76)90203-5. URL `http://www.sciencedirect.com/science/article/pii/0378436376902035`.

[17] An apparatus to measure the thermal conductivity of liquids. *J. Phys. E: Sci. Instrum.*, 9(12):1073, 1976. URL `http://stacks.iop.org/0022-3735/9/i=12/a=020`.

[18] Fangqiang Li, Haisheng San, Meijing Cheng, and Xuyuan Chen. Micro-machined infrared emitter with metallic photonic crystals structure. In *4th International Symposium on Advanced Optical Manufacturing and Testing Technologies: Design, Manufacturing, and Testing of Micro-and Nano-Optical Devices and Systems*, volume 7284, page 728406. International Society for Optics and Photonics, 2009.

[19] Kook-Nyung Lee, Dae-Sung Lee, Suk-Won Jung, Yun-Ho Jang, Yong-Kweon Kim, and Woo-Kyeong Seong. A high-temperature mems heater using suspended silicon structures. *Journal of Micromechanics and Microengineering*, 19(11):115011, 2009.

[20] Woo-Jin Hwang, Kyu-Sik Shin, Ji-Hyoung Roh, Dae-Sung Lee, and Sung-Hoon Choa. Development of micro-heaters with optimized temperature compensation design for gas sensors. *Sensors*, 11(3):2580–2591, 2011.

[21] W Konz, J Hildenbrand, M Bauersfeld, S Hartwig, A Lambrecht, V Lehmann, and J Wollenstein. Micromachined ir-source with excellent blackbody like behaviour. In *Smart Sensors, Actuators, and MEMS II*, volume 5836, pages 540–549. International Society for Optics and Photonics, 2005.

[22] Angela D McConnell, Srinivasan Uma, and Kenneth E Goodson. Thermal conductivity of doped polysilicon layers. *Journal of Microelectromechanical Systems*, 10(3):360–369, 2001.

[23] JB Casady and R Wayne Johnson. Status of silicon carbide (sic) as a wide-bandgap semiconductor for high-temperature applications: A review. *Solid-State Electronics*, 39 (10):1409–1422, 1996.

[24] Hans H Bruun. Hot-wire anemometry: principles and signal analysis, 1996.

[25] John H Lienhard. *A heat transfer textbook*. Courier Corporation, 2013.

[26] Mojtaba Dehghan Manshadi and Mohammad Kazemi Esfeh. Analytical and experimental investigation about heat transfer of hot-wire anemometry. In Salim N. Kazi, editor, *An Overview of Heat Transfer Phenomena*, chapter 3. IntechOpen, Rijeka, 2012. doi: 10.5772/51989. URL `https://doi.org/10.5772/51989`.

[27] Manjula S Raman, Teweldebhran Kifle, Enakshi Bhattacharya, and KN Bhat. Physical model for the resistivity and temperature coefficient of resistivity in heavily doped polysilicon. *IEEE Transactions on Electron Devices*, 53(8):1885–1892, 2006.

[28] Alexander Bunch, Bryan H; Hellemans. *The History of Science and Technology*. Houghton Mifflin Harcourt, April, 2004.

[29] G Hernández and Fabry-Perot Interferometers. vol. 3, 1988.

[30] JH Correia, G De Graaf, SH Kong, M Bartek, and RF Wolffenbuttel. Single-chip cmos optical microspectrometer. *Sensors and Actuators A: Physical*, 82(1-3):191–197, 2000.

[31] L Fonseca, R Rubio, J Santander, C Calaza, N Sabate, P Ivanov, E Figueras, I Gracia, C Cane, S Udina, et al. Qualitative and quantitative substance discrimination using a cmos compatible non-specific ndir microarray. *Sensors and Actuators B: Chemical*, 141 (2):396–403, 2009.

[32] JH Correia, M Bartek, and RF Wolffenbuttel. Bulk-micromachined tunable fabry–perot microinterferometer for the visible spectral range. *Sensors and Actuators A: Physical*, 76 (1-3):191–196, 1999.

[33] Jason S Milne, John M Dell, Adrian J Keating, and Lorenzo Faraone. Widely tunable mems-based fabry–perot filter. *Journal of microelectromechanical systems*, 18(4):905–913, 2009.

[34] AV Tikhonravov, PW Baumeister, and KV Popov. Phase properties of multilayers. *Applied optics*, 36(19):4382–4392, 1997.

[35] P Rüdiger. Encyclopedia of laser physics and technology. *Handbook/Reference Book*, 2008.

[36] CJR Sheppard. Approximate calculation of the reflection coefficient from a stratified medium. *Pure and Applied Optics: Journal of the European Optical Society Part A*, 4(5): 665, 1995.

[37] Max Born and Emil Wolf. *Principles of optics: electromagnetic theory of propagation, interference and diffraction of light*. Elsevier, 2013.

[38] J Brossel. Multiple-beam localized fringes: Part i.-intensity distribution and localization. *Proceedings of the Physical Society*, 59(2):224, 1947.

[39] R Bünnagel, H-A Oehring, and K Steiner. Fizeau interferometer for measuring the flatness of optical surfaces. *Applied optics*, 7(2):331–335, 1968.

[40] NP Ayerden. *A miniaturized optical gas sensor for natural gas analysis*. PhD thesis, Delft University of Technology, 2016.

[41] John R Rogers. Fringe shifts in multiple-beam fizeau interferometry. *JOSA*, 72(5):638–643, 1982.

[42] Mohammad A Rob. Limitation of a wedged étalon for high-resolution linewidth measurements. *Optics letters*, 15(11):604–606, 1990.

[43] Robert R McLeod and Tokuyuki Honda. Improving the spectral resolution of wedged etalons and linear variable filters with incidence angle. *Optics Letters*, 30(19):2647–2649, 2005.

[44] Hongyong Zhang, Hideki Uochi, Toru Takayama, Takeshi Fukunaga, and Yasuhiko Takemura. Method for manufacturing semiconductor device, April 4 1995. US Patent 5,403,772.

[45] Layout and mask conventions. URL https://www.mems-exchange.org/users/masks/guidelines.html.

[46] James M Bustillo, Roger T Howe, and Richard S Muller. Surface micromachining for microelectromechanical systems. *Proceedings of the IEEE*, 86(8):1552–1574, 1998.

[47] N Sharma, M Hooda, and SK Sharma. Synthesis and characterization of lpcvd polysilicon and silicon nitride thin films for mems applications. *Journal of Materials*, 2014, 2014.

[48] Meredith Metzler and Raj Patel. Plasma enhanced chemical vapor deposition (pecvd) of silicon dioxide (sio2) using oxford instruments system 100 pecvd. 2017.

[49] Xiumiao Zhang, Koubao Ding, Ailing Yang, and Diling Shao. Processing and characterisation of pecvd silicon nitride films. *Advanced Materials for Optics and Electronics*, 6(3): 147–150, 1996.

[50] Manjula S Raman, Teweldebhran Kifle, Enakshi Bhattacharya, and KN Bhat. Physical model for the resistivity and temperature coefficient of resistivity in heavily doped polysilicon. *IEEE Transactions on Electron Devices*, 53(8):1885–1892, 2006.

[51] D. Ozevin. 10 - micro-electro-mechanical-systems (mems) for assessing and monitoring civil infrastructures. In M.L. Wang, J.P. Lynch, and H. Sohn, editors, *Sensor Technologies for Civil Infrastructures*, volume 55 of *Woodhead Publishing Series in Electronic and Optical Materials*, pages 265 – 302e. Woodhead Publishing, 2014. ISBN 978-0-85709-432-2. doi: https://doi.org/10.1533/9780857099136.265. URL http://www.sciencedirect.com/science/article/pii/B9780857094322500103.

[52] MY Ghannam and RW Dutton. Resistivity of boron-doped polycrystalline silicon. *Applied physics letters*, 52(15):1222–1224, 1988.

[53] Flir iintroduces thermacam sc 3000 high speed thermal imaging system, Jan 2001. URL https://www.photonicsonline.com/doc/flir-iintroduces-thermacam-sc-3000-high-speed-0001.

[54] Michael H Jones and Stephen H Jones. Optical properties of silicon. *Virginia Semiconductor, Inc*, 2002.